A METHOD FOR RECORDING AND STUDYING CRACK GROWTH IN THE CORROSION FATIGUE OF METALS

Francis J. Cole Scholarship Memoirs

1941-1942

1942-1943

Thesis by

Robert Clarence Brumfield

In Partial Fulfilment

of the Requirements for the Degree of

Doctor of Philosophy

California Institute of Technology

Pasadena, California

1943

To Barbara Katherine Brumfield this thesis is affectionately dedicated.

ACKNOWLEDGMENT

The work described in this thesis was made possible by Professor William Howard Clapp, who first accepted our lack of knowledge of corrosion fatigue phenomena as a personal challenge. Professor Clapp designed the fatigue machine used in the tests, personally financed the first year of operation, and served as faculty adviser during all the tests and development work.

I am further indebted to the late Mrs. Francis J. Cole, who endowed the Institute with funds for the Cole Scholarships; and to the Mechanical Engineering Department for the 1941-1942 and 1942-1943 awards. The Mechanical Engineering Department generously provided additional financial support and encouraged the project in every way.

Dr. Donald E. Hudson lent encouragement and helpful judgment and relieved the author of some of his work in order that this thesis could be finished. Dr. William F. Nash, Jr. gave freely of his time and skill in the Metallography Laboratory. Professor Clapp and Dr. Hudson made many helpful suggestions in reading the text.

Mr. E. M. Wagner, formerly Chief Engineer of the Kobe Company, offered his field experiences with corrosion fatigue phenomena and enlisted the support of his company in furnishing steel, specimens and the corrosive media for the tests.

Mr. Frank Lanni of the Biology Department generously made nearly fifty "pH" determinations on the corrosive media used.

TABLE OF CONTENTS

APPENDICES

ILLUSTRATIONS

1. SUMMARY OF RESULTS AND CONCLUSIONS

A rotating-beam type corrosion fatigue machine and a test procedure were developed for specimens of uniform diameter loaded in pure bending. Twenty SAE X 4130 (normalized) steel specimens were damaged at 1425 rpm in an air-saturated oil-well brine.

A sulfur-print method was developed for analysing the damaged specimens to determine the distribution of the cracks, their profile shapes and depths of penetration.

These studies have led to the following conclusions:

(1) The uniformity of corrosion pitting largely controlled the distribution of fatigue cracks, the amount of interaction between the cracks, their depths of penetration and, hence, the life of the specimen. The distribution of fatigue cracks varied widely under apparently identical laboratory conditions and was found to be the most important factor in causing experimental scatter.

(2) The rates of crack penetration were determined as shown in Figure 18, page 27. The early rates were nearly independent of the loads at the low stresses. It was found difficult to predict the rates of crack penetration at large crack depths.

(3) Lines of constant maximum crack depth are shown on the S-N curve in Figure 19, page 29. These lines resemble McAdam's constant damage lines, particularly for small crack depths. There seems to be no simple relationship between maximum crack depth and failure for different stresses.

(4) Etched axial sections (Figures 20-23, page 31) showed that the pearlite was preferentially attacked by corrosion and cracking.

(5) The corrosion fatigue limit of the steel in air-saturated oil-well brine was 8,750 psi (based on 20 x 10^6 cycles), giving an endurance ratio of 14.3%. When air was excluded and C_2H_2 used instead, the fatigue limit rose to 20,000 psi.

(6) Other possible applications of the sulfur-print method discussed in the thesis are:

(a) The relative merits of materials and the effects of surface finishes, coatings and treatments in retarding crack growth.

(b) Localized corrosion pitting and its effect in producing experimental scatter.

(c) "Size effect".

(7) The sulfur-print method was not found useful in shortening the test procedure, but it allowed considerable additional information to be obtained on the mechanism of crack growth in the corrosion fatigue specimens examined.

2. THE CORROSION FATIGUE PROBLEM

2.1 Sources of Information on Corrosion Fatigue

The recent (1941) state of our knowledge of the fatigue of metals is summarized and discussed in the book "Prevention of the Failure of Metals under Repeated Stress", prepared by the staff of the Battelle Memorial Institute for the Bureau of Aeronautics, Navy Department, (Wiley & Sons, 1941). This publication is referred to as the "Battelle book" in this thesis.

The Battelle book contains an excellent bibliography of 446 references and is conveniently indexed.

In view of the availability and excellence of the Battelle book, the writer has confined his bibliography (Appendix 6) to articles referred to in the thesis and important papers not listed in the Battelle bibliography.

2.2 The Work of Dr. D. J. McAdam, Jr.

McAdam, working at the U. S. Naval Experimental Station, Annapolis, Maryland, and the Bureau of Standards, has written the classical papers in the field of corrosion fatigue. His contributions have been appearing in the literature since 1926. Many of McAdam's papers are included in the Battelle bibliography and others are listed in this thesis. Some of McAdam's data have been summarized by Moore (Ref. 1).

McAdam employed a very logical concept of corrosion fatigue damage in tests which are briefly described as follows:

Fatigue specimens were subjected to two stages of damage in succession:

Stage 1: (Corrosion fatigue stage)

A specimen was damaged a certain amount by cyclic bending stresses and corrosion simultaneously applied for a given length of time. The corrosive

medium was then removed and a protective coating of oil given to the specimen.

Stage 2: (Endurance stage)

One, or several specimens treated in this way were used to find the air-endurance limit of the damaged specimens.

The endurance limit of the damaged specimens, in general, fell below that of the virgin material. The amount of decrease was taken as a measure of the damage. This is a very useful concept. It gives a measure of damage in terms of its effect in reducing the fundamental and well-recognized endurance strength of the material.

McAdam further refined this concept of damage by considering "net damage". If a specimen is allowed to undergo "stressless corrosion" or corrosion without load, its Stage 2 endurance limit will be below that for the virgin material. This type of test is called a "prior corrosion fatigue test" and the damage found called "prior corrosion fatigue damage". "Net damage" is the difference between "(total) corrosion fatigue damage" and "prior corrosion fatigue damage" corresponding to the same time of exposure to the corrosive medium. Net damage is thus a measure of the additional damage caused and made possible by cyclic stress.

McAdam has given us, in addition, photographs of the external surfaces of many damaged specimens, (Ref. 2, etc.). Similar photographs of damaged specimens are shown in Figures 6-13, page 11.

Etched axial sections of specimens E-6 and 8 are shown in Figures 20-23, page 31. McAdam has included many unetched axial sections in his reports (Ref. 2). These axial sections show very clearly the shapes of pits, crevices and fissures corresponding to various degrees of damage, in a plane perpendicular to the plane of the crack.

The stress-corrosion process is thoroughly discussed in a research paper written by McAdam and Geil (Ref. 2). An excellent discussion of the influences of stress range and cycle frequency on surface films is given in Ref. 3.

2.3 The Need for Further Study of the Corrosion Fatigue of Metals

Photomicrographs of axial sections of corrosion fatigue specimens, such as those shown in McAdam's reports (Ref. 2, etc.) and in Figures 20-23, page 31, are of great value in examining the mechanism of the formation and growth of pits and cracks.

These axial sections, however, show the shapes of the cracks in only one plane. The maximum depths reached by the cracks are not necessarily indicated. The picture is thus incomplete. It is desirable that we have other views of the cracks in order to study them in three dimensions.

A simple and accurate way in which another view of the cracks can be obtained is to cut down the diameter of the damaged specimen on a lathe and to examine the "crack pattern" formed by intersection of the cracks and the new cylindrical surface. Cuts may be made to a series of increasing depths (decreasing diameters) and the shapes of the cracks determined to almost any degree of accuracy desired.

In this way the interaction of the cracks, their depths of penetration and profiles can be studied. The effect of stress, time, materials, corrosives, coatings, etc., on crack characteristics can be investigated.

The only practical difficulties lie in the recording and enlarging of these crack patterns for study. Photographic methods might be used, but difficulties would be encountered in making the cracks visible and with distortion due to the surface curvature. Panoramic photography might be used.

The author, in the summer of 1941, conceived a very simple, cheap and accurate sulfur-printing process for recording corrosion fatigue crack patterns. This thesis is chiefly concerned with the technique for making these sulfur prints, their analysis, and the application of the method to the study of twenty corrosion fatigue specimens.

3. EXPERIMENTAL PROCEDURE IN THE PRESENT INVESTIGATION

3.1 Damaging the Specimens

Each specimen was loaded in pure bending and rotated at 1425 rpm while in a gland through which was circulated aeriated oil-well brine. Some of the specimens were run to failure and others partially damaged, as shown on the S-N curve, Figure 1, page 8.

Figure 3, page 10, shows specimen D-7 with corrosion products intact after removal from the fatigue machine. The specimens appear as shown in Figures 6-13, pages 11-13, after being cleaned with fine steel wool. Specimens run at higher stresses were more evenly corroded than those at lower stresses. At a given stress, those run longer were more deeply pitted.

Note that the "D" and "E" series specimens were varnished at the fillets as shown in Figure 29, page 42. Fillet protection is discussed in Appendix 2.4. Specimens C-11 and D-1, which broke early near the fillets, were considered equivalent to specimens stopped early.

3.2 Sulfur (crack) Prints

In order to study the cracks formed in the metal, Figure 14, page 14, halves of damaged specimens were cut in a lathe to successively smaller diameters (greater radial depths). After each cut was made the specimens were etched to open up the cracks, soaked in Na_2S and sulfur prints made of the crack patterns formed at these radial depths. A sample sulfur print is shown in Figure 32, page 47. Series of sulfur prints made at successive radial depths in specimens E-5, 6, 7, and 8 are shown in Figure 16, page 15.

The sulfur print method is described in more detail in Appendix 3.

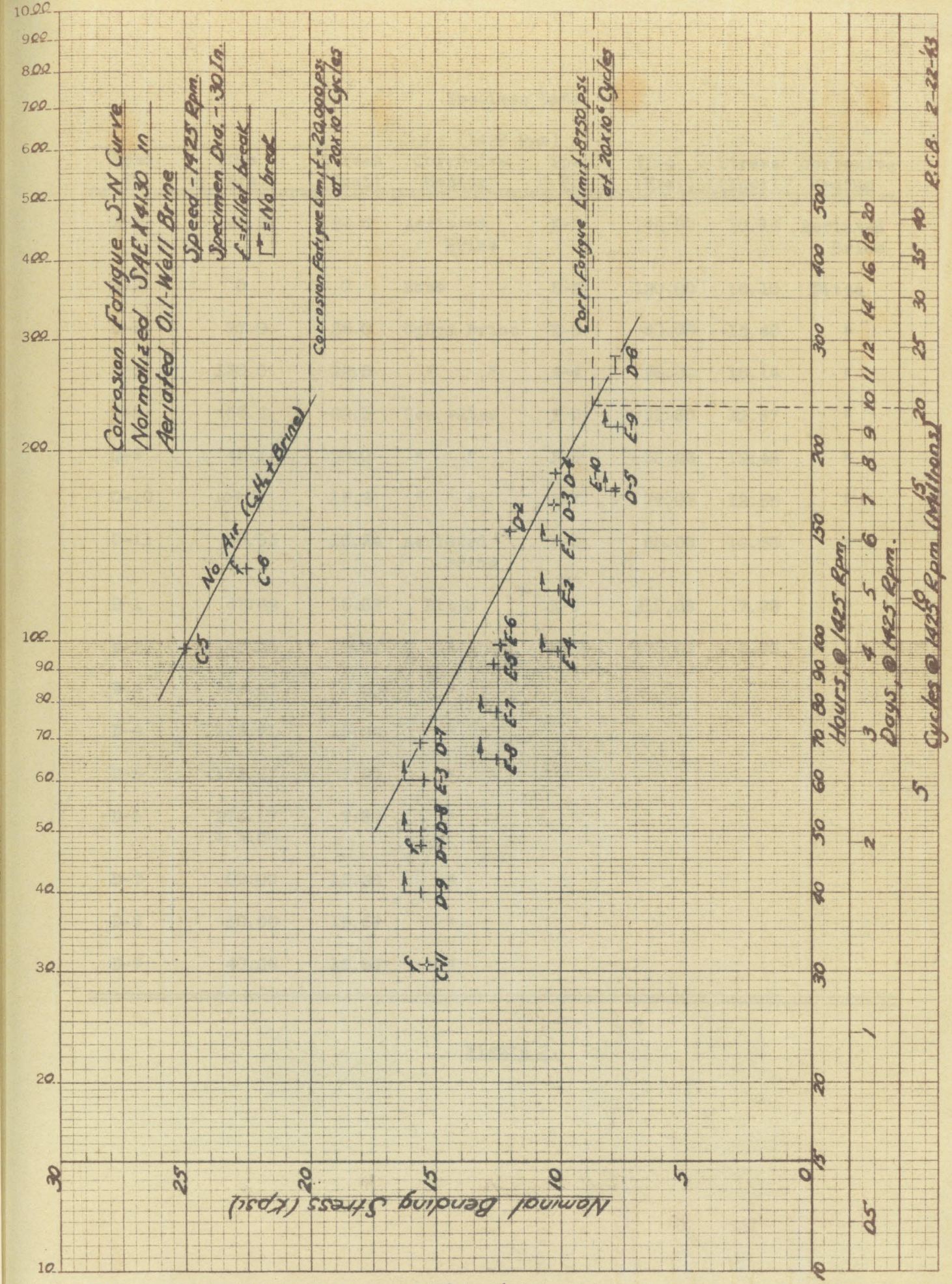
Corrosion Fatigue S-N Curve
Normalized SAE 4130 in
Aerated Oil-Well Brine
Speed - 1425 Rpm.
Specimen Dia. - .30 In.
F=fillet break
=No break
Corrosion Fatigue Limit = 20,000 psi
at 20x10⁶ Cycles
No Air (C.H. + Brine)
Corr. Fatigue Limit = 8750 psi
at 20x10⁶ Cycles
Nominal Bending Stress (Kpsi)
Hours @ 1425 Rpm.
Days @ 1425 Rpm.
Cycles @ 1425 Rpm (Millions)
E.G.B. 2-22-43

Fig 1

Specimen Data

(1425 Rpm)

Spec. No.	Time (Hrs.)	Stress (Kpsi)	Corrosive Medium	Spec. No.	Time (Hrs.)	Stress (Kpsi)	Corrosive Medium
A-2	143.0	24.6	Aeriated Brine	E-1	144.00	10.14	Aeriated Brine
A-9	0	0	None	E-2	120.00	10.10	Ditto
C-5	97.0	25.0	C_2H_2& Brine	E-3	60.00	15.48	"
C-6	130.0	22.5	" "	E-4	96.00	10.14	"
C-8	53.6	22.5	Sea water	E-5	91.80	12.67	"
C-9	43.1	20.0	" "	E-6	98.23	12.46	"
C-10	104.2	15.3	" "	E-7	77.03	12.55	"
C-11	30.83	15.34	Aeriated Brine	E-8	65.00	12.53	"
D-1	47.42	15.62	Ditto	E-9	218.08	7.73	"
D-2	149.25	12.01	"	E-10	173.67	7.73	"
D-3	164.17	10.20	"				
D-4	183.91	10.22	"				
D-5	173.67	7.80	"				
D-6	273.17 ± 9.00	7.80	"				
D-7	69.00	15.60	"				
D-8	50.00	15.59	"				
D-9	40.08	15.59	"				

Figure 2.

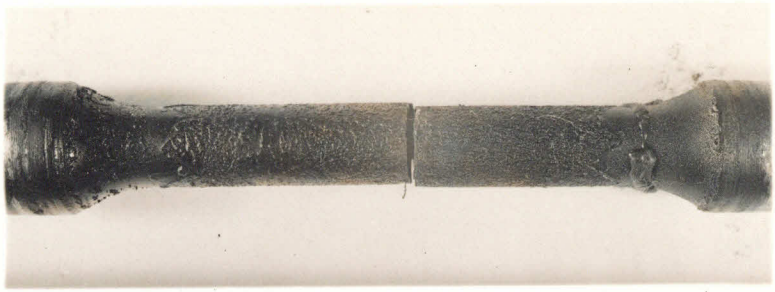

Fig. 3. Specimen D-7 with Corrosion Products.

C-8 C-10 C-9

Fig. 4. Specimens after Running in Sea Water.

Fig. 5. Specimens Pulled in Tension before and after Damage.

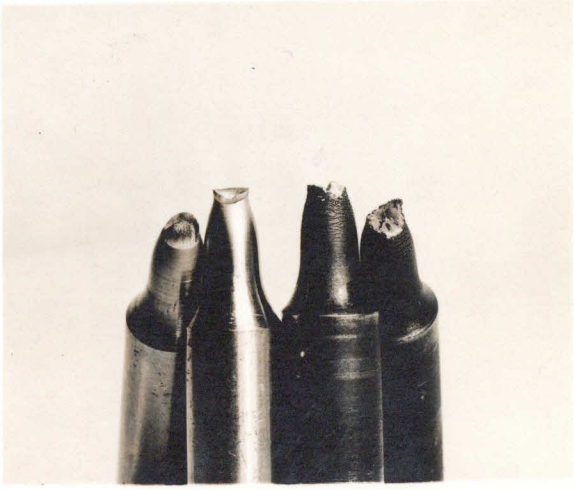

A-9	A-2
Syp. = 119 kpsi	Syp. = 112 kpsi
Sult. = 132 kpsi	Sult. = 126 kpsi

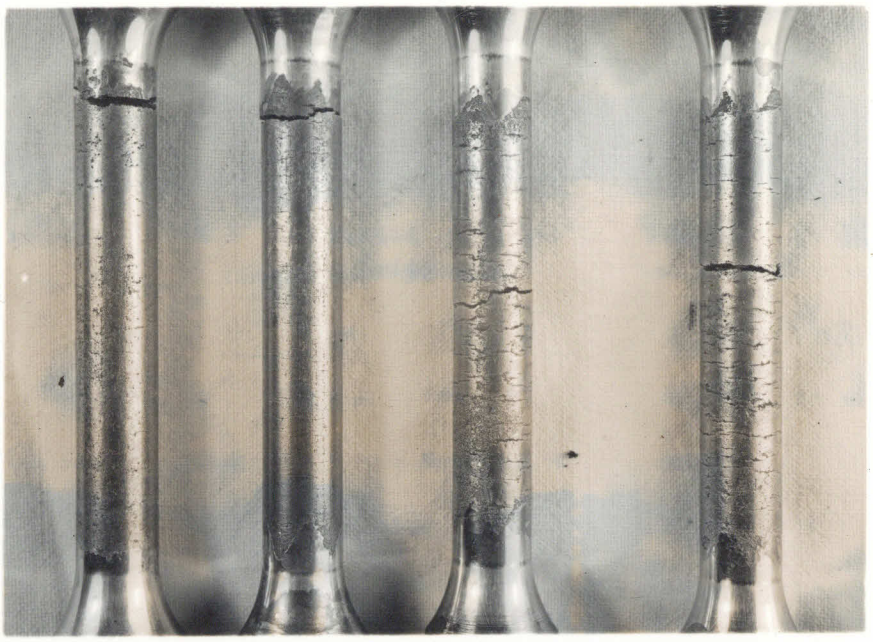

D-1 D-2 D-3 D-4

Fig. 6.

Fig. 6-13. Specimens Damaged in Air-Saturated Oil-Well Brine. Corrosion Products Removed.

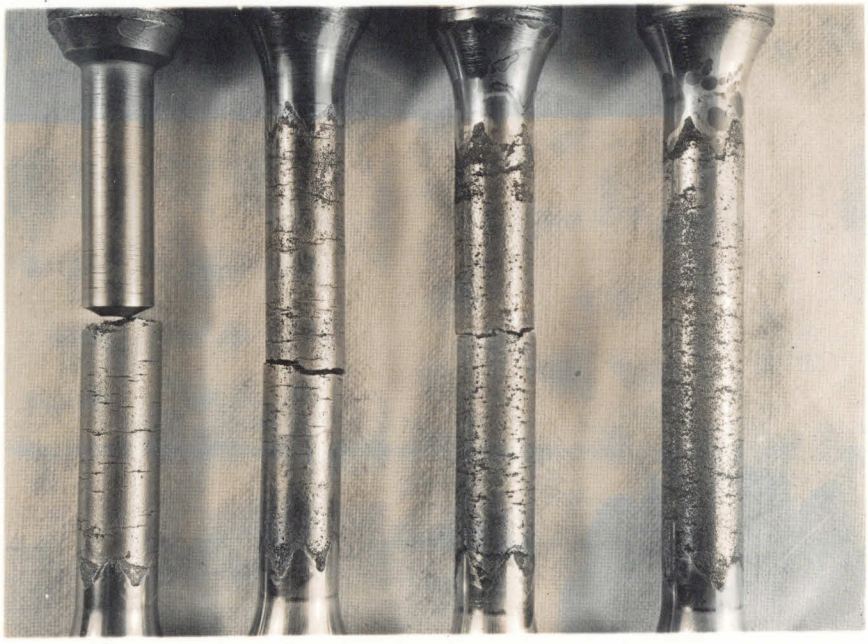

D-5 D-6 D-7 D-8

Fig. 7.

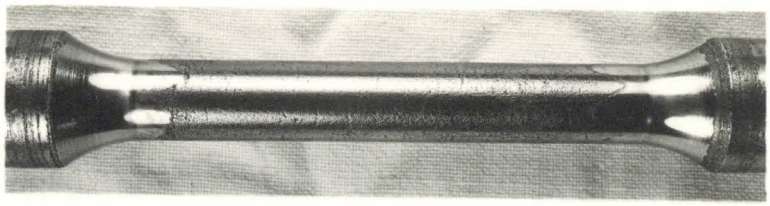

Fig. 8. D-9.

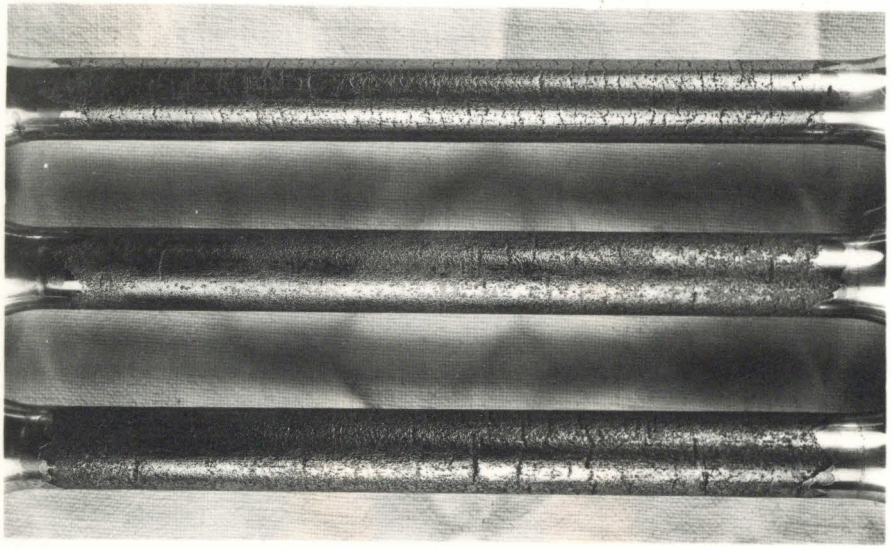

Fig. 9.

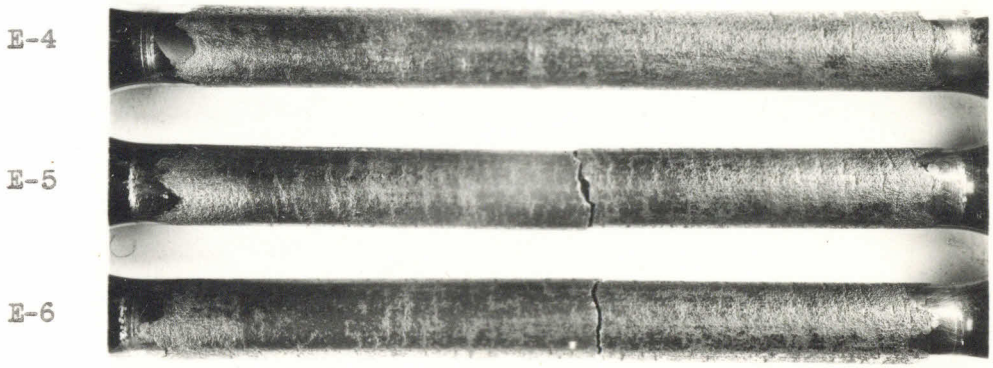

Fig. 10.

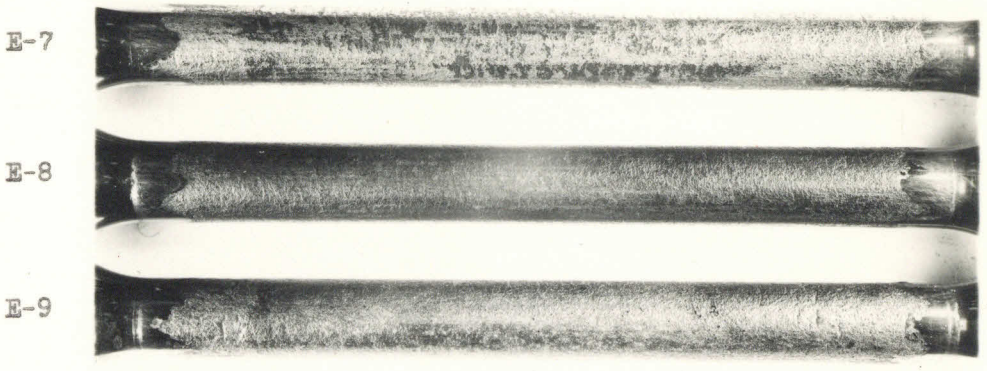

Fig. 11.

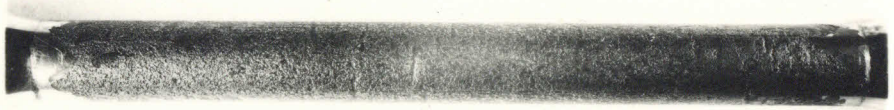

Fig. 12. E-10.

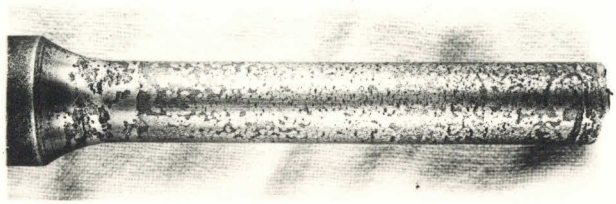

Fig. 13. C-11.

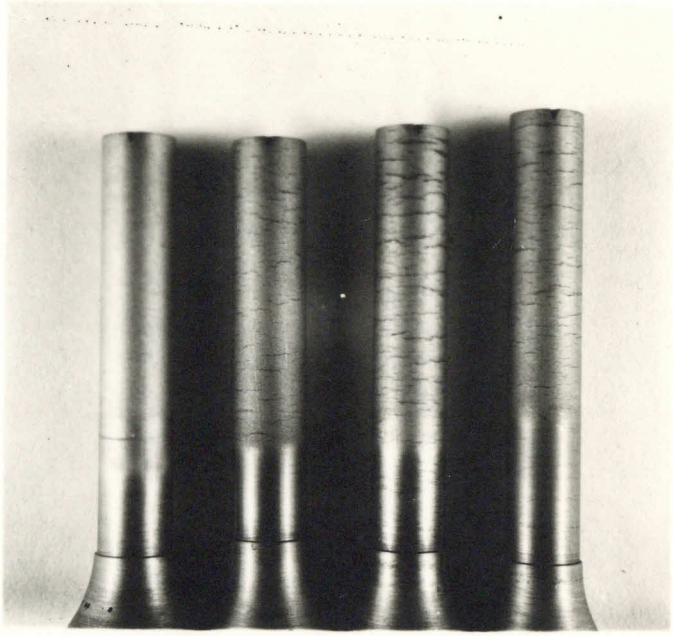

E-8 E-7 E-5 E-6

Fig. 14. Damaged Specimens Cut to a Radial Depth of 7% and Etched to Show Cracks. (Time of Damage at 12.5 kpsi Increases, Left to Right.)

E-5
Right Half

E-6
Right Half

E-5
Left Half

E-6
Left Half

Fig. 15. End Views of Corrosion Fatigue Fractures.

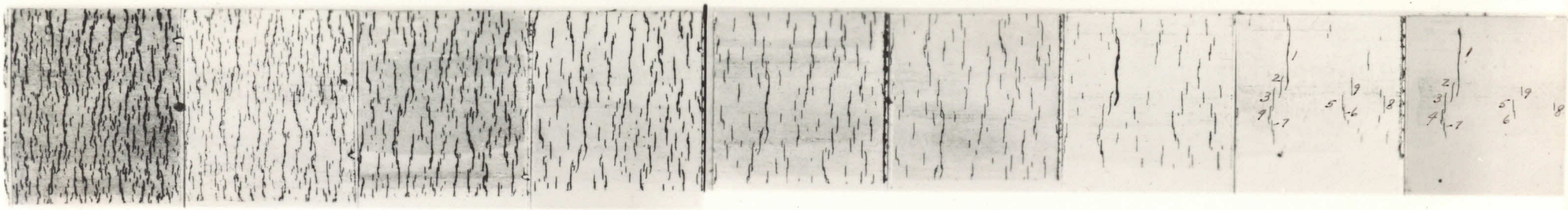

E-5-n(6.9%) o(8.5%) p(10.9%) q(14.1%) r(18.3%) s(20.7%) u(25.9%) w(33.6%) y(40.9%)

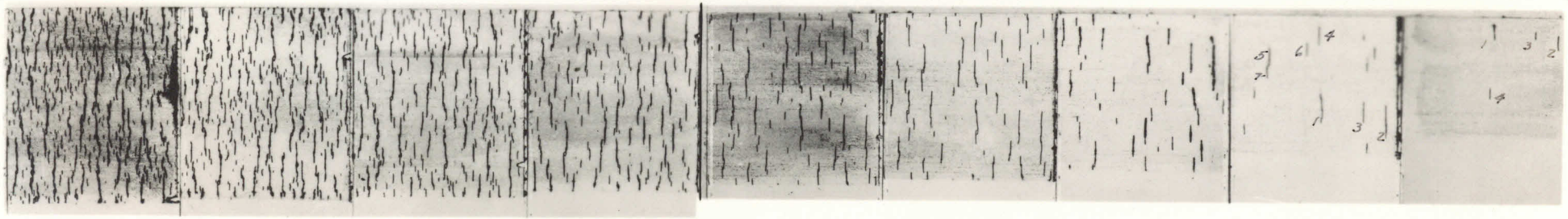

E-6-n(7.3%) o(9.3%) p(11.5%) q(14.7%) r(18.9%) s(21.3%) u(26.7%) w(34.7%) y(41.5%)

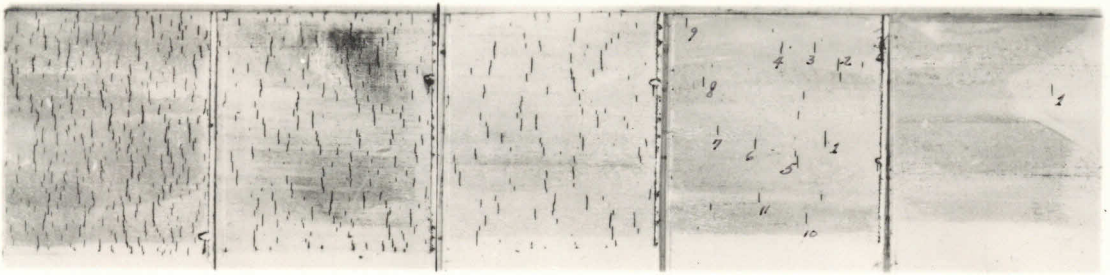

E-7-n(7.1%) o(9.3%) p(11.1%) q(14.5%) r(18.5%)

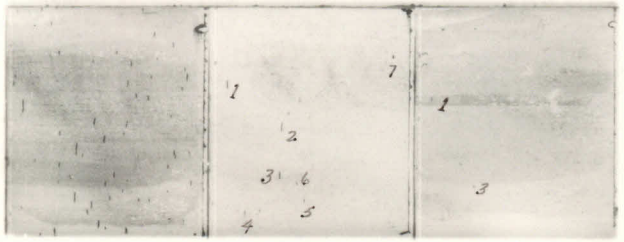

E-8-n(7.1%) o(9.0%) p(11.5%)

Spec.	Stress	Time	Print Mag.
E-5	12.67	91.8	1.47 X
E-6	12.46	98.2	1.41 X
E-7	12.55	77.0	1.45 X
E-8	12.53	65.0	1.34 X

Fig. 16. Sulfur Prints of Crack Patterns at Increasing Depths in Specimens E-5, 6, 7, and 8. (Numbers in parentheses are depths as percentage of radius.)

3.3 Analysis of the Sulfur Prints

After completion of the printing operations, a series of sulfur prints made at successive radial depths on a given specimen were photographically enlarged for study, (Figure 33, page 51). It can be seen that the individual cracks make traces on the prints which are easily recognized and followed through the entire series. The five to ten deepest cracks in each half-specimen were selected for study and numbered as shown in Figure 33. The circumferential arc-lengths were then measured. This provided the data necessary for plotting the crack profiles.

Analysis of the sulfur prints is further described in Appendix 3.3.

3.4 Axial Sections

Axial sections were made of specimens E-6 and 8. Halves of the damaged specimens were cleaned, copper-plated, and cut approximately on axial planes. The sections were mounted in bakelite, polished, etched and photomicrographs were made at 100 and 500X (Figures 20-23, page 31). The preparation of these sections is further described in Appendix 3.4.

4. RESULTS AND CONCLUSIONS

4.1 Experimental Scatter and the Distribution of Fatigue Cracks

Experimental scatter, as measured by extraordinary crack growth and early or late failure was found to be correlated with the distribution of fatigue cracks on the specimen surface. Even distributions tended to retard crack growth by minimizing interaction and joining and, conversely, uneven distributions led to high local crack populations which promoted crack growth through interaction and joining. For example, specimen D-2 developed a very even, shallow crack distribution and enjoyed a correspondingly long life. Specimens D-5 and D-6 failed very early as a result of deep crack growth concentrated in band-like areas around the specimens.

Fatigue cracks are known to grow from corrosion pits and thus, other things being equal, the extent and distribution of corrosion pitting largely determines the number and distribution of the cracks formed. Most of the experimental scatter encountered was therefore probably not due to differences in materials or controllable test conditions (Sec. 4.3), but to the erratic behavior of the stress-corrosion process. In a late (1940) paper, (Ref. 2, p. 701), McAdam pointed out the unpredictable nature of corrosion pitting:

> "The evidence indicates that stress-corrosion pits in steel corroded in fresh water are merely modifications of pits formed by stressless corrosion. The number of pits per unit area and their distribution, consequently, are determined by the same uncontrollable variables that determine the number and distribution of pits formed

by stressless corrosion. Great differences may be found in the number and distribution of these anodic regions after apparently identical corrosion conditions. The size of the pits, moreover, generally varies inversely with the number."

The author encountered similar difficulties, particularly at the lower stresses where corrosion was relatively more important in the damaging process (see Section 4.3).

The erratic behavior of stress-corrosion evidently tends to complicate corrosion fatigue tests by causing scatter. It does not appear, however, that this difficulty can be avoided by even the most careful laboratory control. Large amounts of experimental scatter are, from the practical standpoint, a natural characteristic of corrosion fatigue tests. Special studies should be made to determine the laws, if any, which govern the magnitude and frequency of scatter.

4.2 The Crack Profiles

The crack profiles were drawn as described in Appendix 3.3. The profiles, to the writer's knowledge, are the first ever made for fatigue specimens. Note that these are half-profiles drawn assuming that the cracks are symmetrical about radial lines. Actually, the shapes are somewhat dependent on the direction of rotation of the specimen. The symmetry assumption should not appreciably affect the crack depth indicated.

The profile shapes near the surface are not known. This region is hopelessly complicated by a network of pits and cracks. Some cracks were separated at the bottom and joined at the top. These were treated as separated in drawing the profiles. Two branches are shown on crack E-7-(m)-1

(Appendix 7) to show how it joined with another crack and increased in width near the surface.

The shapes of the cracks at large depths were considered as more important, since growth occurs in that direction. The profiles are very accurate from the half to full-depth levels, except for the symmetry assumptions.

The cracks studied were selected for their great depth. The widths vary widely, depending on the amount of joining which took place. Many cracks were "undercut"; i.e., had arcs which subtended larger angles at greater depths. This undercutting was probably made possible by the stress relief in the heavily pitted and cracked material near the surface. The existence of undercutting was verified under the microscope in the axial section of specimen E-6.

4.3 Rates of Crack Growth or Penetration

The sulfur print method is obviously a destructive type of test. It is not possible, by use of this method, to measure the rate of crack growth in a single specimen. It is necessary to compare the cracks in a number of specimens which have been tested under apparently identical conditions for different lengths of time. The accuracy of such tests evidently depends on the consistency of response of the several specimens to the damaging influences.

The small number of specimens tested and the experimental scatter encountered made accurate determination of the rate curves impossible, but at least the trends have been indicated.

Curves of maximum crack depth versus time were drawn for four stresses (15.5, 12.5, 10.1, and 7.8 kpsi), as shown in Figure 17a, b, c and d, pages 23-26. The crack depths corresponding to a number of the deeper cracks

(approximately 10 per inch of working length studied) were measured directly from the crack profiles.

Consider the 15.5 kpsi graph (Figure 17a, page 23). The top line was drawn through the points of maximum crack depth for specimens C-11, D-8, and E-3. The maximum crack depths for D-9 and D-1 lie a little below the line. Specimen D-7 was retarded in crack growth quite considerably. This specimen failed, however, and must have contained one very deep crack which, of course, could not be studied.

The top line was taken as the curve representing maximum crack depth versus time. The lower curve was drawn to show the range of depths covered by the first six or so cracks studied. Notice that the distance between the curves increases with time. This indicates that the cracking process becomes increasingly unpredictable with time and large crack depths. Note that if the maximum points for the D-8 and E-3 specimens were neglected, a smooth curve could be drawn which would go through the D-9 and D-1 maximum points. In such cases the investigator should let his conscience be his guide.

In the 12.5 kpsi graph (Figure 17b, page 24), specimens E-5 and 6 are inconsistent. This can also be seen in Figure 14, page 19, and in the crack prints, Figure 16, page 15. Joining explains the extraordinary damage in the E-5 specimen. Both E-5 and E-6 failed. The early failure of E-5 is not surprising in view of the deep cracks that developed.

The specimens on the 10.0 kpsi graph (Figure 17c, page 25) are very consistent in behavior, except for E-4. Many of the important cracks in E-4 had neighbors which probably helped their growth; otherwise the E-4 crack patterns were quite normal. The upper curve was drawn in below the

E-4 points on the strength of the data given by the other specimens.

The data for the lowest stress, 7.8 kpsi (Figure 17d, page 26) are rather confusing. Specimens E-10, E-9, and D-6 are quite consistent, except that the E-10 distribution appears high. D-5, as has been discussed in Section 4.1, was extraordinarily damaged due to localized corrosion and subsequent joining of the cracks. Its early failure is not surprising. The D-5 points all fall above the maximum crack depth curve used (Line "A"). Line "B" marks the lowest depths of the cracks studied. Line "C" was drawn on the basis of the E-9 and D-6 data and Line "D" through the maximum depth found in specimen D-5.

In regard to the inconsistencies discussed above, it should be noted that they cannot be correlated with specimen design (as indicated by the specimen prefix letter C, D, or E (Appendix 2.2)). Similarly, these inconsistencies cannot be correlated with the order in which the tests were run: C-11, D-1, 2, 3 .....9, E-1, 2, 3 .....10.

The curves of maximum crack depth, chosen as described above, for four stresses are collected in Figure 18, page 27. All point symbols have shapes characteristic of the stress at which the corresponding specimens were run. Points are labeled with the specimen numbers and also the letter identifying the half of the specimen studied when both halves were analysed. The dotted line on the 12.5 kpsi curve (Figure 17b, page 24) goes through the maximum crack depth for specimen E-5. Specimen E-5 has undergone extraordinary damage as can be seen by comparison with the curves for the other stresses.

All the curves are drawn dotted near the origin, since in this region cracking had not as yet started. The curves for the lower three stresses

are very similar near the origin, indicating that the early part of the damaging process at these stresses is nearly independent of the load. The 15.5 kpsi curve climbs sharply upward, showing that, at this higher load, the interaction of corrosion and cyclic stress starts very early. The rate of crack growth, as measured by depth, becomes extremely large near failure, particularly for the higher stresses.

Specimen D-2, of which the maximum crack depth is indicated by the circle, was the only specimen run at 12.0 kpsi. D-2 failed very late and showed a very even, shallow crack distribution.

The rate curves given in Figure 18, page 27, were drawn neglecting the data from specimens E-5 at 12.5 kpsi, E-4 at 10.1 kpsi, and D-5 at 7.8 kpsi, on the strength of apparent inconsistencies in behavior by comparison with the other specimens tested. These three specimens all gave crack depths greater than those indicated by the "maximum" crack depth lines. These inconsistencies should be kept in mind when the data are interpreted.

4.4 Lines of Constant Maximum Crack Depths on the S-N Curve Sheet

Lines of equal maximum crack depths were drawn on the standard S-N curve sheet by the use of Figure 18, page 27. This was done by plotting the combinations of stress and time resulting in a given maximum crack depth as lines, as shown in Figure 19, page 29. Maximum crack depth lines of over 80% were not determined accurately enough for plotting.

It is interesting to note the position of these lines relative to the S-N curve. There is evidently no simple relationship between maximum crack depth and failure for all stresses.

In the lower stress ranges, the early rates of crack growth are almost independent of the loads, as was mentioned in Section 4.3. There is a

SUBJ. ME 140

BY R.C.B.

CALIFORNIA INSTITUTE OF TECHNOLOGY
DEPARTMENT OF MECHANICAL ENGINEERING

PG. 23 OF ... PGS.

DATE 3-23-43

NO 15.5 Kpsi.

Crack Depth vs. Time

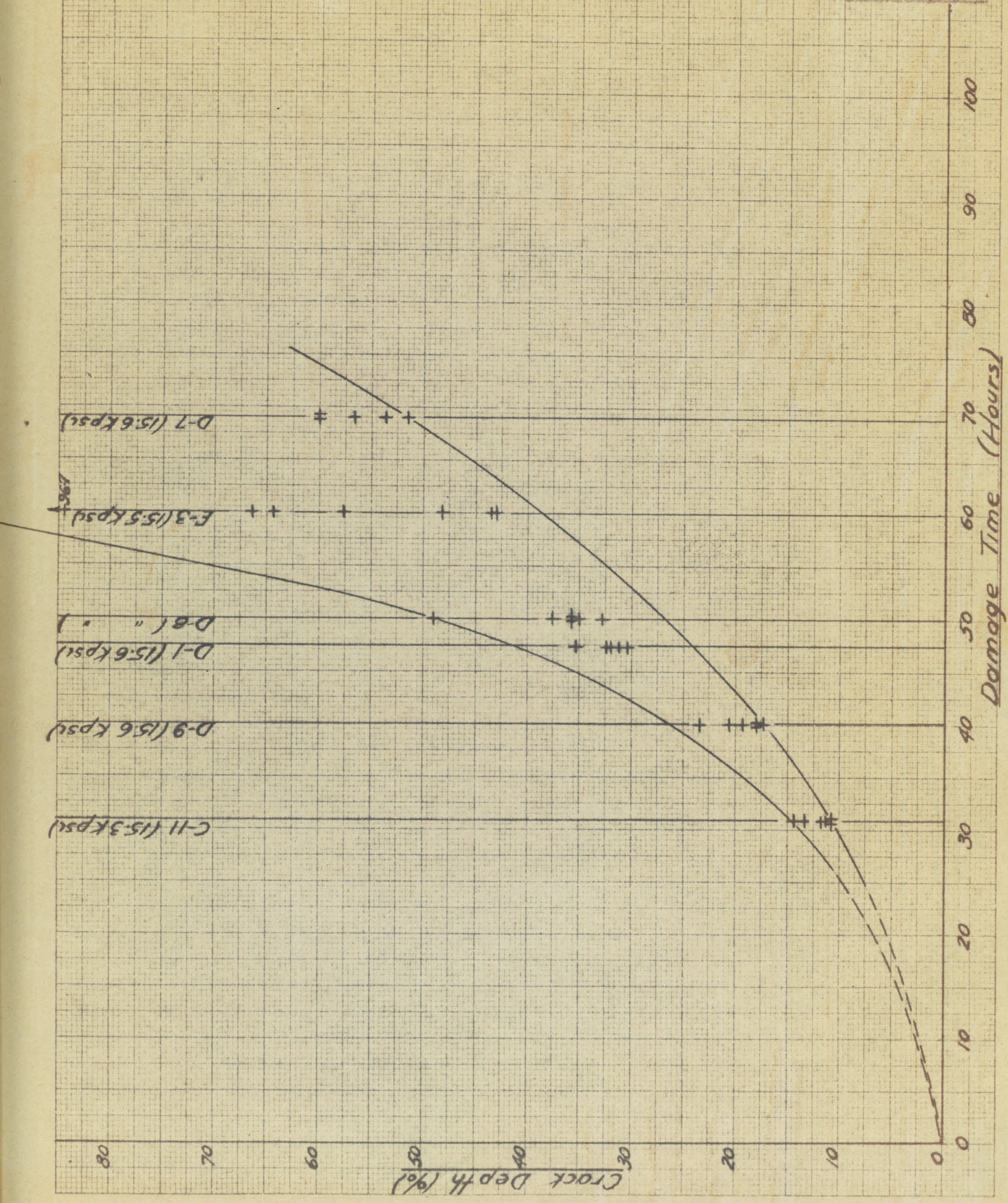

Fig 17a

SUBJ ME 140

BY RCB

APR

CALIFORNIA INSTITUTE OF TECHNOLOGY
DEPARTMENT OF MECHANICAL ENGINEERING

PG. OF. PGS.

DATE 3-23-43

NO. 12.5 Kpsi

Crack Depth vs Time

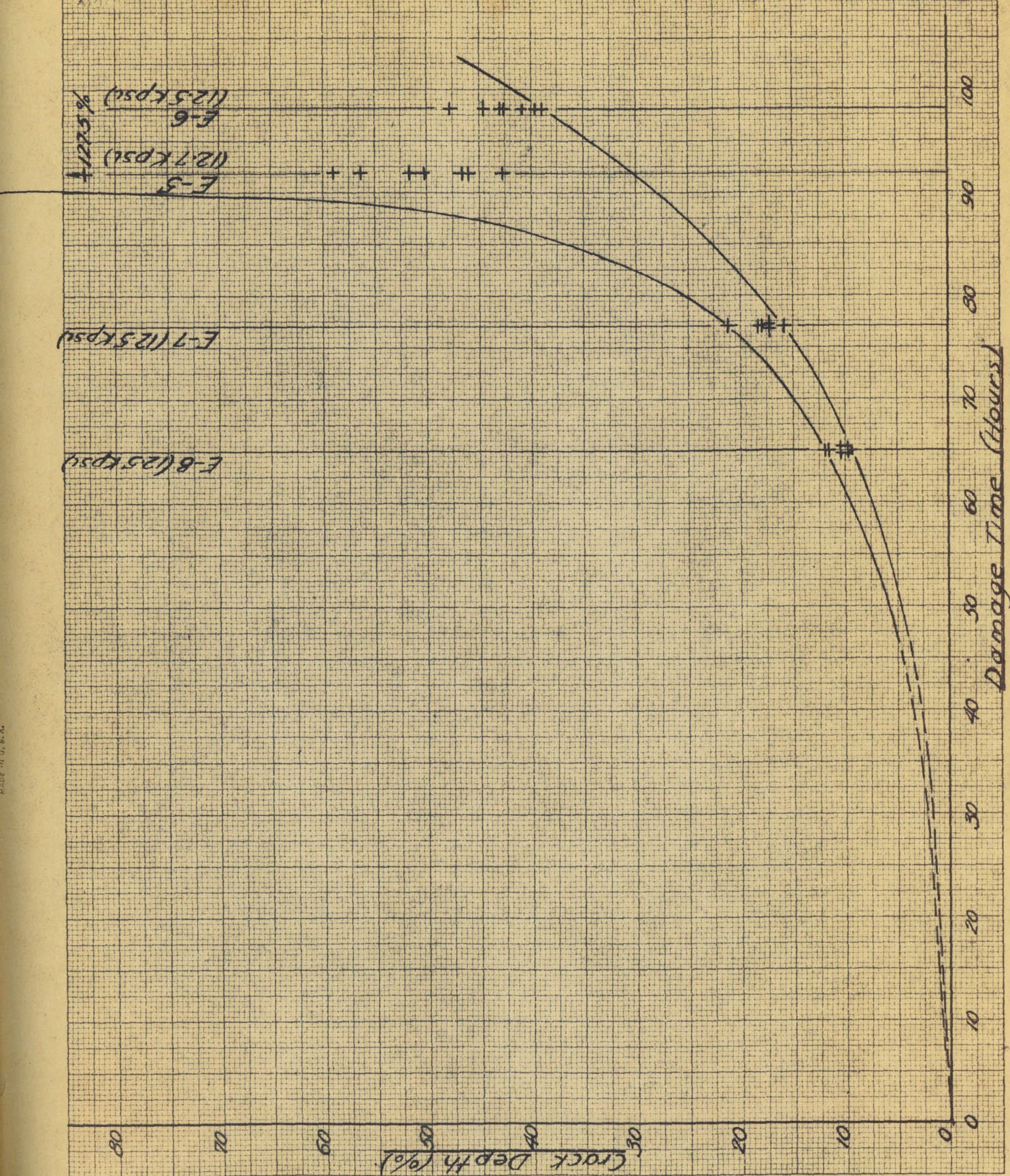

Fig. 17b

Crack Depth vs. Time

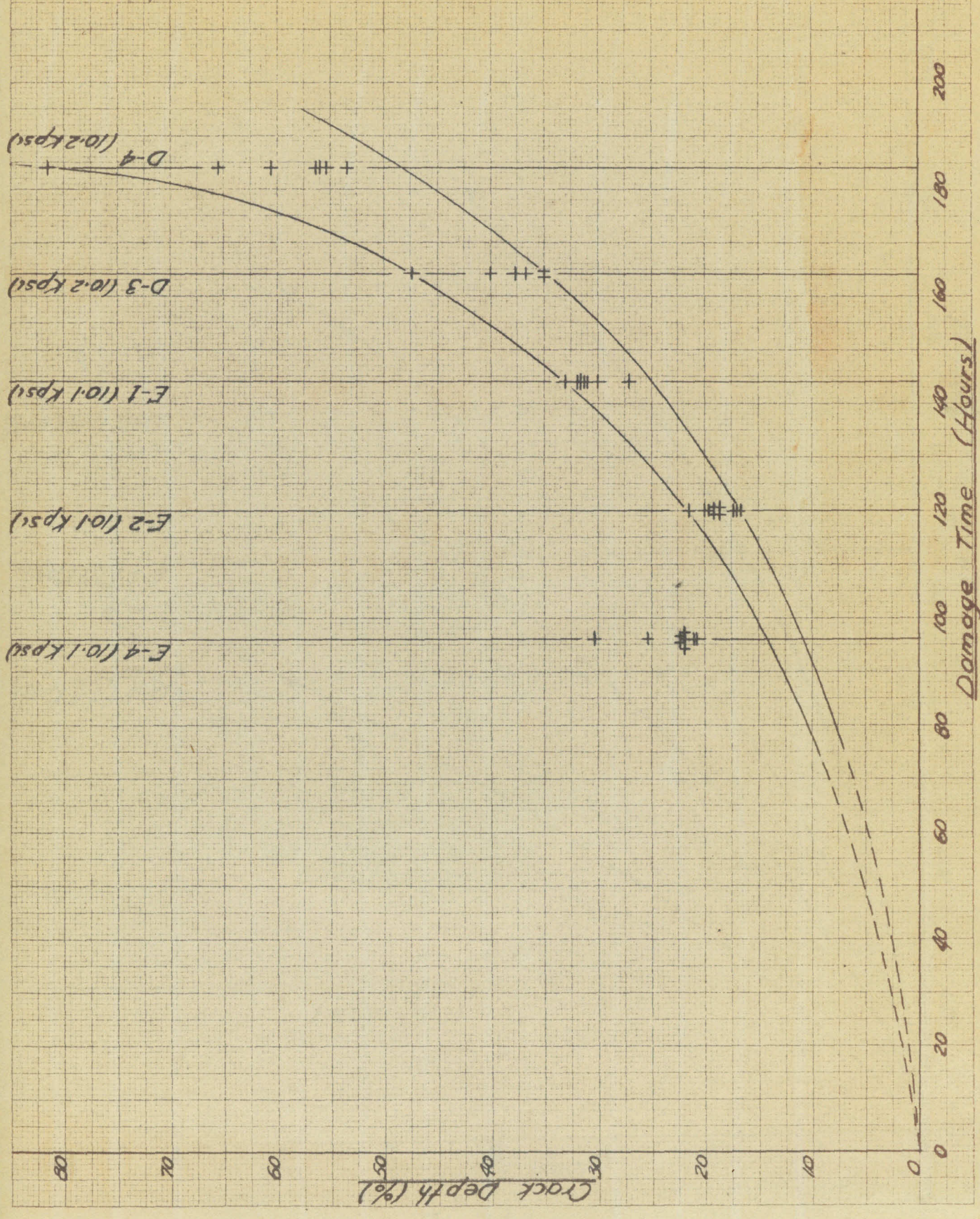

Fig 17c

S.U.I. ME 140

BY R.C.B.

APP

CALIFORNIA INSTITUTE OF TECHNOLOGY
DEPARTMENT OF MECHANICAL ENGINEERING

PG. 26 OF ___ PGS.

DATE 3-23-43

NO. 7.8 Kpsi

Crack Depth vs. Time

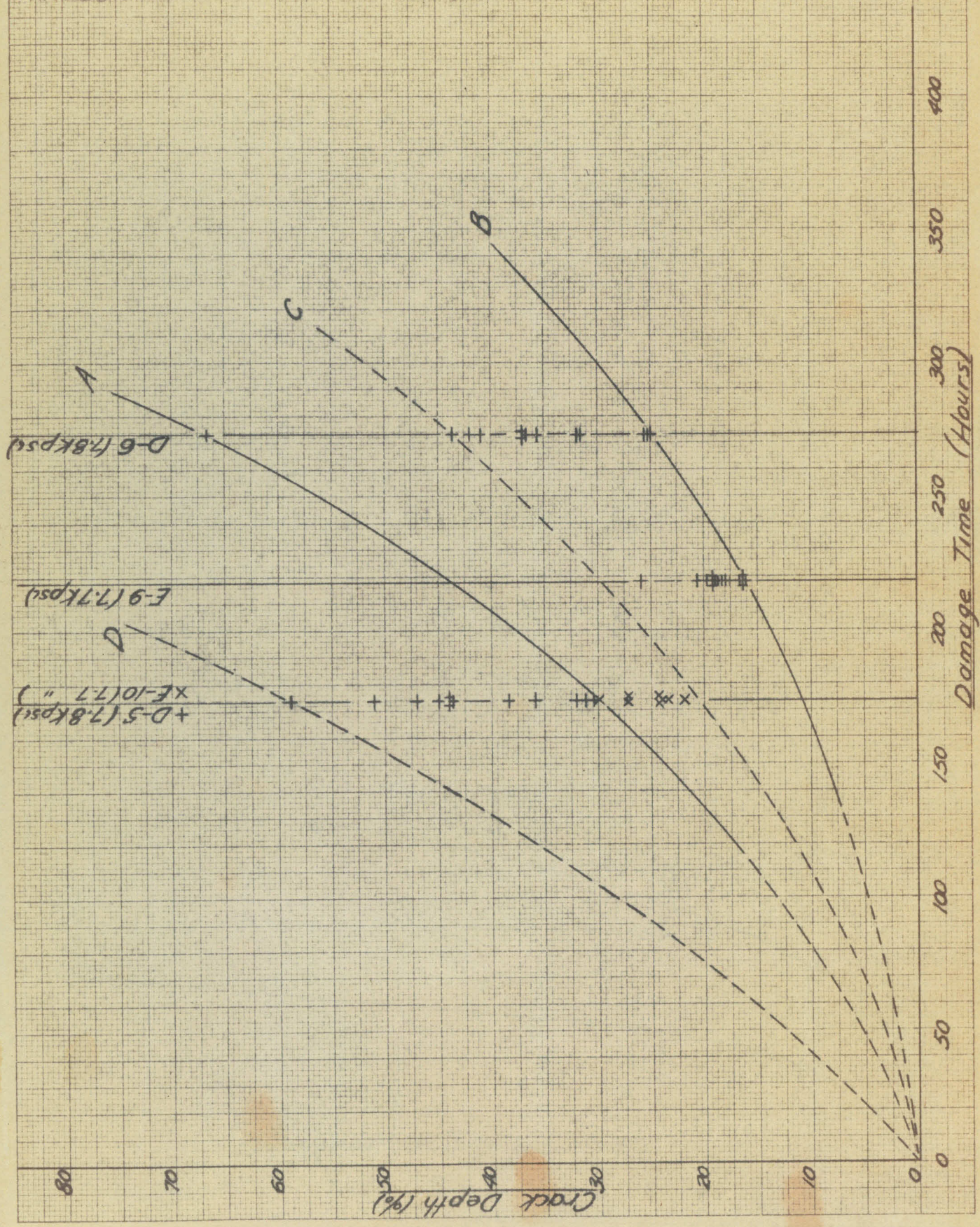

Fig 17d

SUBJ. ME 140

BY R.C.B.

APP.

CALIFORNIA INSTITUTE OF TECHNOLOGY
DEPARTMENT OF MECHANICAL ENGINEERING

PG. 27 OF PGS.

DATE 3-23-43

NO.

Maximum Crack Depth vs. Time

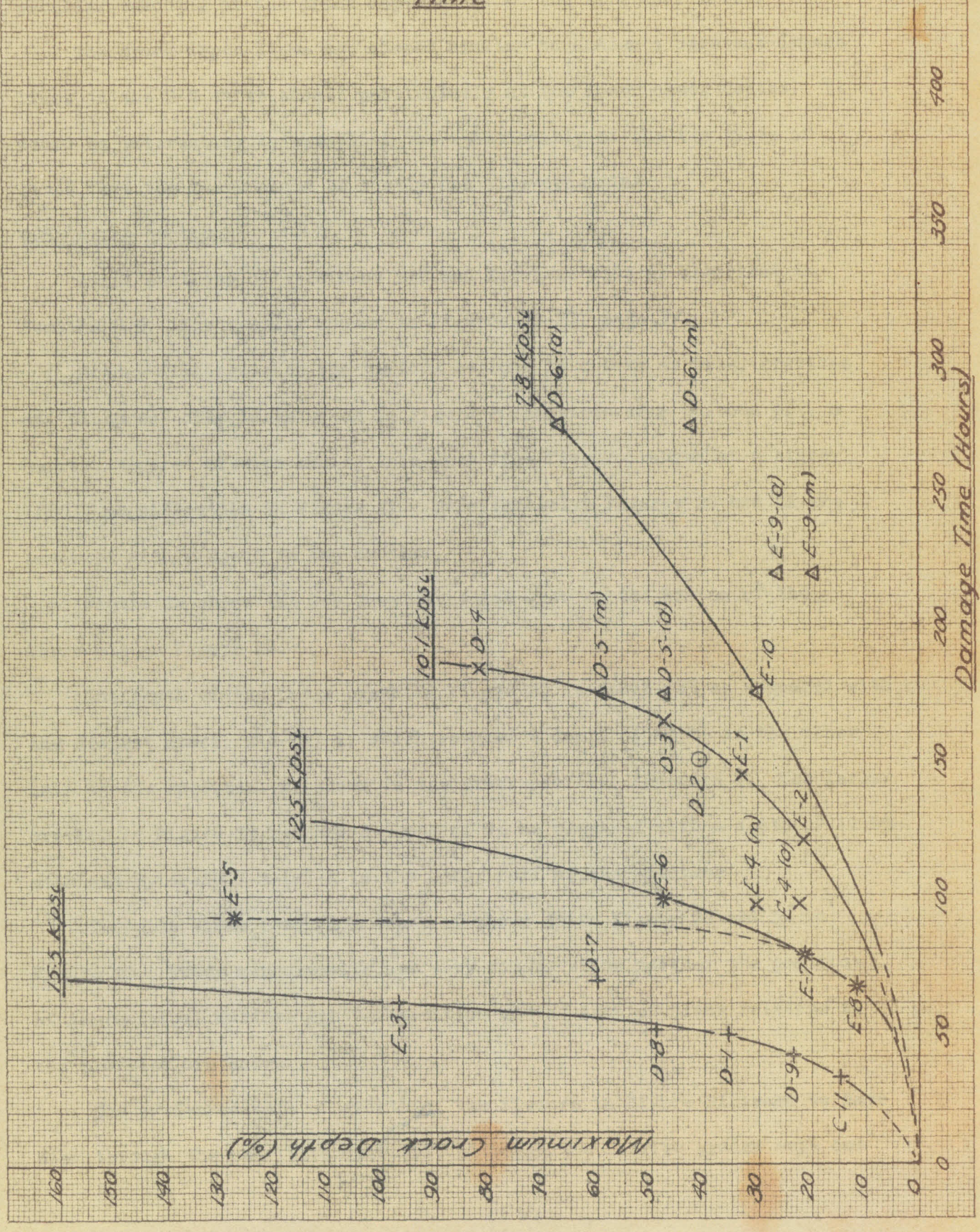

Fig 18

peculiar bunching of the crack depth lines at the 12.5 kpsi level.

The crack depth lines are shaped similar to McAdam's constant-damage lines on the S-N curve sheet, particularly at the lower crack depths. It would be interesting to establish the relationship of the two types of lines, but the tests would be costly and time-consuming.

4.5 Axial Sections

Axial sections of specimens E-6 and E-8 were made as described in Section 3.4. The results appear in Figures 20-23, page 31.

McAdam distinguishes the various regions in cracks as pits, crevices, and fissures. The large crack in Figure 20 consists of a bulbous pit, a narrow, tapered crevice ending in a very fine fissure, shown at a higher (500X) magnification in Figure 21. Unfortunately, Figures 20 and 21 are inverted with respect to one another.

Figure 22 shows the two crevices which grew at the bottom of the large pit in Figure 23.

The depth of the large crack in Figure 20 is about 23% as compared with the deepest crack, E-6-(m)-1, which reached a depth of 47.8% in the other half of the specimen, as shown in the crack profile, Appendix 7. The larger crevice in Figure 22 reached a depth of 9% as compared with a depth of 11.9% attained by crack E-8-(m)-1 in the other half of the specimen.

The pits shown reached a depth of about 3% in Figure 20 and 5% in Figure 23. These measurements are very rough, since neither the position of the original surface nor the position of the section plane relative to the profiles are known.

The preferred path of growth of the fissure in Figure 21 seems to have been through the pearlitic material, although the ferrite grains were cut

SUBJ: ME 140

BY: R.C.B.

APR:

CALIFORNIA INSTITUTE OF TECHNOLOGY
DEPARTMENT OF MECHANICAL ENGINEERING

PG. 29 OF ____ PGS.

DATE 3-24-43

NO.

Lines of Constant Maximum Crack Depth (%) with S-N Curve

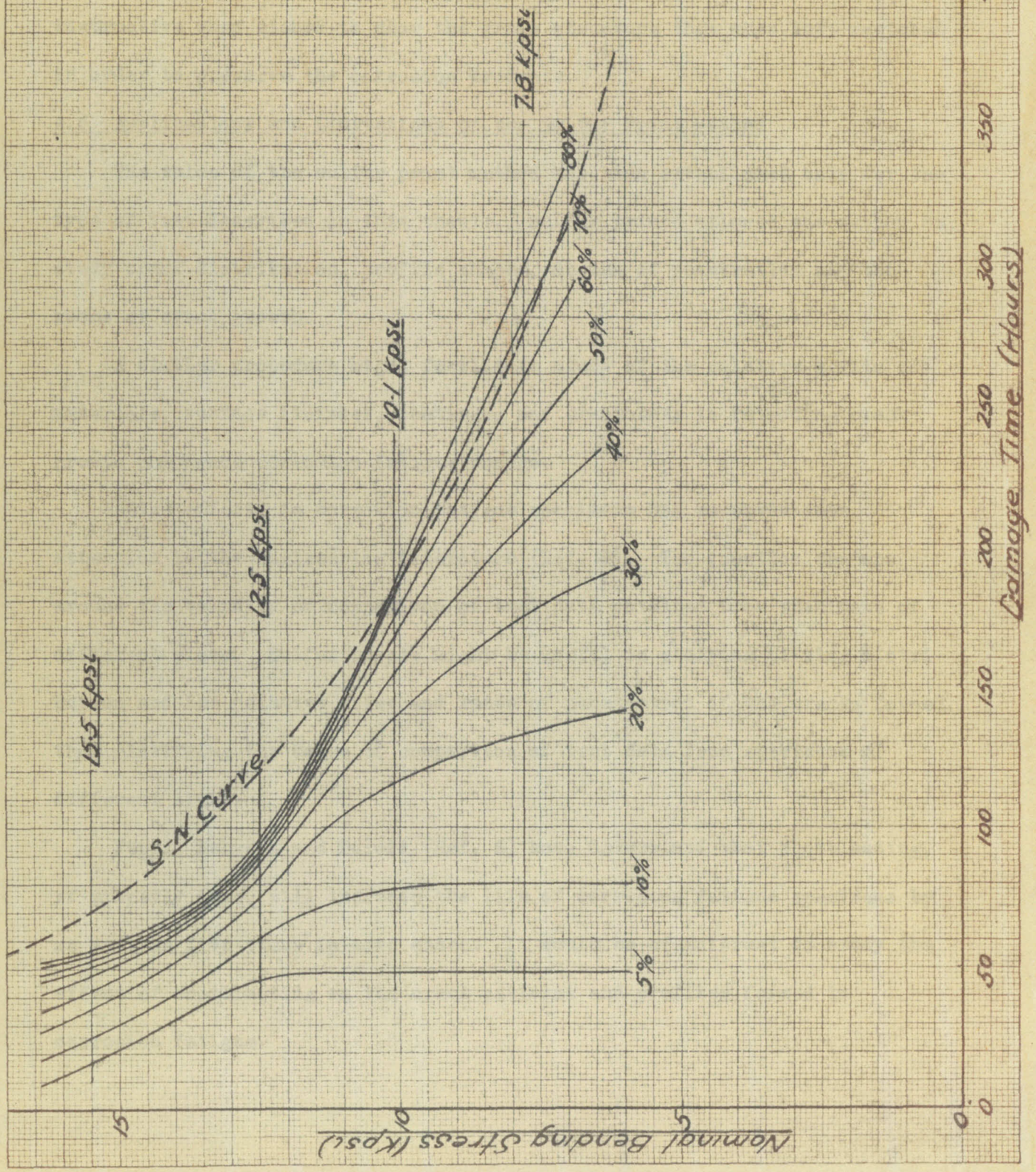

Fig 19

when they could not be detoured. Figure 22 seems to show that in pitting, the pearlite was attacked more readily than the ferrite grains.

The author believes, in general, that axial sections are more instructive when etched to show the grain structure than when left unetched in order to preserve the corrosion products.

4.6 Applications and Limitations of the Sulfur Print Method

The value of the sulfur print method has been established only for the type of test described in this thesis. Sulfur prints allowed the author to study crack distribution, profile shapes, depths of penetration and the rates of crack growth.

A similar procedure might facilitate study of the relative merits of materials, surface finishes, coatings, and treatments in retarding crack growth and hence corrosion fatigue damage.

"Size effect" in corrosion fatigue specimens has received some attention in the engineering literature (Ref. 4). The question centers around the validity of comparison of test data obtained from specimens of different sizes. Sulfur prints might be useful in studying pitting distribution and the relative sizes and rates of penetration of the cracks formed, thus clarifying the bases of comparison of test data from specimens of different sizes.

Föppl, Behrens and Dusold (Ref. 5) have determined that shotblasting, if properly done, will increase the life of corrosion fatigue specimens by as much as five times in some cases. It would be of interest to study the effect of shotblasting on the crack patterns and profiles formed in corrosion fatigue.

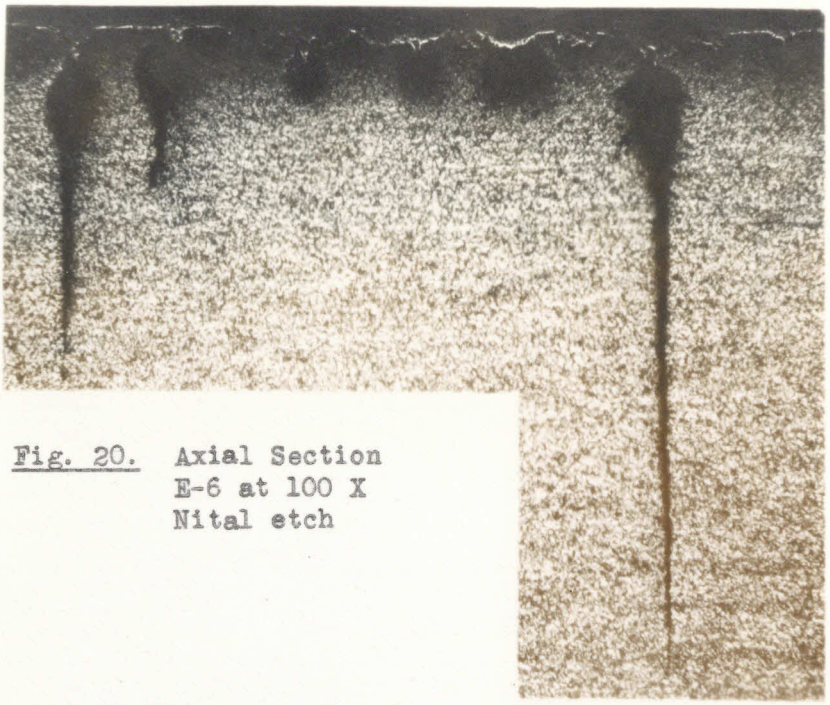

Fig. 20. Axial Section
E-6 at 100 X
Nital etch

Fig. 21. (Right)
Fissure in E-6
at 500 X.

Fig. 22. E-8 at 500 X.

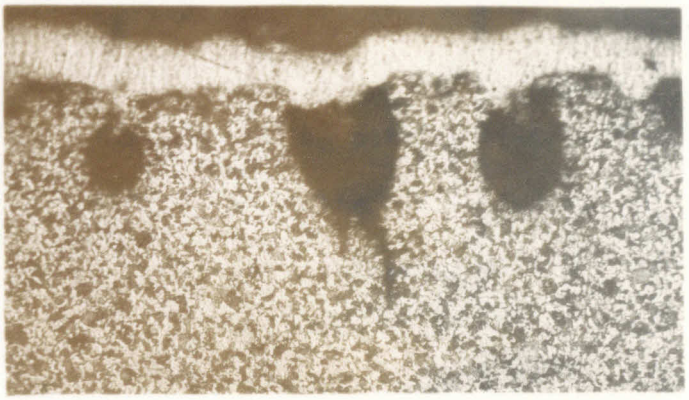

Fig. 23. E-8 at 100 X.

Corrosion inhibiters are known to benefit corrosion fatigue specimens (Ref. 6), but in some cases they promote localized corrosion. These tendencies could be studied to some advantage by the sulfur print method.

The shapes of quenching and grinding cracks could be studied by making sulfur prints of the damaged material at successive depths.

The sulfur print method does not constitute an "accelerated" test procedure. It does not make possible a "short cut" method of locating the S-N curve. It is probably more time-consuming than McAdam's method for evaluating corrosion fatigue damage (Section 2.2).

The destructive nature of the sulfur print method limits its application to laboratory tests.

The sulfur print method cannot be used to study the particular cracks that have caused failure in a specimen, since such cracks are at the ends of the broken halves. These ends are trimmed smooth in the test procedure.

Specimens to be used for making sulfur prints should be at least 0.4 inches in diameter. In the thesis tests, the specimens were 0.3 inches in diameter. It was found difficult to make good sulfur prints on diameters less than 0.2 inches, which corresponds to a depth of only 33% of the radius.

APPENDIX I.

The Fatigue Machine

1.1 The machine used (Figures 25a and b, page 37) was of the rotating beam type operating at 1425 rpm.

1.2 The stresses were induced by the bending moment set up by weights on the loading rack. The bending moment diagram was trapezoidal in form and the specimen was in the region of constant bending moment. As the specimen rotated, it was subjected to sinusoidally varying bending stresses. On an undamaged specimen, the maximum stress amplitude occurred at the surface and is given by S = 1.191 W kpsi (for a .3000 in. diameter specimen), where "W" is the total rack load in pounds. This is the "nominal bending stress" plotted on the S-N curve (Figure 1, page 8). The amplitudes of the local stresses in damaged specimens were not known.

Since there is one stress cycle per revolution of the specimen, the machine speed in rpm is numerically equal to the frequency of stress variation in cycles per minute.

1.3 Counterweights were used to balance the gravity load of the machine parts. The bending stresses were thus practically zero when no weights were on the loading rack.

1.4 The spindles (Figures 24 and 27, pages 34 and 38) were of annealed SAE 1035 steel. They were bored on the inside ends to hold the specimen. The tapers were sufficiently accurate to prevent water from seeping into the spindles. Damaged specimens were pushed out of the spindles with screw-operated push rods which fastened on the back end of the spindles.

1.5 The water gland (Figures 24 and 27, pages 34 and 38) consisted of two bakelite sleeves, each formed by pressing two bakelite tubes together. These

GLAND DESIGN

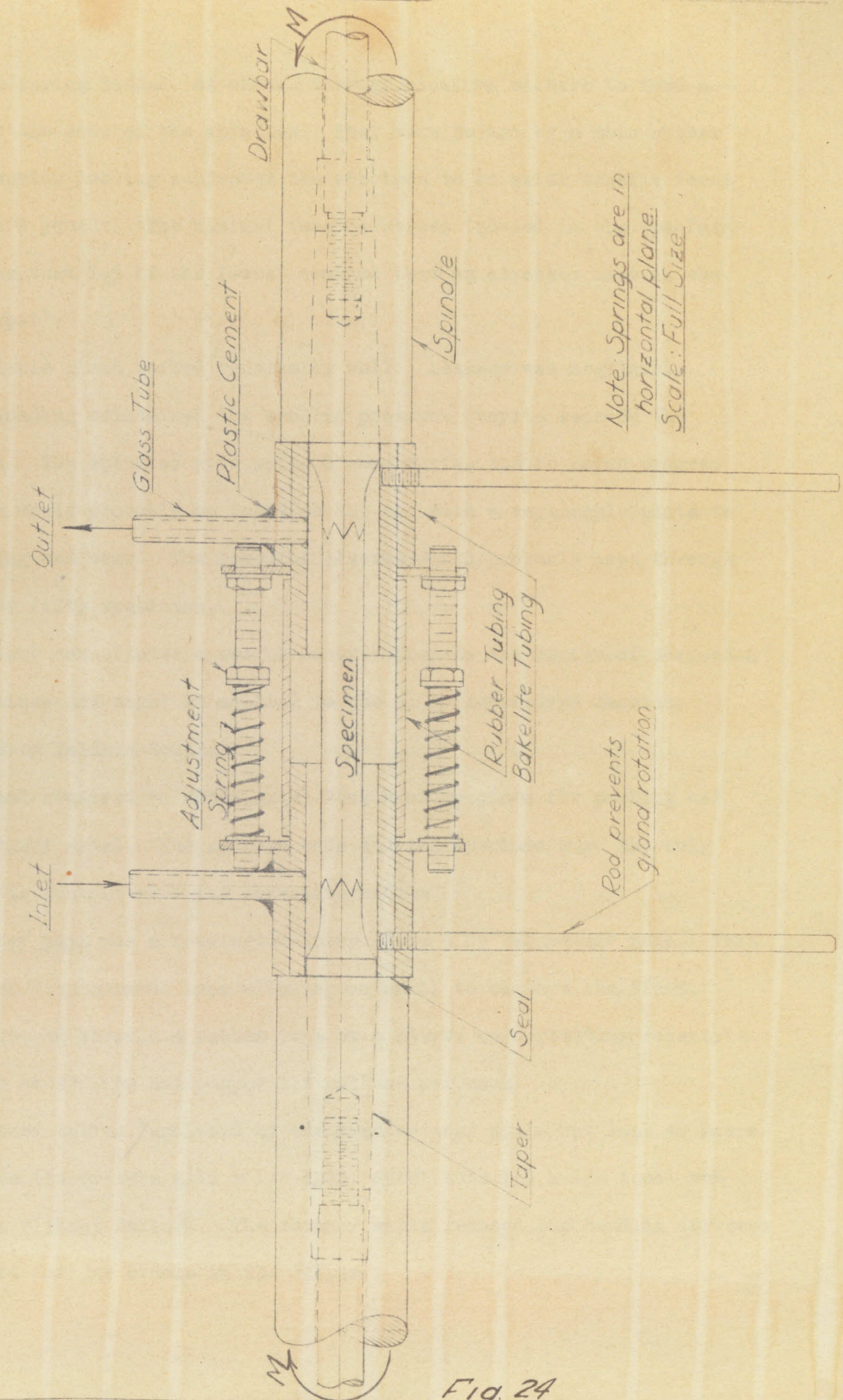

Fig. 24

sleeves were spring loaded, as shown, through aluminum washers to form a seal against the ends of the spindles. They were joined by a thin rubber tube. The spring loading subjected the specimen to an axial tensile force of less than 8 pounds. The nominal tensile stress induced in the specimen was thus less than 1½% of the lowest nominal bending stresses used in the tests (7.8 kpsi).

This simple gland worked remarkably well. Leakage was negligible. The spring loading maintained the sealing pressure despite wear on the spindle ends. The spindles were refaced once during the research program. The spindles could probably be faced on the end with a replacable plate to avoid refacing and wear. The bakelite sleeves would probably last through tests on over fifty specimens.

This gland constitutes a useful contribution to the design of corrosion fatigue machines and might be applied to the R. R. Moore-type machine, manufactured by Baldwin-Southark.

The gland required no extra axial length of specimen for packing and was made without metal. The spindle ends and the specimen were the only metal parts in contact with the corrosive medium.

1.6 The water pump was a Downington-Huber (Size 4 U) "squeegee" pump. This is a positive-displacement type allowing no metal to contact the fluid. Water is squeezed through a rubber tube by a sleeve on a rotating eccentric. The pump ran at 290 rpm and pumped 1.7 gallons per hour.

The rubber tubing furnished by the manufacturer would not last 48 hours. A double tube (inner tube 1/16 x 1/8 inch, outer tube 1/8 x 1/4 inch) ran over 10 days without failure. The thinner walls reduced the bending stresses and prevented fatigue cracks in the rubber.

A gear-type oil pump circulated cool oil through the spindle drums and kept the machine temperature down. The drum journal bearings were not packed off, but oil-leakage was caught and returned to the circuit. The absence of packing friction reduced the heat generated near the specimen and the torque transmitted by the specimen. All oil connections were of soft gum rubber to allow free drum movement as the specimen deflected under load.

1.7 The coupling driving the left spindle was a rubber tube (O.D. = 1, I.D. = 3/4 inch) with a free-length of $1\frac{1}{2}$ inch. It was allowed to run without bending by jacking up the drive-pulley stand to the proper angle and elevation to allow for specimen bending under load. The ends of the coupling were pin-connected (in perpendicular directions) to their respective shafts. Tests made on the turning coupling indicated that it was 52 times as flexible as the "D" series specimen and 32 times as flexible as the "E" series specimens in preventing drum rotation about the horizontal axis and thus probably did not load the specimen except in torsion.

1.8 An automatic shut-off switch was used to stop the machine when the specimen broke. The broken specimen allowed the left drum to move down under the rack load and break the circuit.

1.9 The counter mechanism originally used was much too noisy. A 60 cycle clock was put in the circuit to measure the time of specimen failure. In order to increase the clock period beyond 12 hours, a 50 cycle clock was also put in the circuit and the time gain during the test noted. The period was thus increased to $2\frac{1}{2}$ days.

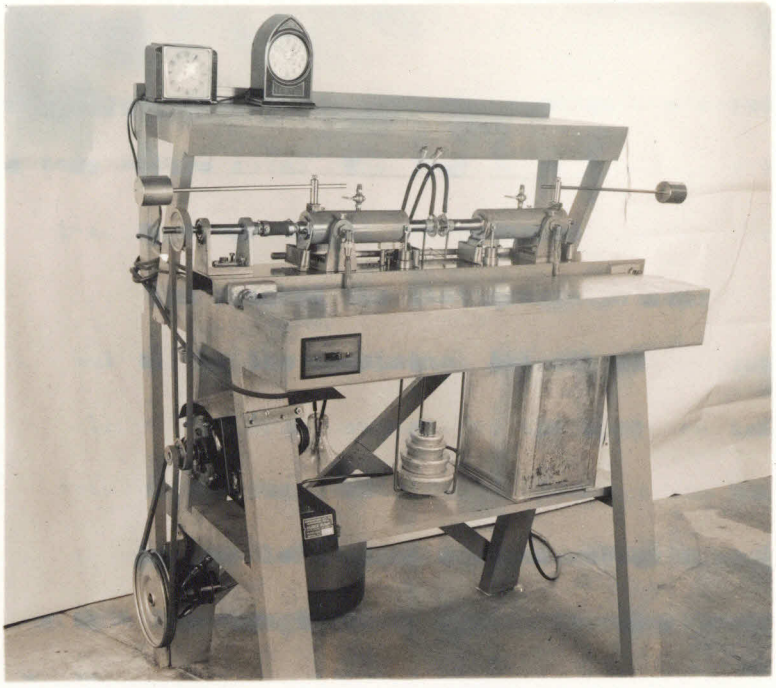

Fig. 25a. Corrosion Fatigue Machine. Front View.

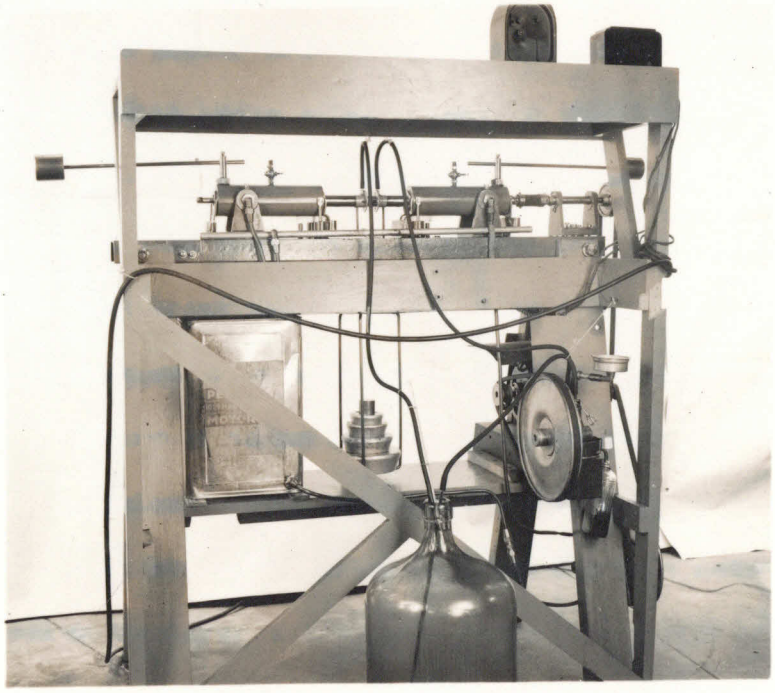

Fig. 25b. Back View.

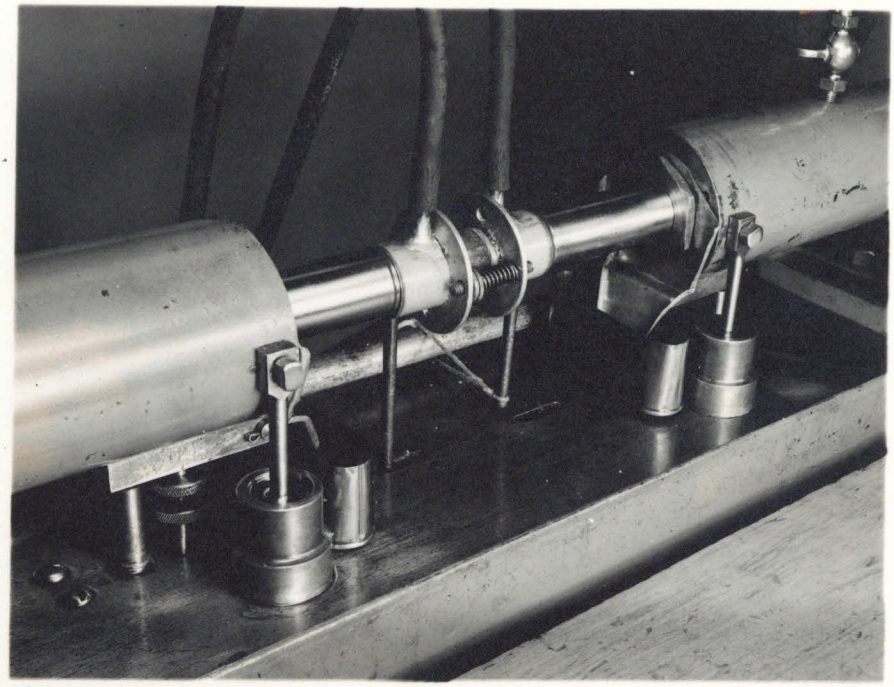

Fig. 26. Fatigue Machine (Center Section).

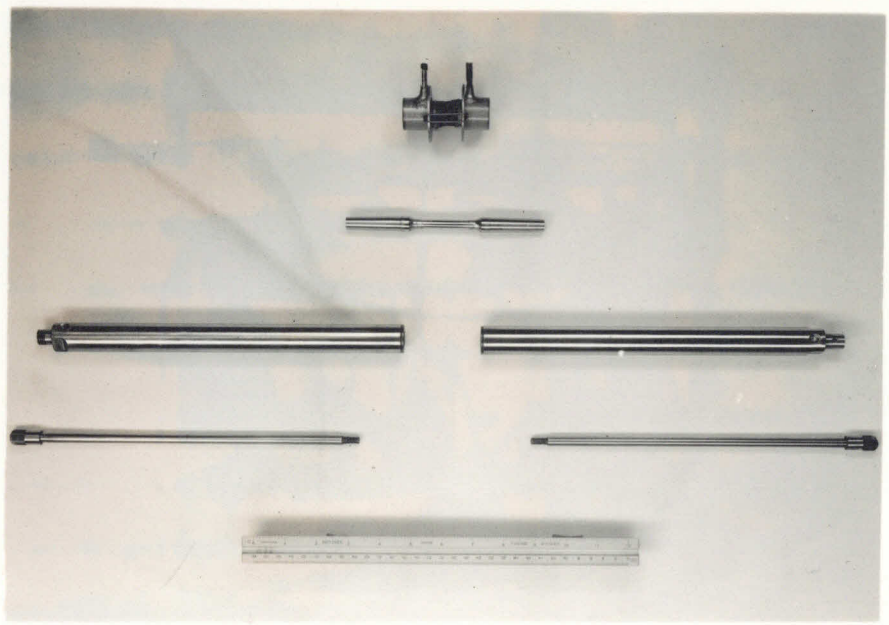

Fig. 27. Gland, D Series Specimen, Sprindles and Drawbars.

APPENDIX 2.

The Specimens

2.1 Material and physical properties.

All the specimens used were made of SAE X4130 of the following composition:

Carbon	.30%	Silicon	.017%
Manganese	.46	Chromium	.92
Phosphorus	.023	Molybdenum	.17
Sulfur	.020	Heat No. 23A	-052

The specimens were cut from 3/4 inch round stock which had been cold drawn, annealed, and then normalized by holding at 1650° F. for one hour and cooling in air. The C, D, and E series materials were normalized separately, but the heat-treatment specifications were the same in all cases.

The microstructure is shown in Figure 28, page 41. Standard tension tests on the normalized steel were not run because of material shortages. The tension test of the virgin specimen A-9 indicated a "drop of the beam" at 119 kpsi and an ultimate strength of 132 kpsi. Figure 5, page 10, shows the specimen and the shape of the fracture. The diameter was .300 inches.

According to the Battelle book (page 101) the endurance limit in air for normalized SAE X4130 is 61 kpsi. The hardness of the material was approximately Rockwell B-89.

Tests run by Dr. D. E. Hudson (Thesis: "Internal Damping in Metals", California Institute of Technology, 1942) indicated that the annealed

steel had a mean specific damping capacity of .0003 at a maximum torsional stress of 900 kpsi. Many steels show specific damping capacities which are six or seven times as great.

2.2 Specimen designs.

Specimens of three different designs were used in the tests; namely, the "C", "D", and "E" series specimens. The design of the "E" series is shown in Figure 29, page 42. The earlier "C" and "D" series designs differed from "E" series design as shown in the table on Figure 29. A photograph of one "D" and one "E" series specimen, taken just before testing is shown in Figure 30, page 43.

The changes in specimen design came as logical developments in the evolution of the test methods.

The differences in design were confined to shoulder and specimen lengths and could not be correlated with experimental scatter, as discussed in Section 4.3.

2.3 The method of surface finish.

The "C" and "D" series specimens were received with a circumferential, fine grind finish and the "E" series with a very smooth machine cut. All specimens were fastened in a lathe and circumferentially polished with No. 400 Aloxite metallography paper until all sub-surface deformations from grinding and cutting were removed. The specimens were then carefully hand finished by rubbing longitudinally with No. 1/o, 2/o, 3/o and 4/o emery papers in succession.

After varnishing the fillets (Appendix 2.4), the finished surface was protected with grease and wrapped in paper. Before testing, the

Fig. 28a. Specimen Steel SAE X 4130 at 500 X, Nital Etch.

Fig. 28b. Specimen Steel SAE X 4130 at 100 X, Nital Etch.

ME 140

42

KCB

2-21-73

W.P. No. W.1110.

CORROSION FATIGUE SPECIMEN

NO. ME 140-5

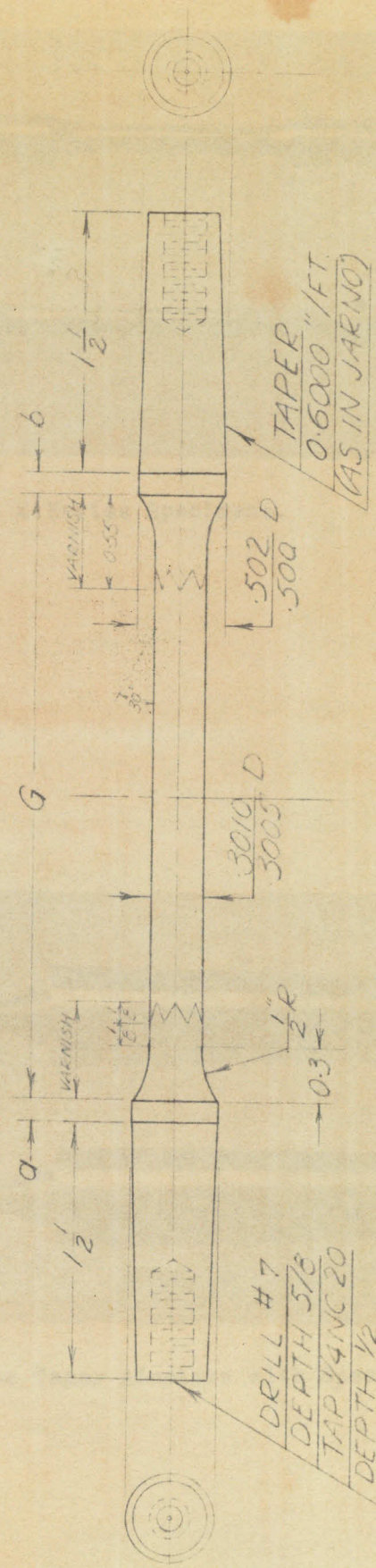

SCALE - ACTUAL SIZE OF "E" SERIES SPECIMENS (1"=1")

SPEC. SERIES	a	b	G
C	13/16	9/16	2 3/8
D	1/8	1/8	2 3/8
E	1/8	1/8	3 1/8

Fig 29

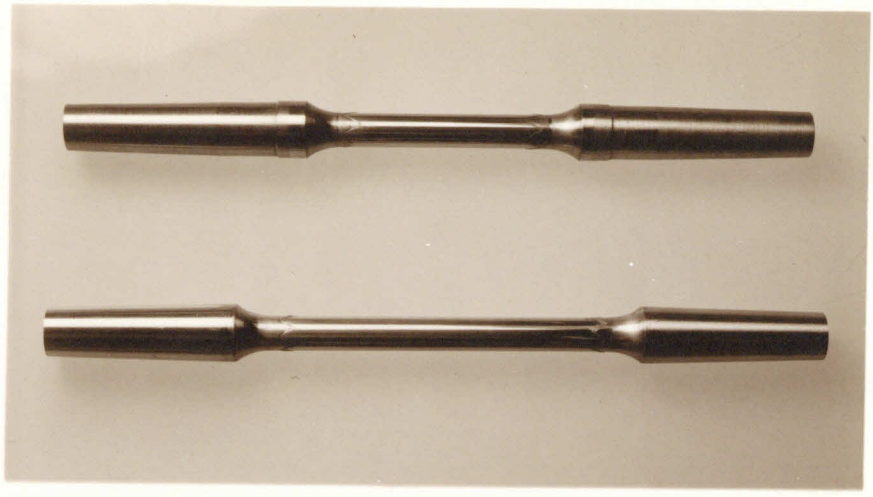

Fig. 30. D and E Series Specimens.

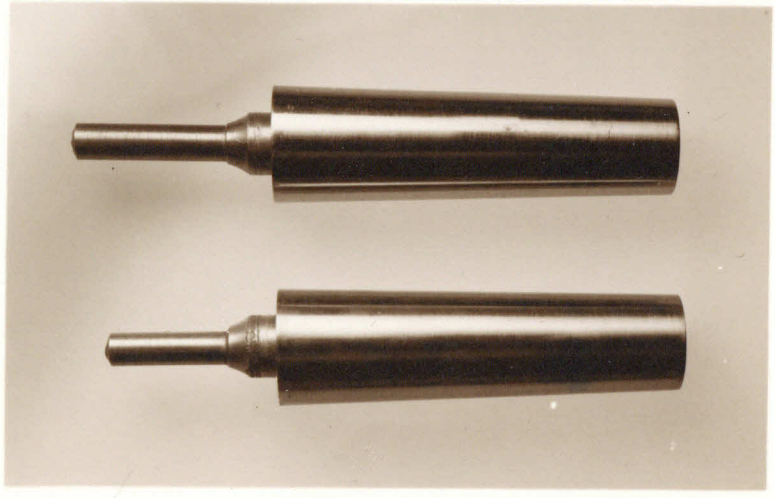

Fig. 31. Lathe Taper Adapters with Specimen Halves.

specimen was carefully washed in benzine (C_6H_6), dried with a clean cloth and then rubbed lightly with 4/o paper on the working section.

2.4 The method of fillet protection.

In this test procedure, it was necessary to use a specimen of uniform diameter. Fillets were therefore necessary. When unprotected, specimens almost invariably failed at the ring of tangency of the fillets and the working surface.

Fillets can be protected by varnish or other coatings. If the coating were ended abruptly on the working surface, a sharp ring of discontinuity in corrosion resistance would be created and early failure would occur at this section.

Professor Clapp suggested that this sharp ring of discontinuity be avoided by serrating or pinking the edge of the varnish coat. Pinked tape was used accordingly to protect the working section and the fillets were varnished as shown in Figures 29 and 30, pages 42 and 43.

The method proved completely successful. Specimen C-11 was not varnished. Only specimen D-1 failed near the fillets. This was due to a poor varnish coat. This method prevented early failure of the specimens and made possible the determination of the S-N curve. Specimens which failed early at the fillets were taken as equivalent to partially damaged specimens stopped early.

APPENDIX 3.

Analysis of the Damaged Specimens

3.1 Cutting of the specimens.

The damaged specimens that had not been broken were cut in two near the middle and at least one-half used for making sulfur prints. The "(m)" half was taken as the longer portion and used for making prints m, n, o, etc., at the cut depths labeled on the profiles (Appendix 6) as m, n, o, etc., respectively. Similarly, the shorter "(a)" half was used for making prints a, b, c, etc. at the depths a, b, c, etc., respectively, as labeled in the profiles, (Appendix 7).

A specimen half was rigidly fastened into the headstock of a Southbend 9 inch lathe by means of a taper adapter (Figure 31, page 43) and drawbar and the end was trimmed smooth. A fine cutting tool was then used to remove the desired amount of damaged metal from the surface. The new cylindrical surface was then made smooth with No. 320 grit emery cloth.

The diameters of specimens cut in this way were measured to ± 0.3 mils with a Brown and Sharpe micrometer. These data were tabulated and the depths of cuts below the polished surfaces of the virgin specimens calculated. Each depth and the sulfur print made at that depth were identified by a lower case letter suffixed to the specimen number. Thus, "D-6-p" identifies a sulfur print made on the "(m)" half of specimen D-6 and at the depth "p".

The specimens were then ready for etching and sulfur printing.

Figures 7, 14, and 31, pages 11, 14, and 43, show specimens which have been cut down. Those in Figure 14 have been etched to open up the cracks.

3.2 The method for making sulfur prints.

Specimens with some of the damaged material removed, as described above, were treated as follows:

a. Washed in alcohol to remove the cutting oil and then dried.

b. Soaked in concentrated (Technical) HCl for 30-40 minutes to open up the cracks smeared over by the cutting tool and the emery cloth.

c. Quickly and singly removed from the HCl, washed in tap water, and dried thoroughly with paper towels. The specimens then appeared as shown in Figure 14, page 14.

d. Left soaking in a water solution of Na_2S (1 part of $Na_2S.9\ H_2O$ + 2 parts distilled water) for 45 minutes, or longer, until the writer was ready to print them one at a time.

e. A specimen was removed from the Na_2S solution, quickly and thoroughly dried. If a clean surface was not obtained, the specimen was dipped back in the solution and then dried again. (The cleanliness of the surface determines the lightness and uniformity of the crack print background. Light, uniform backgrounds are attractive, but they are not essential to prints used for analysing.

f. A small piece of sulfur printing paper (prepared as described below) was then carefully wrapped around the specimen to avoid smearing; overlapped, pressed firmly in place, and removed from the specimen surface. If carefully done, a clear and distinct reproduction of the crack pattern was transferred to the printing paper immediately on contact with the steel. An actual sample of a crack print is shown on the next page.

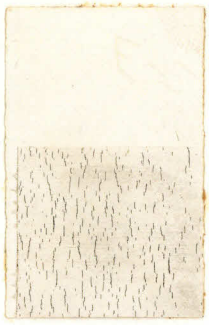

Figure 32. Sample of Sulfur (crack) Print (No.E-2-a)

The sulfur print was then marked for identification, fixed in hypo, washed, ferro-typed, and dried. If the first print was not satisfactory, the specimen was dipped back in the Na_2S, dried, and the process repeated.

After trimming, a number (12 to 20) sulfur prints were mounted on a 3 x 5 inch card and a 5 x 7 inch negative made (Commercial ortho film). From this negative, an 11 x 14 inch enlargement was made for analysing and studying the crack patterns at the total magnification of about 3.5 x (Figure 33, page 51).

The type of paper recommended for making sulfur prints is a No. 4 Azo or Velox, glossy, single weight photographic printing paper.

The printing paper was cut into small rectangles 1 x $1\frac{1}{2}$ inches. These pieces were soaked in tap water for 15 minutes or more to soften up the paper and the gelatin. The soft paper was then "preformed" to help in bending around the small specimen diameters. The preforming was done by rolling the paper in the fingers around a small (1/8 inch diameter) glass rod.

Just before removing the fatigue specimen from the Na_2S for the purpose of printing, one of these pieces of paper was blotted carefully between paper towels to remove all excess surface moisture. This

helped to prevent skidding by giving the printing paper surface a tacky consistency which readily adherred to the dried specimen surface.

Sulfur printing requires a certain amount of skill and care, particularly for the production of prints with light, uniform backgrounds. For analysing, however, such a background is not necessary. The degree of skill required is not different from that necessary to "roll your own" without spilling half of the tobacco.

The following precautions are advisable:

a. In making the sulfur prints, use (for example) the left hand to hold only printing paper and paper towels. Use the right hand to hold the specimen. This was found almost necessary to avoid staining the photographic paper with Na_2S.

b. Guard against lint from paper towels, etc., both on the specimen and the printing paper. Lint from the specimen, in particular, stains the printing paper.

The author found it convenient to work with 5 to 15 specimen halves in a group. Small glass vials ($\frac{1}{2}$ x 2 inches) filled with HCl or Na_2S solution were used to soak the specimens. The vials were held in a wooden rack. Sulfur prints can be made very economically with a fairly large group of specimens.

In the sulfur printing process, corrosion products and iron sulfide probably fill the cracks and help to retain sodium sulfide, which gives an insoluable dark precipitate of silver sulfide in the photo-sensitive gelatin when contact occurs. The resulting sulfur-prints are permanent records of the minute details of the crack pattern.

Figure 16, page 15, shows four series of sulfur prints at approximately 1.5 X. Figure 33, page 51, shows enlarged photographs of six prints as used for analysing.

3.3 The method for analysing sulfur prints.

The enlarged photographs of crack prints, Figure 33, were examined to determine the crack profiles shown in Appendix 7. The method of analysis was as follows:

The deep cracks were taken to be the more important. These were the cracks that remained on the prints made at the greater depths. By examination of the latter prints, a number of the deep cracks were selected for study. These cracks were traced easily and numbered on the prints made at successively lesser depths, as shown in Figure 16, page 15, and Figure 33, page 51.

The lengths of the crack arcs, "a_i" were measured from photographs such as Figure 33. The angle "α_i" subtended by the "i^{th}" crack was calculated as:

$$\alpha_i = \frac{a_i}{M\pi d} \times 360^\circ \quad \text{at a} \quad \text{"\% Depth"} = \frac{d_o - d}{d_o} \times 100\%$$

where:

M = magnification of the photograph used.

d_o = original diameter of the specimen.

d = diameter of the cut specimen on which the particular print was made.

The profiles, (Appendix 7) were drawn using the data, obtained as described above, giving "α_i" vs. "% Depth" for the cracks studied, i = 1, 2, 3, etc.. Note that some of the profiles were drawn to a scale of 50:1,

others at 100:1.

The radial coordinate "% Depth" varies from 0% at the virgin surface to 100% at the center of the specimen. The angular coordinate, the "Total Crack Angle, α_i", is labeled as twice the geometrical angle represented since only the half-profiles are represented.

The crack profiles were drawn under the assumption of symmetry about radial lines. This simplified the measuring process in analysing the crack prints.

The accuracy of the analyses is discussed in Appendix 5.5.

3.4 Axial sections.

The axial sections (Figures 20 to 23, page 31) were made according to the following procedure:

a. The corrosion products were removed from the specimens with fine steel wool.

b. The surfaces were electrolytically plated with copper in a $CuSO_4$ bath.

c. The damaged material was cut approximately on an axial plane and mounted in bakelite.

d. The sections were then wet polished, ending with No. 600 grit, levigated alumina and then magnesium oxide.

e. The sections were etched with 1% Nital, photographed at 500 X, etched again and photographed at 100 X.

Some difficulty was experienced in polishing the specimens because of abrasive carried in the pits which scratched the surfaces during the later polishing operations. The microstructure in Figure 20 is slightly out of focus. This was done to show the crack shape more clearly.

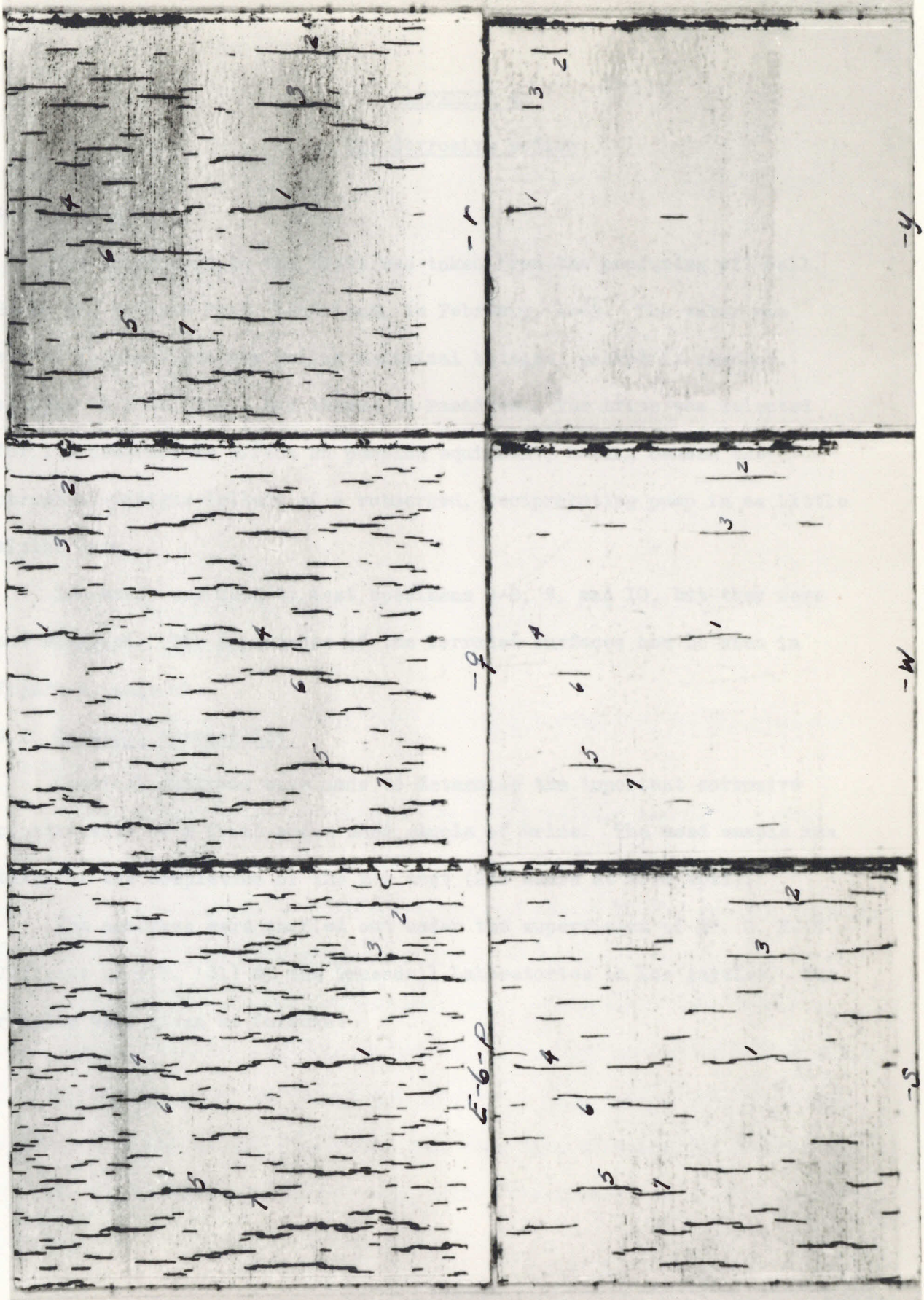

Fig. 33. Enlarged (3.8X) Photographs of Sulfur Prints as Used for Analysing. Prints E-6-p, q, r, s, w, and y.

APPENDIX 4.

The Corrosive Medium

4.1 Source.

The brine used in the tests was taken from the producing oil-well, Rambo #7, Rodessa Pool, Louisiana, in February, 1942. The water was stored in air-tight one gallon medicinal bottles, packed in sawdust, shipped to Kobe, Inc., and thence to Pasadena. The brine was selected for its destructive effect on pumping equipment, having caused the corrosion-fatigue failure of a submerged, reciprocating pump in as little as nine days.

Sea-water was used to test specimens C-8, 9, and 10, but they were not analysed. The appearance of the corroded surfaces can be seen in Figure 4, page 10.

4.2 Chemical composition.

Chemical analyses were made to determine the important corrosive constituents of a fresh and a used sample of brine. The used sample was taken at the completion of the E-9 test (218 hours at 7.73 kpsi).

The analyses were carried out under the supervision of Dr. C. E. T. Jeffreys (C.I.T. '31) at the Truesdail Laboratories in Los Angeles. The results were given as follows:

	Sample	
	Fresh	Used
Total solids	107,400 ppm	105,600 ppm
Loss on ignition	13,800	11,600
pH (glass electrode) at 20° C.	5	4.8
Acidity ±	50	48
Chloride	60,500	61,100
Sulfate	20	92
Nitrate	11.4	8.7
Ferrous Iron	5.2	5.9
Ferric Iron	1.5	1.1

± Acidity Mineral acids + Sulfates of Iron and Aluminum as Calcium Carbonate.

The conclusions, as quoted from the report submitted by the Truesdail Laboratories, were as follows:

"These waters are acid brines which would be expected to be highly corrosive to metals. A small amount of acid in the presence of iron salts can cause corrosion for an indefinite period because of the ease of hydrolysis of iron salts. Also, the presence of metal chlorides such as $MgCl_2$ which are easily hydrolyzed will produce continuous corrosion. Such brines as these usually contain significant amounts of Mg, Ca, and Sr chlorides along with sodium chloride. Nitrates are equally as injurious as the chlorides, and sulfates are somewhat less so. The very high chloride and significant sulfate and nitrate content of these brines along with the acidity easily accounts for their corrosive nature."

It should be noted that there were no important differences in the corrosive constituents of the fresh and the used samples of brine. This indicates that the corrosive media were very constant in composition during the tests.

4.3 Storage and volume used.

The brine used in the tests was kept in air-tight medicinal bottles packed in sawdust until ready for use.

Each specimen test was started with a fresh sample of the brine. The volume used was 1 gal. for each of the "C" and "D" series specimens, and 1-3/4 gal. for the "E" series. This was equivalent to 141 cu.in. per sq. in. of working area for all specimens.

The circulation rate was 1.7 gal. per hour (6.7 cu.in. per minute) in all cases, or 4.0 cu. in. per min. per sq. in. for the "C" and "D" specimens and 2.5 for the "E" series specimens.

4.4 Aeriation and circulation rate.

Twenty-four hours before each test started, a fresh sample of brine was placed in a 5 gallon bottle, shaken and allowed to stand open in order to saturate the brine with air. The water was pumped from the open bottle, piped through rubber and glass tubing to the specimen gland and returned. The water discharge was allowed to run down and spread out over the inner surface of the bottle. According to the discussion of oxygen absorption given in Harvey's "Chemistry and Physics of Sea Water", page 62, (1928), the brine must have been completely saturated with air at all times during the tests.

Specimens C-5 and C-6 were run in an air-free brine atmosphere kept under C_2H_2 pressure, as shown on the S-N curve, Figure 1, page 8. The

tests provide, then, an indication of the effect of air on the position of the S-N curve. Due to a shortage of data, the air-free test curve is but roughly located. It was drawn parallel to the air-saturated test curve in Figure 1.

4.5 pH Variation.

The variation in the brine pH values is recorded in Figure 34, page 56, for specimens D-3, 4, 5, and 6. These pH readings were made by Frank Lanni of the Biology Department on a Beckman pH meter (Model G), a glass electrode type of instrument.

The brine is quite acid, probably due to the presence of complex organic swamp acids. The range of pH variation was not excessive.

A chemical analysis of a fresh and a used brine sample is given in Appendix 4.2.

4.6 Temperature variation.

The room temperature during the tests was always within the range 20 to 25° C. (68 to 77° F.). The brine was usually 3-4° C. above the room temperature due to energy dissipation in friction. The temperature variation during the day was typically $1\frac{1}{2}$° C. from early morning to late afternoon.

pH Variation

"pH" Variation During Operation for Specimens D-3, 4, 5 & 6, also for brine standing open.

Data by Frank Lonn. Instrument: Beckman pH Meter Model "G".

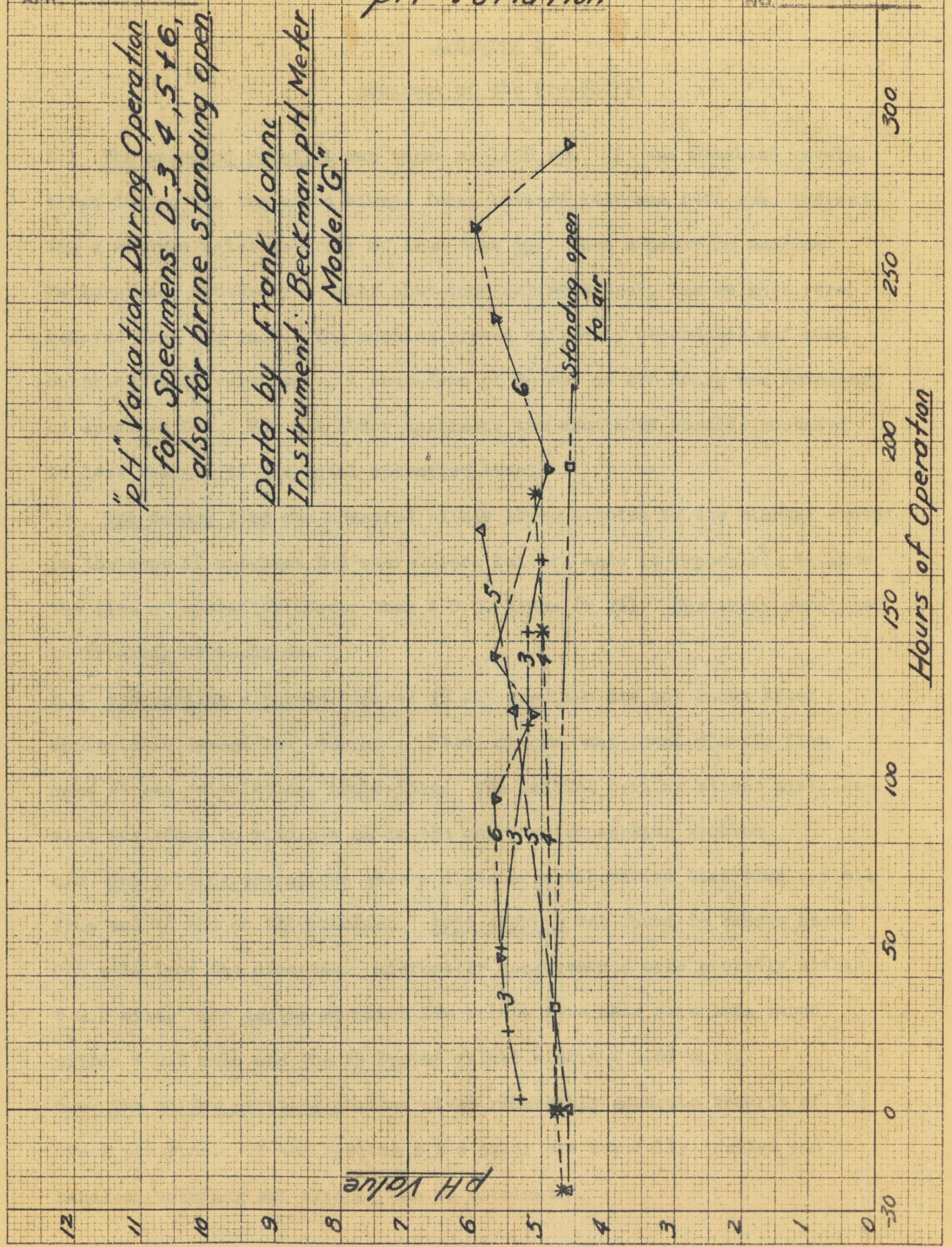

Fig 34

APPENDIX 5.

Accuracy of the Procedure

5.1 The speed of rotation was taken as 1425 rpm. It was measured several times during the tests and always found between 1419 and 1428 rpm, indicating a maximum relative error of less than $\frac{1}{2}$%. When a power or machine failure made necessary a brief shut-down during a test, the weights were removed from the rack. The machine proved extremely dependable and such occasions were very rare. A shut-down of $2\frac{1}{2}$ out of 273 hours was necessary on specimen D-6. For all other specimens the shut-down periods amounted to less than 1% of the total operation time.

The damage time was measured within three minutes by the clocks, except in the case of specimen D-6 where clock failure made it impossible to know the time of operation closer than ± 9.00 hours (± 3%). Specimens persisted in breaking on weekends.

5.2 The bending stresses induced in any specimen are not known after appreciable damage has occurred. Pits, cracks, and local plastic flow make stress calculations impossible. The initial bending stress distribution was known to within ± 2% in the unprotected working section.

5.3 The cutting operations gave a diameter which varied less than 0.5 mil from end to end on the specimen. Acid etching was found to remove about 0.8 mils from the diameter. Micrometer measurements were probably within ± 0.3 mils. The depths at which the prints were made were thus known within ± 0.7 mils and the "% Depth" values within ± 0.5% units.

5.4 The sulfur printing process gives remarkably accurate records of the crack patterns. If the specimens and paper are carefully treated and handled, smearing and sliding can be eliminated.

During the cracking process many little slivers of metal are isolated by the joining of cracks. Some of these are only a few mils in diameter and appear as tiny "islands" in the crack patterns. The fact that these islands can be transferred without blotting is good evidence of the accuracy of transfer that can be obtained even with very complex patterns (see Figures 16 and 33, pages 15 and 51).

If double printing occurs, it can be detected easily since the second impression is much lighter than the first. Sliding is also easily detectable.

Measurements made on paper just before printing and on finished prints showed paper shrinkage to be less than 2%.

5.5 Crack arc measurements were usually made on enlargements at about 3.5 X. The ends of the cracks were marked with the sharp point of a drafting instrument and then measured within ± .005 in. This corresponds to ± .15 inches on the 100 X profiles, and ± .08 in. on the 50 X profiles. In some of the earlier analyses of crack prints at large depths, arc measurements were made directly on the prints. (These print depths are marks on the crack profiles (Appendix 7) as follows: u^o , v^o , w^o, etc.). This practice is not advisable, but the measurements were very carefully made with an accuracy corresponding to ± 0.3 in. on the profiles at 100 X. Inaccuracy in arc measurements at large depths does not greatly affect the crack depths indicated because of the small slopes near the crack bottoms.

It may be seen from Figures 16 and 33 that some cracks do not lie in a plane perpendicular to the axis. This was ignored in drawing the profiles, since the error introduced is not more than 3% in the worst

cases. The cracks are all nearly perpendicular to the axes at the greater depths.

Some of the earlier prints were made on velvet instead of glossy finish paper and the crack lengths were difficult to measure. Fortunately, several sulfur prints were made at each depth so that the true lengths of cracks could be checked by comparison of several prints.

5.6 The crack profiles were drawn on the assumption of symmetry about a centerline. This assumption greatly simplified the measurements and calculations. The actual crack profiles are somewhat dependent upon the direction of specimen rotation and chance joining with other cracks. The error introduced does not seriously affect the crack depth indicated.

The crack profiles were drawn in as smooth curves. Actually they are somewhat rough in outline. This may help to explain some of the scatter of the experimental points about the smooth curve. No important error is introduced by drawing the profiles as though smooth.

5.7 The overall accuracy of the method is such that crack depths can be determined with an accuracy of ± 1.5 mils or ± 1% unit on the "% Depth" scale. This accuracy is much greater than that required in the measurement of the rate of crack penetration.

In general, the sulfur print process as described in this thesis gives results which are more accurate than the corrosion fatigue process is consistent, predictable, or can be reproduced with the best laboratory control.

APPENDIX 6.

BIBLIOGRAPHY

1. H. F. Moore, "Corrosion Fatigue of Metals", in "Metals Handbook", A.S.M., 1939, Ed. pp. 147-153.

2. D. J. McAdam, Jr., and G. W. Geil, "Influence of Cyclic Stress on Corrosion Pitting of Steels in Fresh Water, and Influence of Stress Corrosion on Fatigue Limit", J. Research National Bur. Standards, v. 24, 1940, pp. 685-722.

3. D. J. McAdam, Jr., "Influence of Cyclic Stress on Corrosion", A.I.M.E., Inst. Metals Div. Tech. pub. No. 329, 1930.

4. Battelle Memorial Institute "Prevention of the Fatigue of Metals", (Book) 1941, Appendix 6, p. 123.

5. O. Föppl, O. Behrens, T. Dusold. z. Metallkunde v. 25, 1933, p. 279-281.

6. F. N. Speller and P. F. Mumma, "Influence of Corrosion Accelerators and Inhibitors on Fatigue of Ferrous Metals", Proc. A.S.T.M. v. 29, 1929, pt. 2, p. 238. Also, v. 28, 1928, pt. 2, p. 159-173.

7. U. R. Evans, "Metallic Corrosion, Passivity and Protection", (Book), Arnold & Co., London, 1937.

8. U. R. Evans, "The Passivity of Metals and Its Relation to Problems of Corrosion", Trans. A.I.M.E., Inst. of Metals Div., 1929, p. 7.

9. H. J. Gough and D. G. Sopwith, "Corrosion Fatigue Characteristics of and Aluminum Specimen Consisting of Two Crystals", J. Inst. of Metals, v. 52, 1933, p. 57.

10. H. J. Gough, "Corrosion Fatigue of Metals", J. Inst. of Metals, v. 49, No. 2, 1932, p. 17.

11. H. J. Gough and G. Forest, "The Behavior of a Single Crystal of Aluminum Subject to Stressless Corrosion in Tap Water, Followed by Test in Air to Destruction ~~in Air~~ under Alternating Torsional Stresses", Aero. Research Com. Reports and Mem. No. 1476, 1932.

12. H. J. Gough and D. G. Sopwith, "The Behavior of a Single Crystal of Aluminum under Alternating Torsion Stresses while Immersed in a Slow Stream of Tap Water", Proc. Royal Soc. (London),(A) 135, 1932, p. 392.

13. H. J. Gough and R. V. Southwell, "On Stress Concentration in the Neighborhood of a Small Spherical Flaw, and on Propagation of Fatigue Fractures in a Statistically Isotropic Material", British Aero. Research Com. Reports and Memoirs, No. 1003, 1926.

14. D. J. McAdam and G. W. Geil, "Influence of Stress on the Corrosion Pitting of Steel in Distilled Water", A.S.M. Trans., v. 30, No. 4, Dec. 1942, p. 1159.

15. D. J. McAdam and G. W. Geil, "Pitting and Its Effect on the Fatigue Limit of Steels Corroded under Various Conditions", A.S.T.M. Preprint No. 33, 1941.

16. D. J. McAdam, "Influence of Stress on the Corrosion Pitting of Aluminum Bronze and Monel Metal in Water", U.S.B.R. J. Research, v. 26, 1941, R.P. 1366, p. 135.

17. D. J. McAdam, "Influence of Water Composition on Stress Corrosion", Proc. A.S.T.M. v. 31, pt. 2, 1931, p. 259.

18. D. J. McAdam, "Stress and Corrosion", Proc. Third International Congress of Applied Mech., Stockholm, v. 2, 1930, p. 269.

19. D. J. McAdam, "Corrosion of Metals under Cyclic Stress", Trans. Am. Soc. Mech. Eng., v. 51, pt. 1, 1929, APM-51-5, p. 45.

20. D. J. McAdam, "Corrosion of Metals as Affected by Stress, Time, and Number of Cycles", Trans. A.I.M.E., Inst. Metals Div. 1929, p. 56.

21. D. J. McAdam, "Corrosion of Metals as Affected by Time and by Cyclic Stress", Trans. A.I.M.E., Proc. Inst. of Metals Div., 1928, p. 571.

22. D. J. McAdam, "Some Factors Involved in Corrosion and Corrosion Fatigue of Metals", Proc. A.S.T.M., v. 28, pt. 2, 1928, p. 117.

23. D. J. McAdam, "Corrosion Fatigue of Non-ferrous Metals", Proc. A.S.T.M., vol. 27, pt. 2, 1927, p. 102.

24. D. J. McAdam, "Stress-Strain-Cycle Relationships and Corrosion Fatigue of Metals", A.S.T.M. Proc., v. 26, pt. 2, 1926, p. 224.

25. B. Westcott and C. N. Bowers, "Economical Selection of Sucker Rods", Trans. A.I.M.E., v. 114, 1935, pp. 117-192.

APPENDIX 7.

A Collection of Crack Profiles

SUBJ. ME 140

CALIFORNIA INSTITUTE OF TECHNOLOGY
DEPARTMENT OF MECHANICAL ENGINEERING

PG. ____ OF ____ PGS.

BY. R.C.B.

DATE 2-18-43

APR. W.H.G.

NO. C-11

Crack Profiles

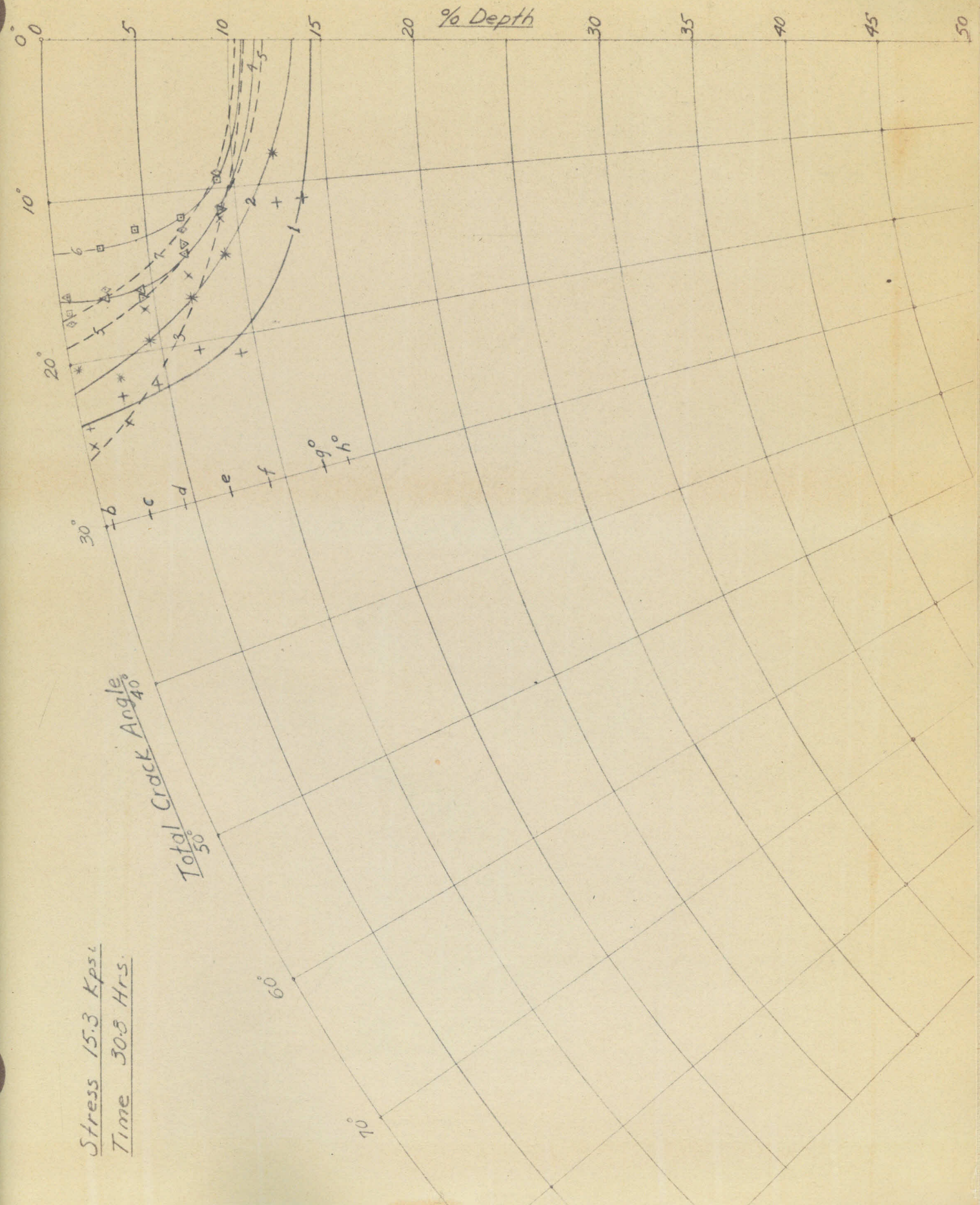

Stress 15.3 Kpsi.

Time 30.3 Hrs.

SUBJ. ME 140

BY R.C.B.

APR. W.H.G.

CALIFORNIA INSTITUTE OF TECHNOLOGY
DEPARTMENT OF MECHANICAL ENGINEERING

PG. ____ OF ____ PGS.

DATE 2-18-43

NO D-1

Crack Profiles

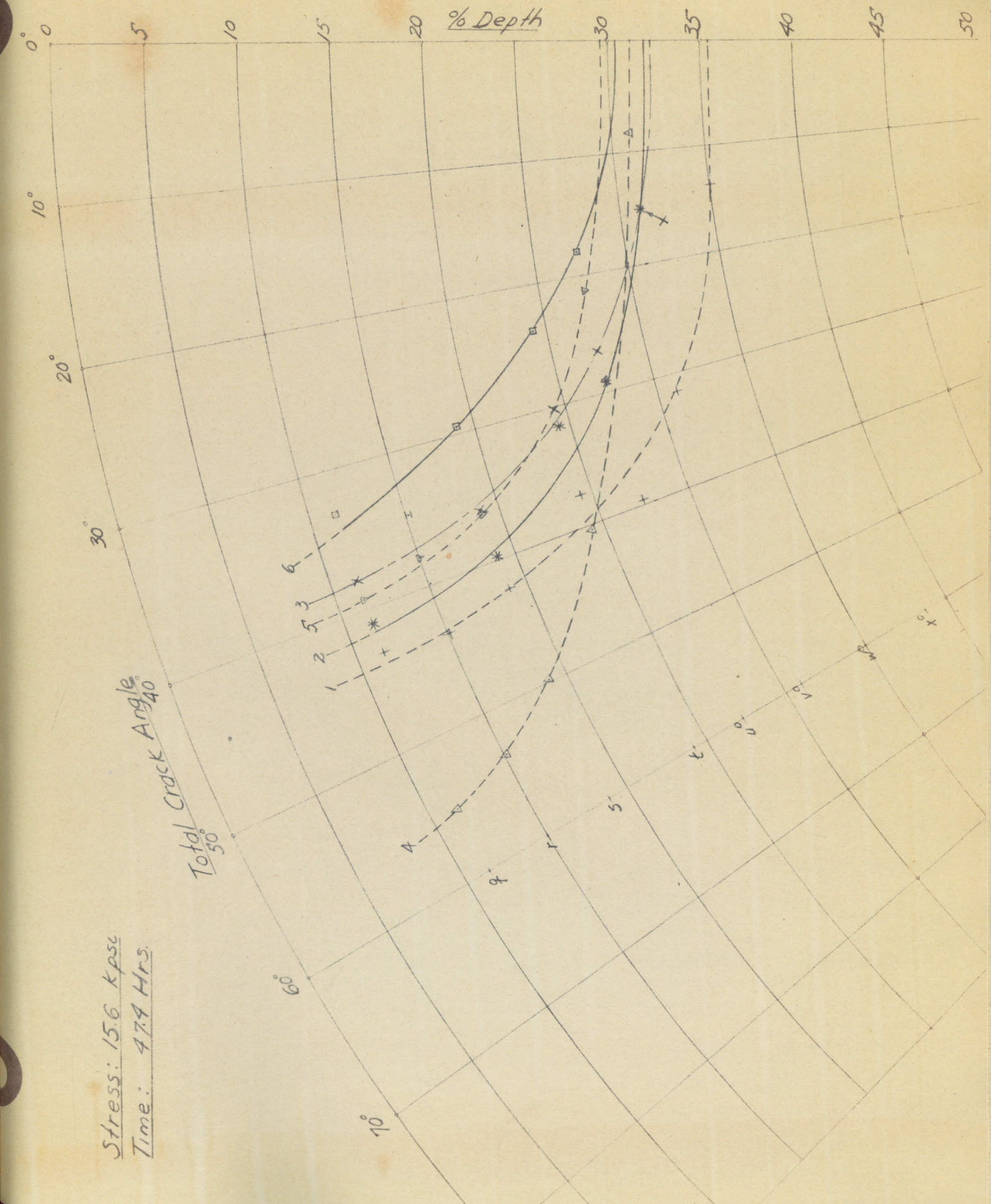

Stress: 15.6 Kpsi
Time: 474 Hrs.

SUBJ. ME 140

BY R.C.B.

APR W.H.L.

CALIFORNIA INSTITUTE OF TECHNOLOGY
DEPARTMENT OF MECHANICAL ENGINEERING

PG. ___ OF ___ PGS.

DATE 2-20-43

NO. D-2

Crack Profiles

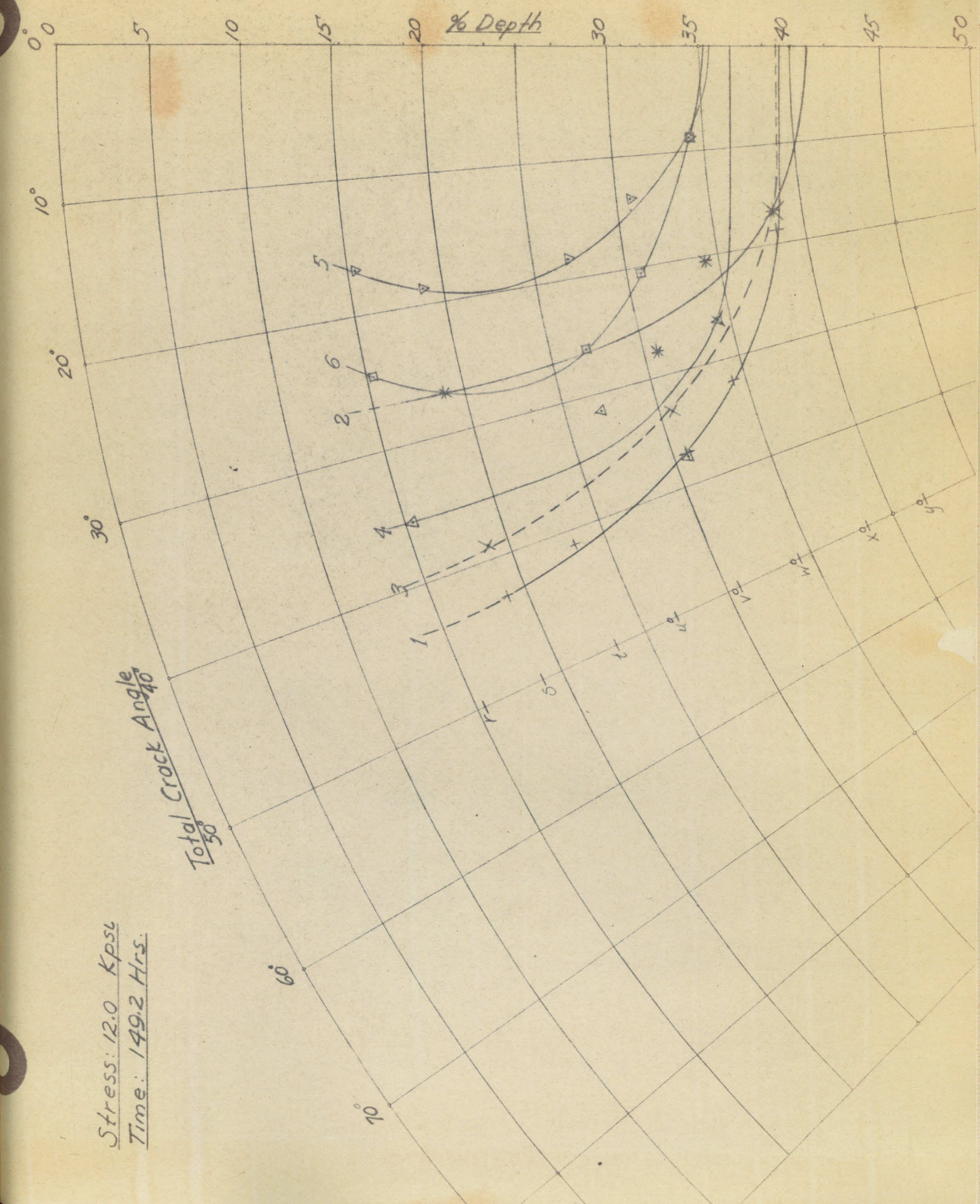

Stress: 12.0 Kpsi
Time: 149.2 Hrs.

Crack Profiles

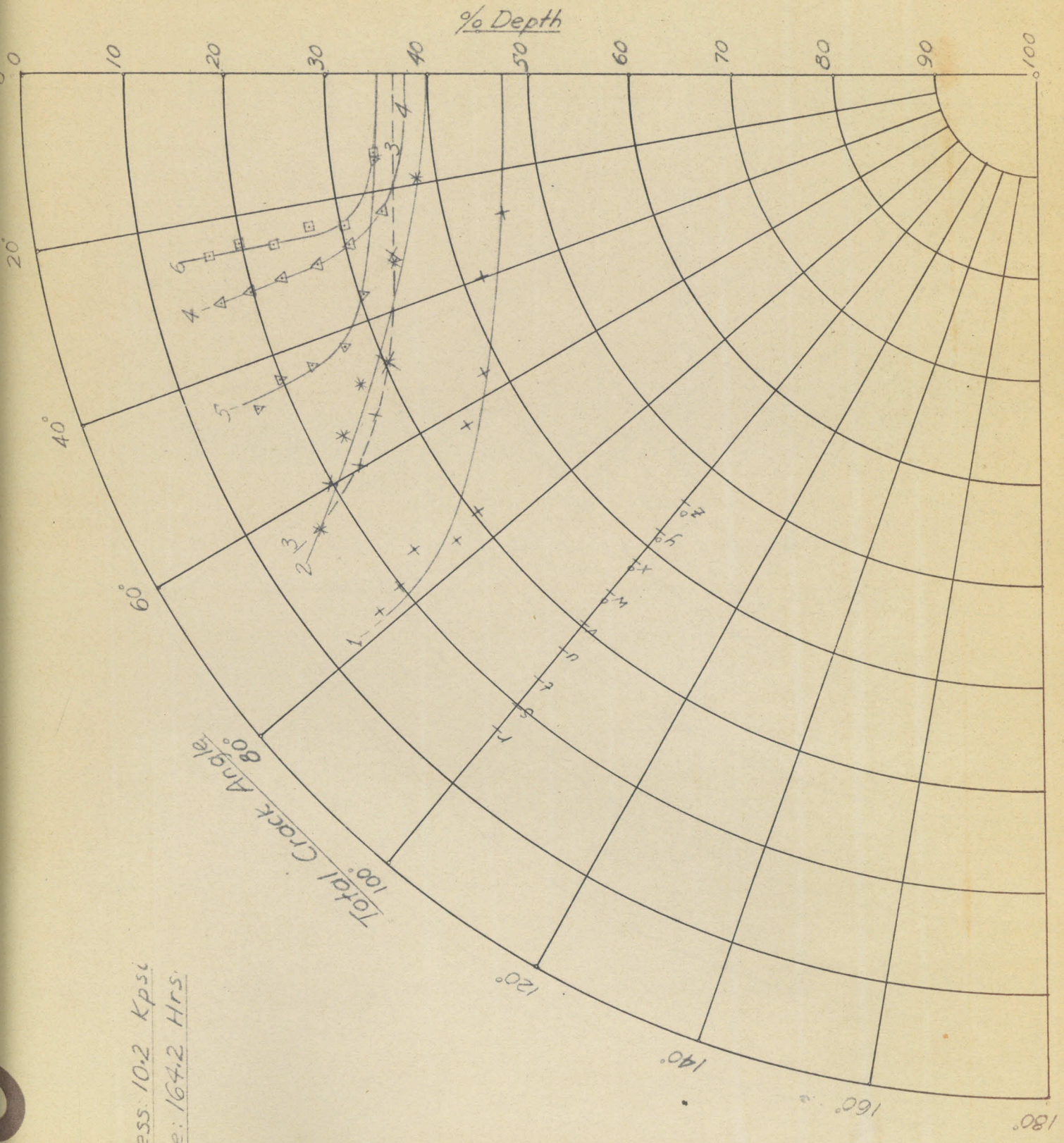

Stress: 10.2 Kpsi
Time: 1642 Hrs.

SUBJ ME 140

BY R.C.B.

APP W.H.d.Le.

CALIFORNIA INSTITUTE OF TECHNOLOGY
DEPARTMENT OF MECHANICAL ENGINEERING

PG. ____ OF ____ PGS.

DATE 2-19-43

NO. D-4

Crack Profiles

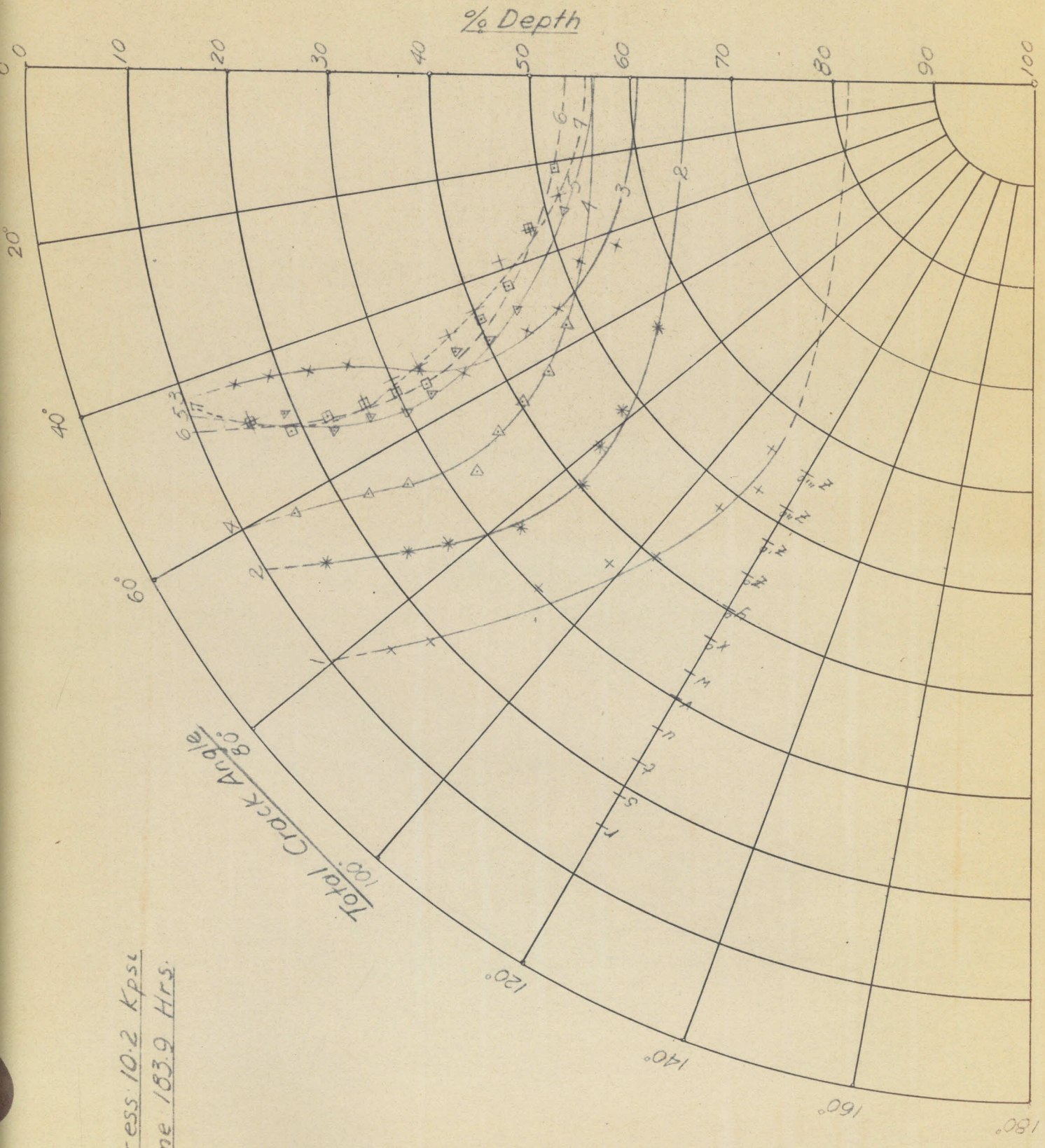

Stress 10.2 Kpsi
Time 1839 Hrs.

SUBJ. ME 140

BY. R.C.B.

APR. Wtle.

CALIFORNIA INSTITUTE OF TECHNOLOGY
DEPARTMENT OF MECHANICAL ENGINEERING

PG. ____ OF ____ PGS

DATE 3-20-43

NO. D-5

Crack Profiles

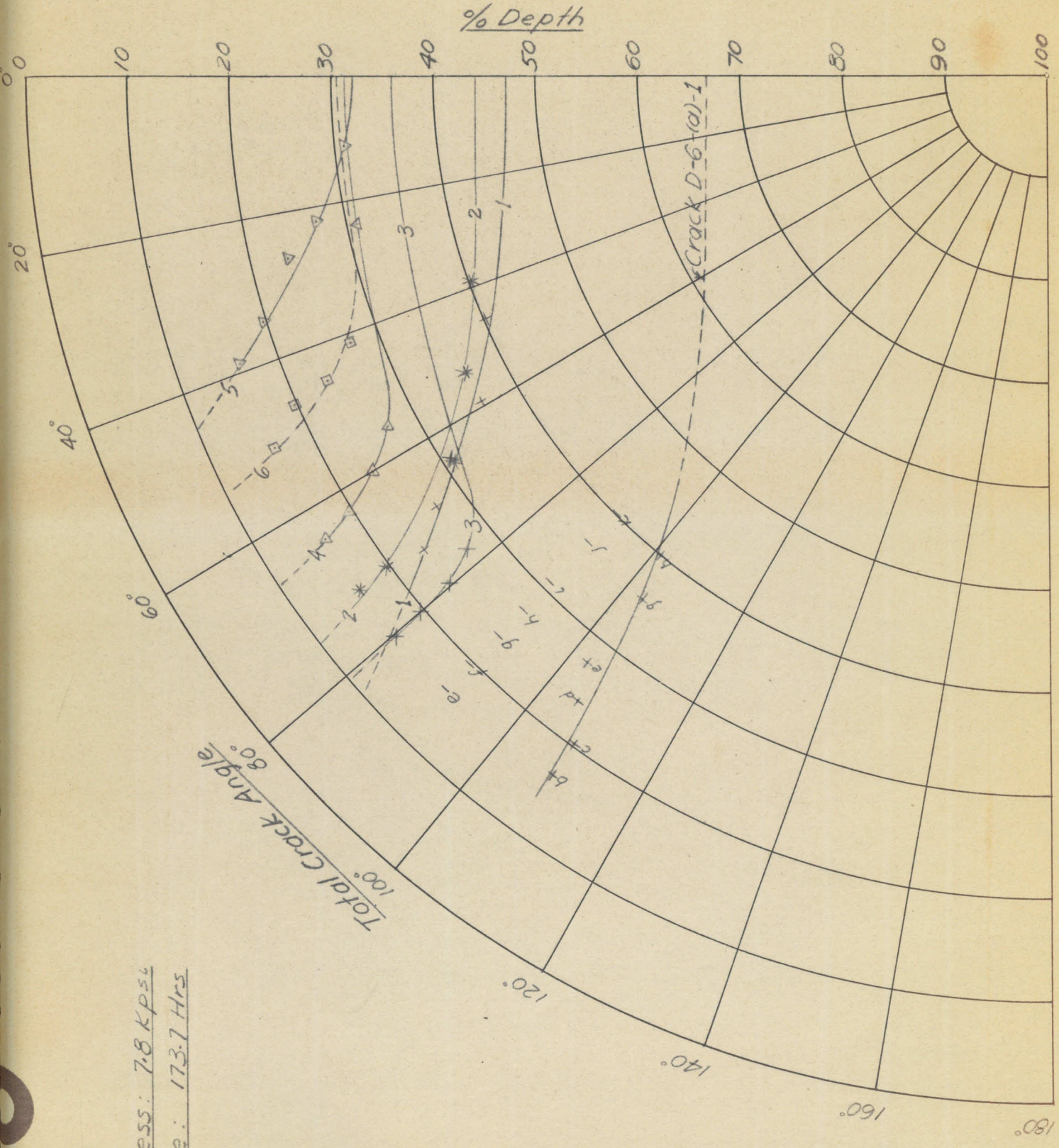

Stress: 7.8 kpsi

Time: 173.7 Hrs

SUBJ ME 140

BY RCB

APP Ubbe.

CALIFORNIA INSTITUTE OF TECHNOLOGY
DEPARTMENT OF MECHANICAL ENGINEERING

PG ____ OF ____ PGS

DATE 2-20-43

NO D-5

Crack Profiles

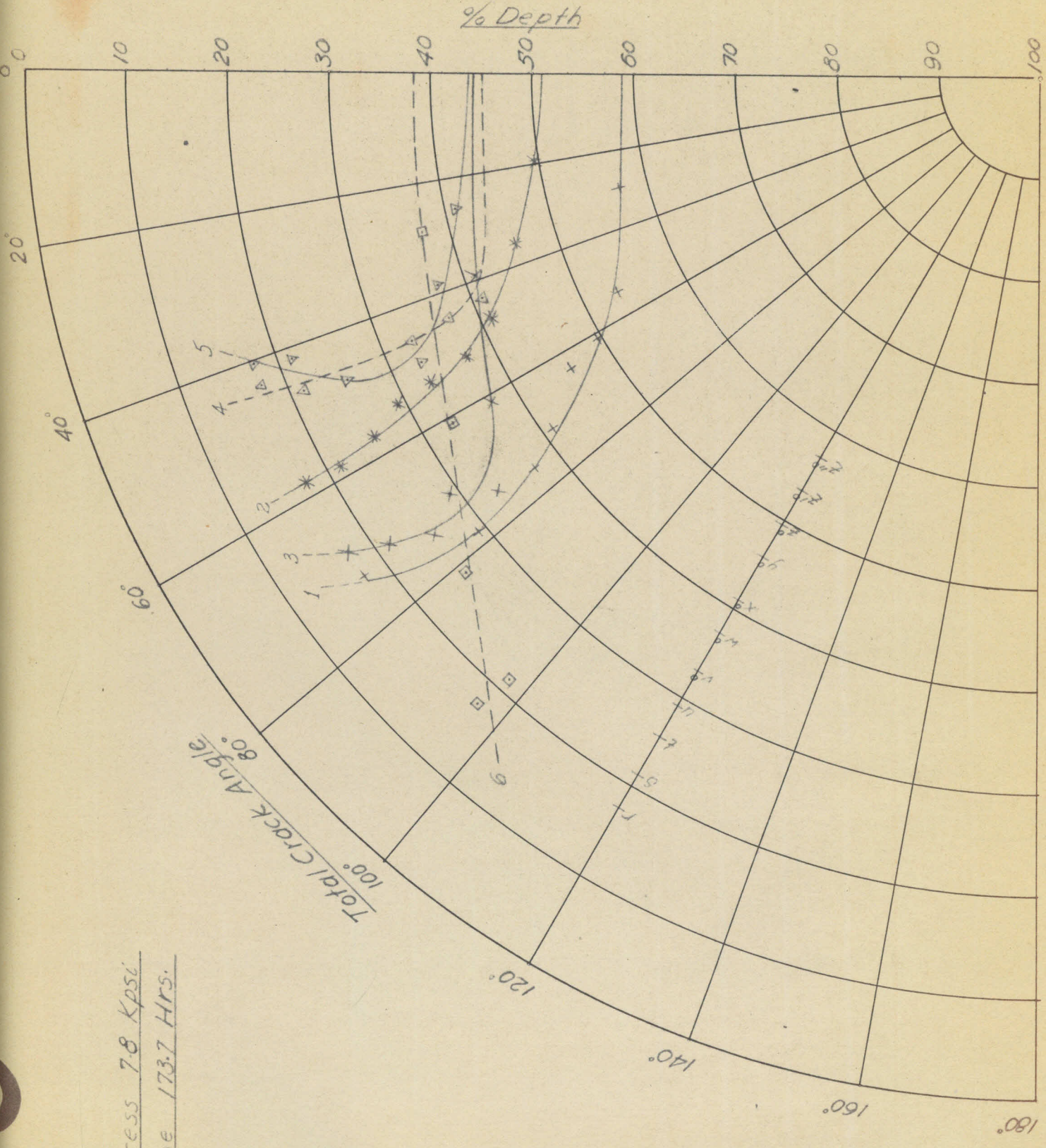

Stress 7.8 Kpsi

Time 1737 Hrs.

SUBJ ME 140

BY R.C.B

APR W.H.G.

CALIFORNIA INSTITUTE OF TECHNOLOGY
DEPARTMENT OF MECHANICAL ENGINEERING

DATE 3-20-93

NO D-6

Crack Profiles

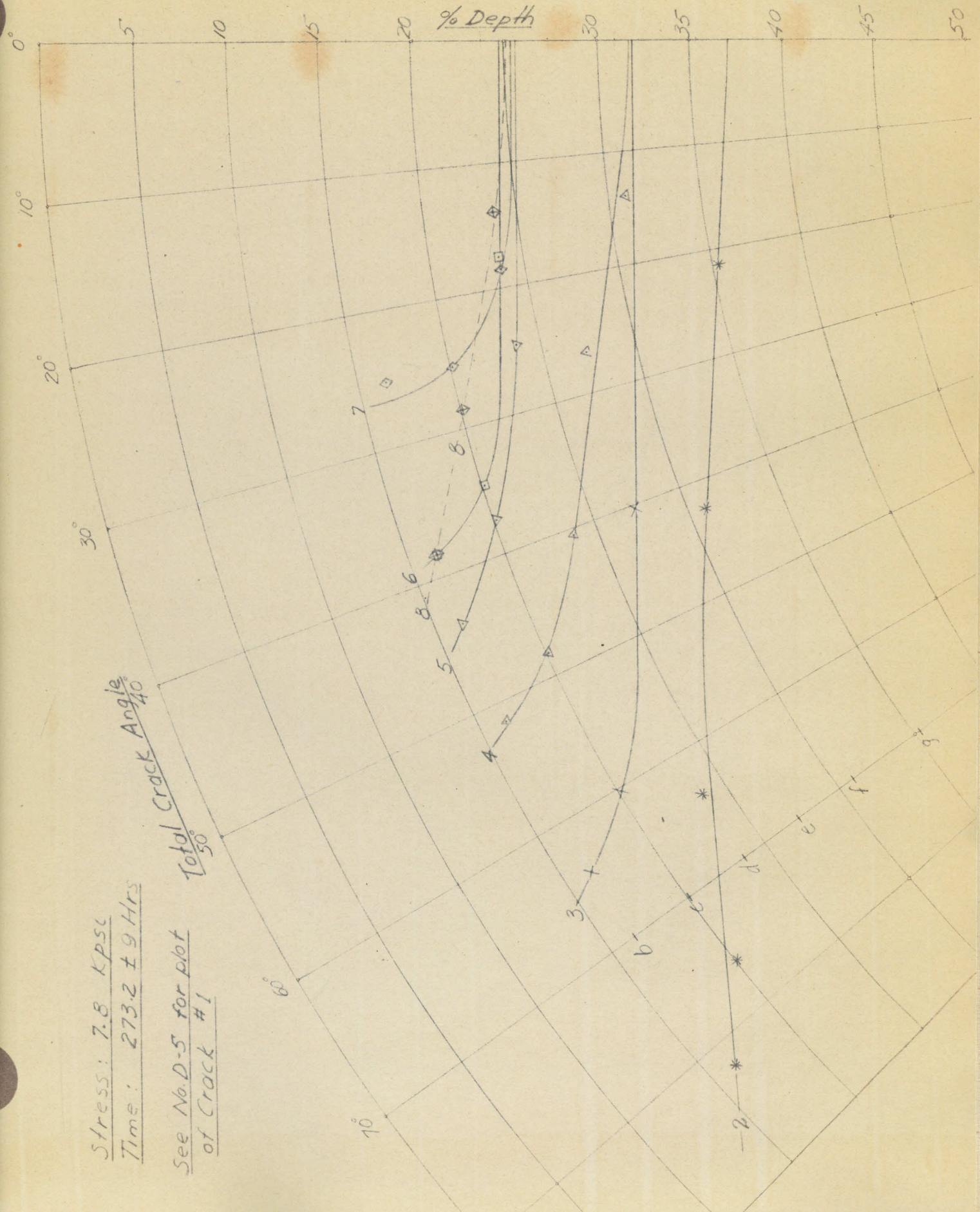

Stress: 7.8 KPSI
Time: 273.2 ± 9 Hrs

See No. D-5 for plot of Crack #1

SUBJ ME 140

BY R.C.B.

APR Little

CALIFORNIA INSTITUTE OF TECHNOLOGY
DEPARTMENT OF MECHANICAL ENGINEERING

PG ____ OF ____ PGS.

DATE 2-20-43

NO. D-6

Crack Profiles

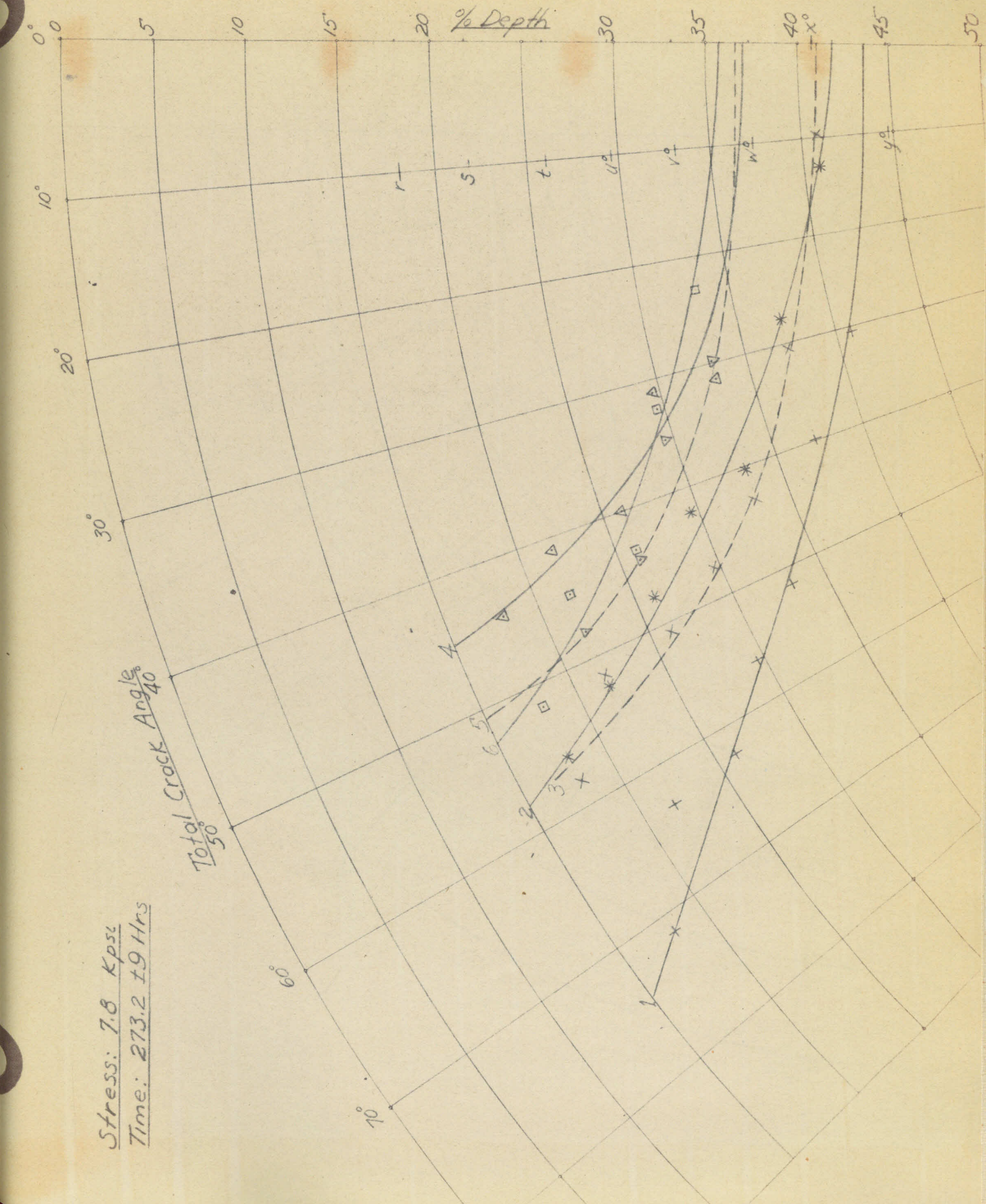

Stress: 7.8 Kpsi
Time: 273.2 ± 9 Hrs

Crack Profiles

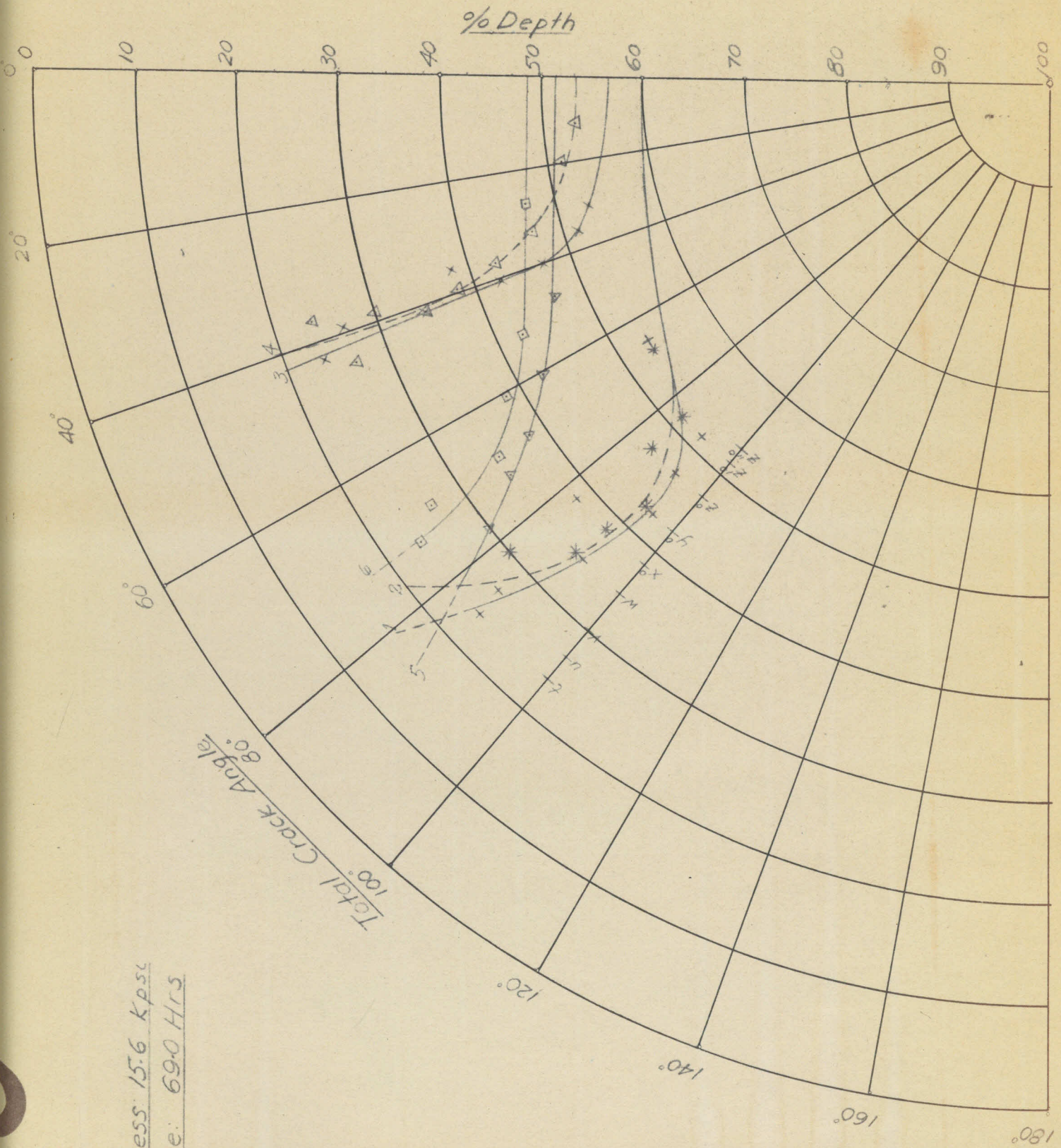

Stress: 15.6 kpsi
Time: 69.0 Hrs

SUBJ ME 140

CALIFORNIA INSTITUTE OF TECHNOLOGY
DEPARTMENT OF MECHANICAL ENGINEERING

BY R.C.B.

DATE 2-18-43

APR W.H.e.

NO. D-8

Crack Profiles

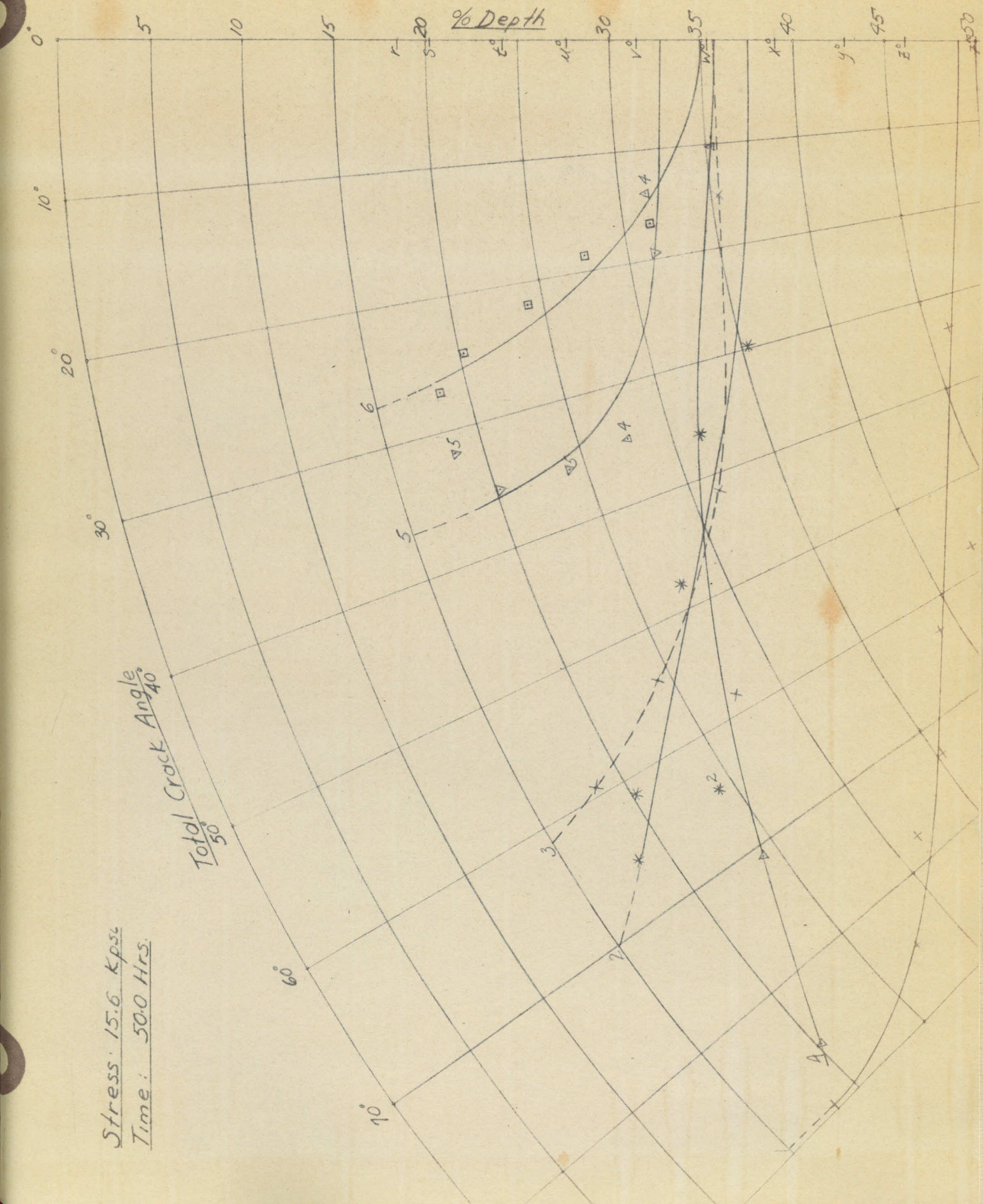

SUBJ. ME140

BY R.C.B.

APR W.H.e.

CALIFORNIA INSTITUTE OF TECHNOLOGY
DEPARTMENT OF MECHANICAL ENGINEERING

PG. ____ OF ____ PGS.

DATE 2-18-43

NO D-9

Crack Profiles

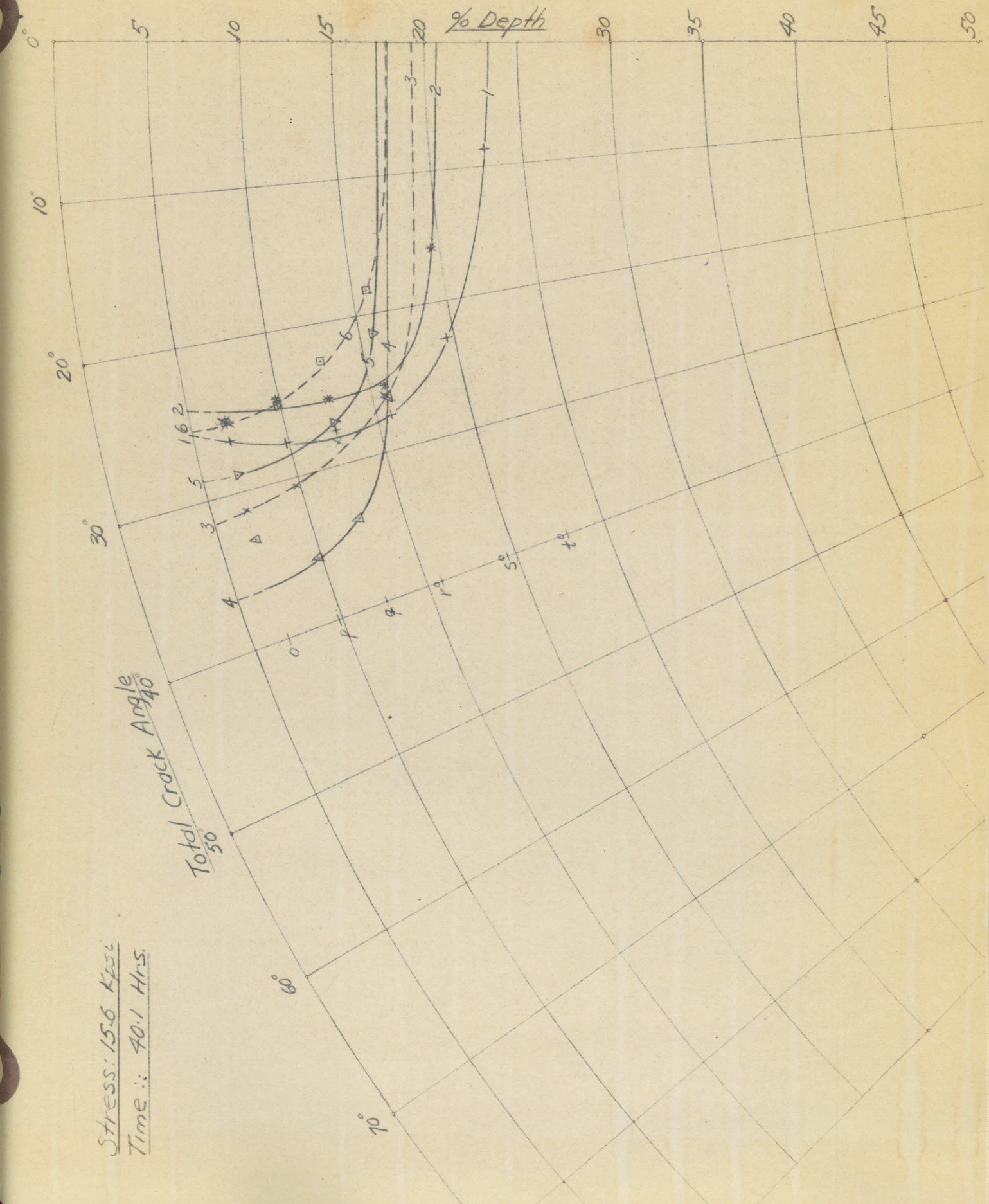

SUBJ. ME 140

CALIFORNIA INSTITUTE OF TECHNOLOGY
DEPARTMENT OF MECHANICAL ENGINEERING

PG. ____ OF ____ PGS.

BY R.C.B.

DATE 2-20-93

APR W.H.G.

Crack Profiles

NO. E-1

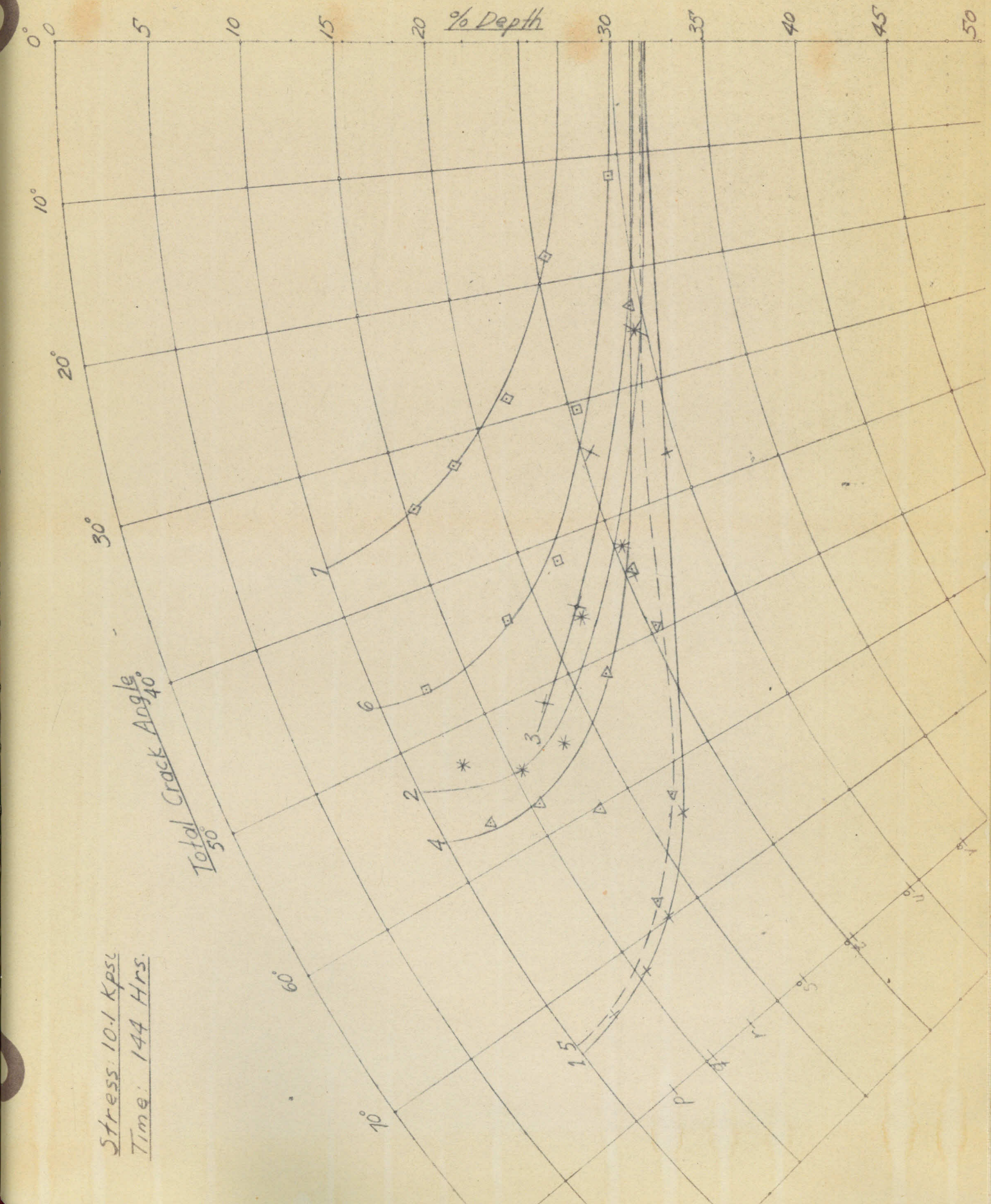

Stress: 10.1 Kpsi
Time: 144 Hrs.

SUBJ ME140

BY R.C.B

APR Ubl6.

CALIFORNIA INSTITUTE OF TECHNOLOGY

DEPARTMENT OF MECHANICAL ENGINEERING

PG ___ OF ___ PGS.

DATE 3-20-43

NO. E-2

Crack Profiles

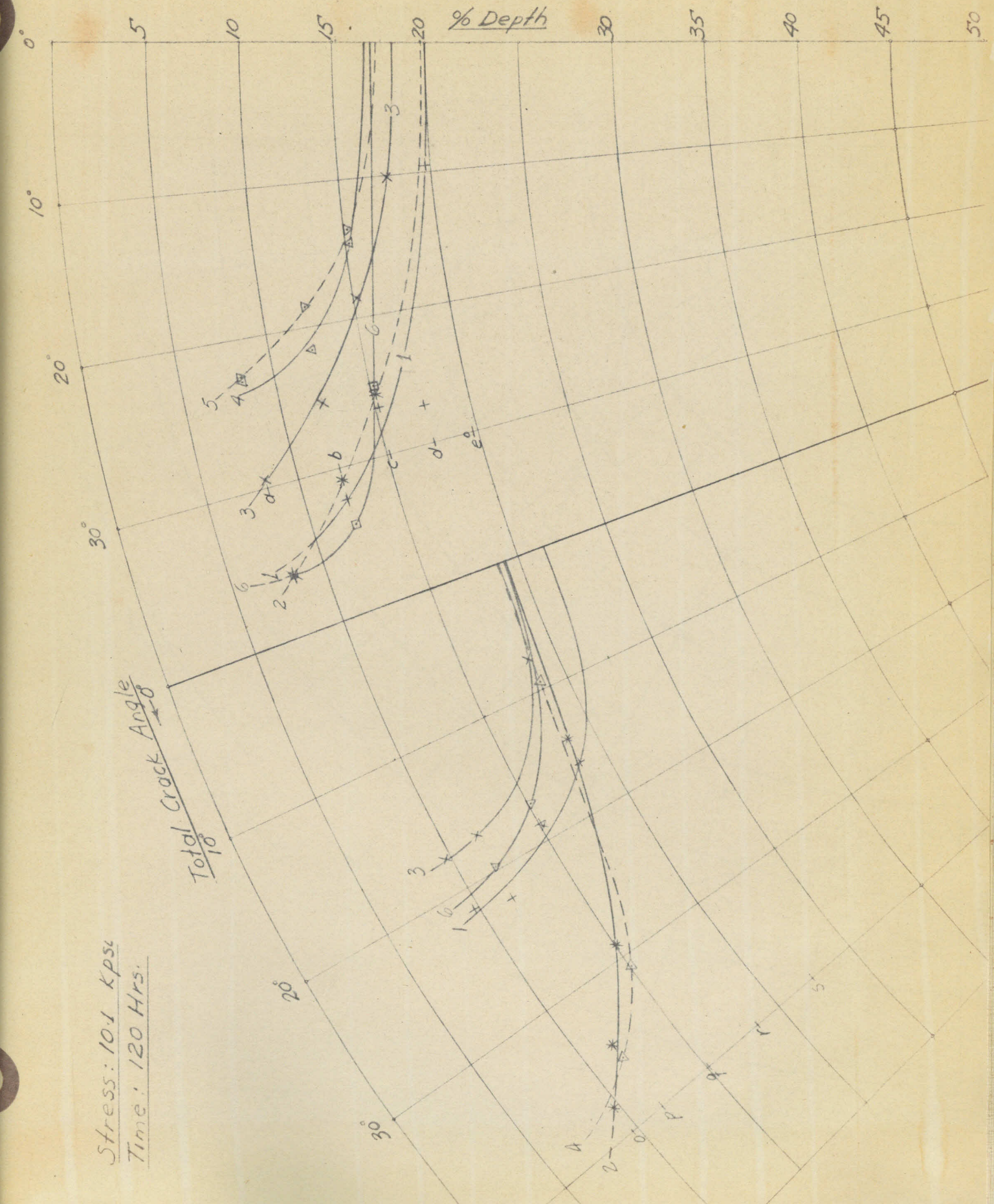

SUBJ ME 140

BY R.C.B.

APP

CALIFORNIA INSTITUTE OF TECHNOLOGY
DEPARTMENT OF MECHANICAL ENGINEERING

PG. OF PGS.

DATE 2-19-43

NO. E-3

Crack Profiles

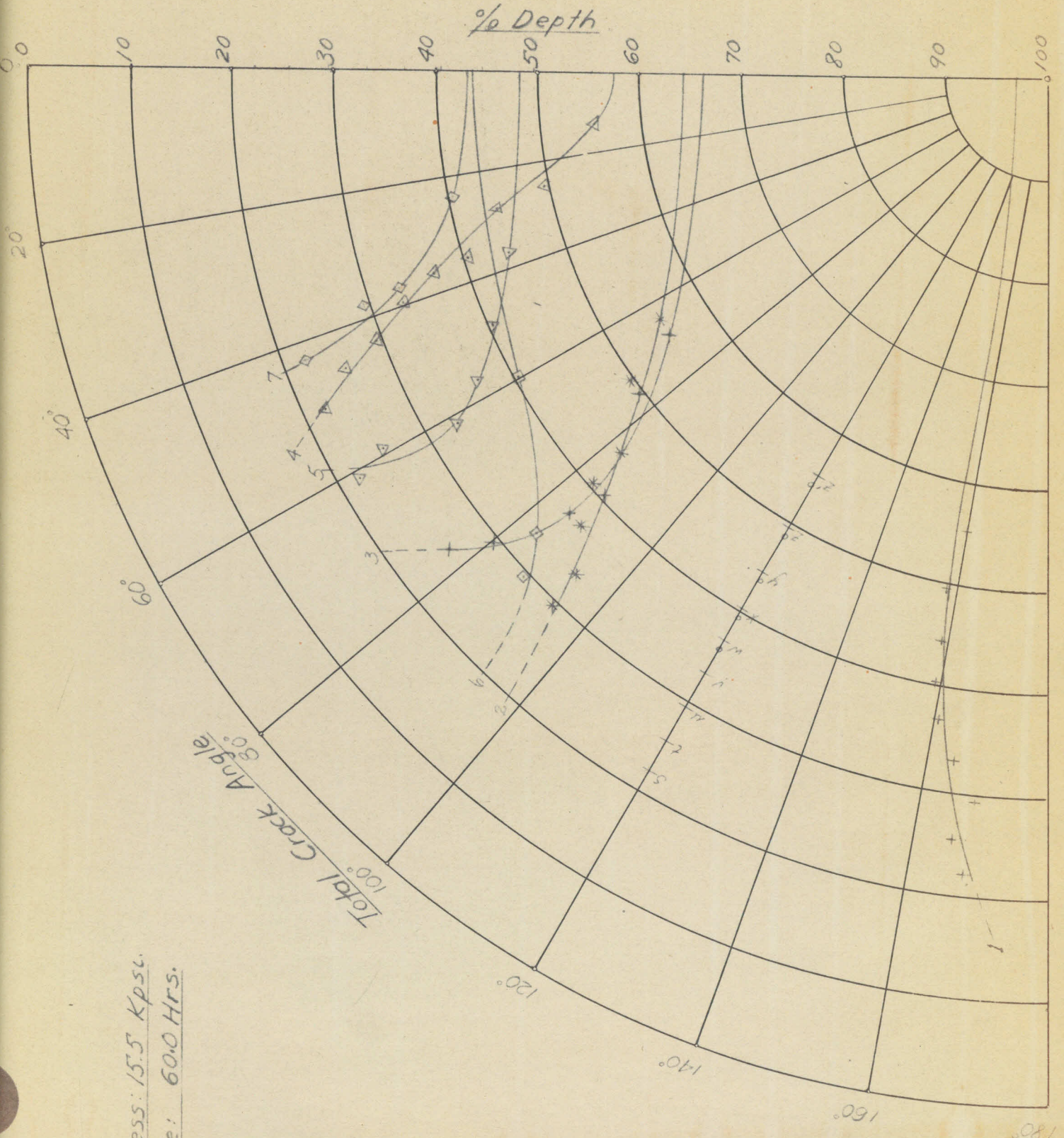

Stress: 15.5 Kpsi.

Time: 60.0 Hrs.

Crack Profiles

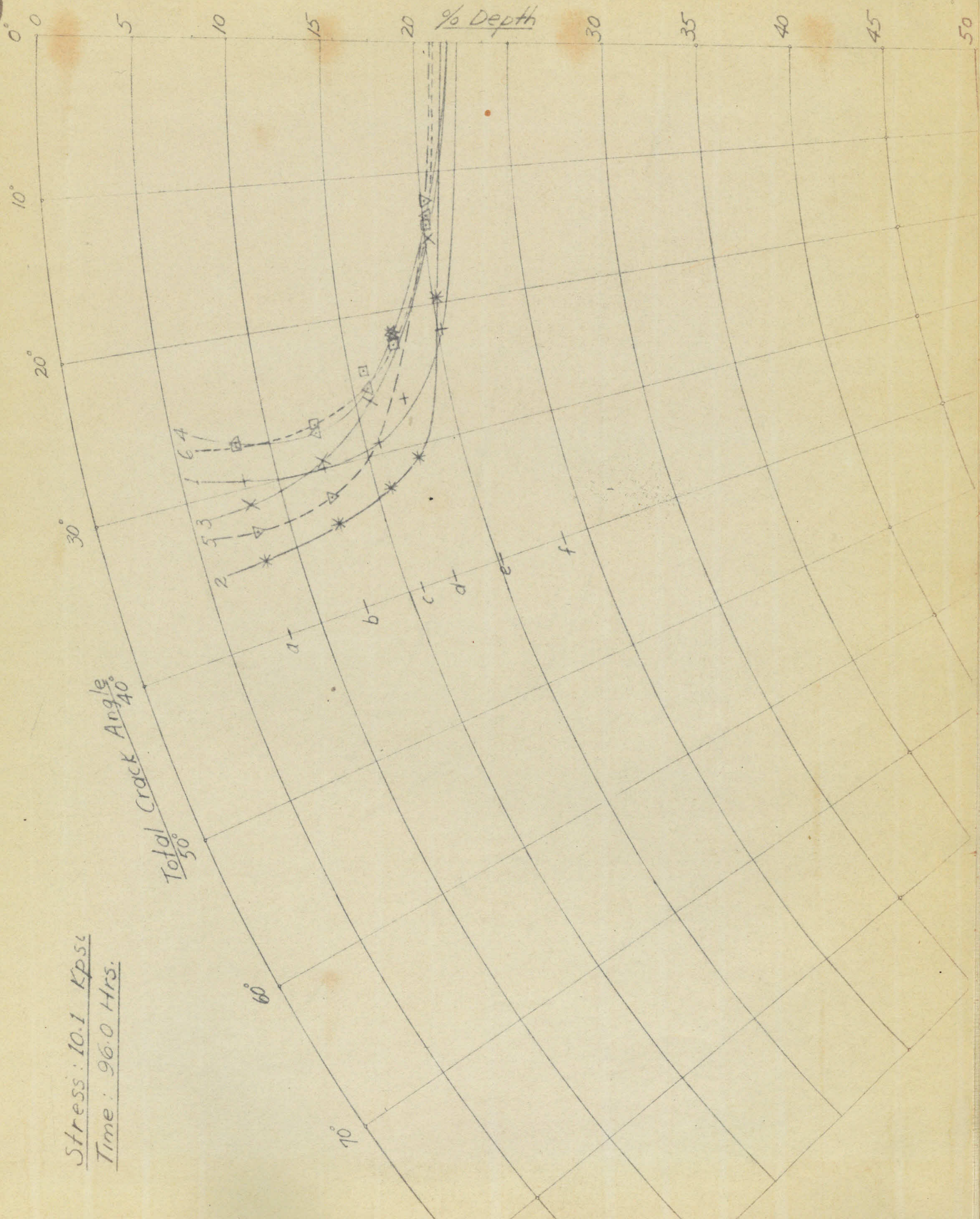

ME 140

R.C.B.

41-6.

3-22-43

E-4

Crack Profiles

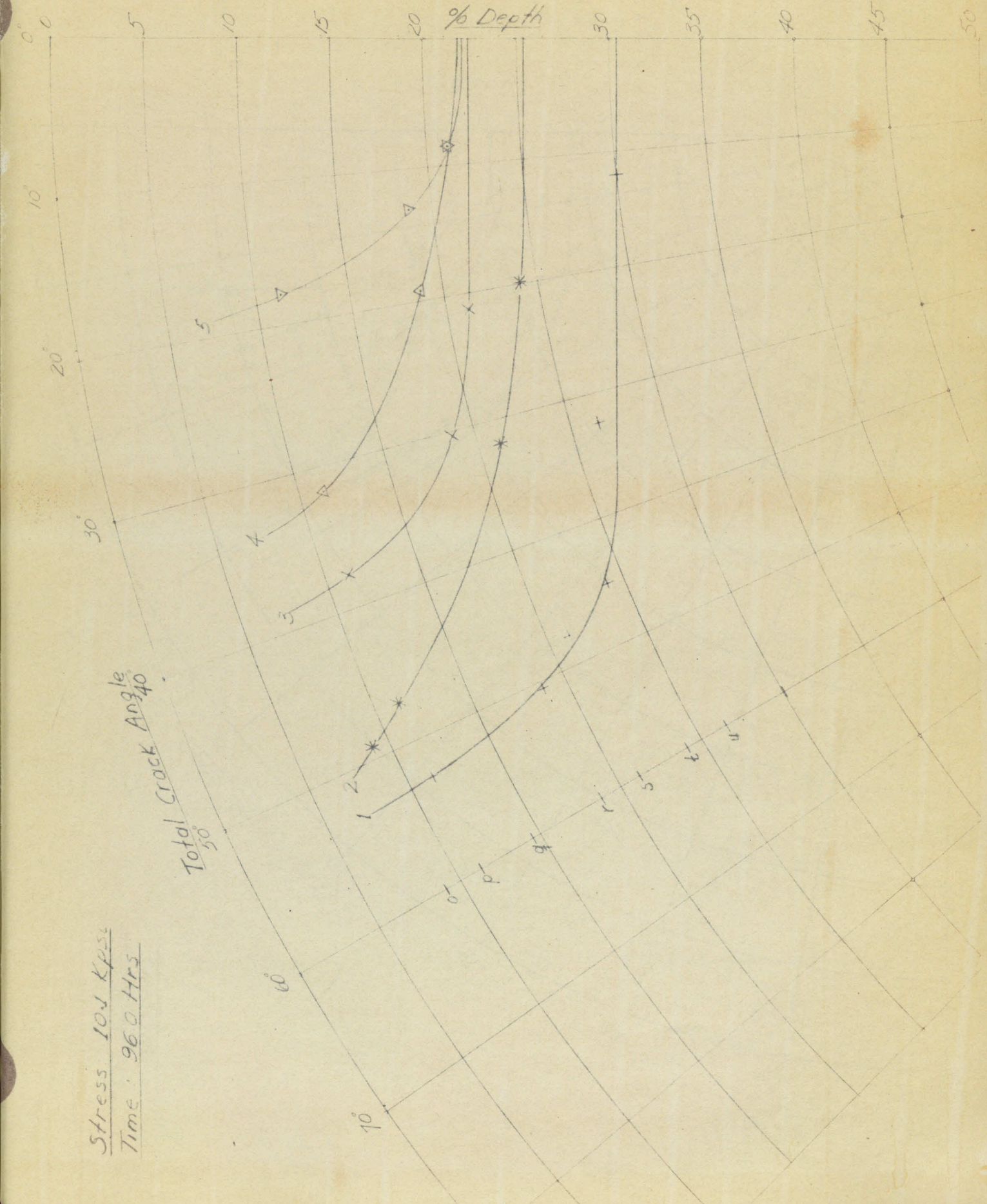

Stress 10.4 Kpsi

Time: 960 Hrs

ME 140

R.C.B.

4.11.6.

CALIFORNIA INSTITUTE OF TECHNOLOGY
DEPARTMENT OF MECHANICAL ENGINEERING

DATE 3-22-43

E-5

Crack Profiles

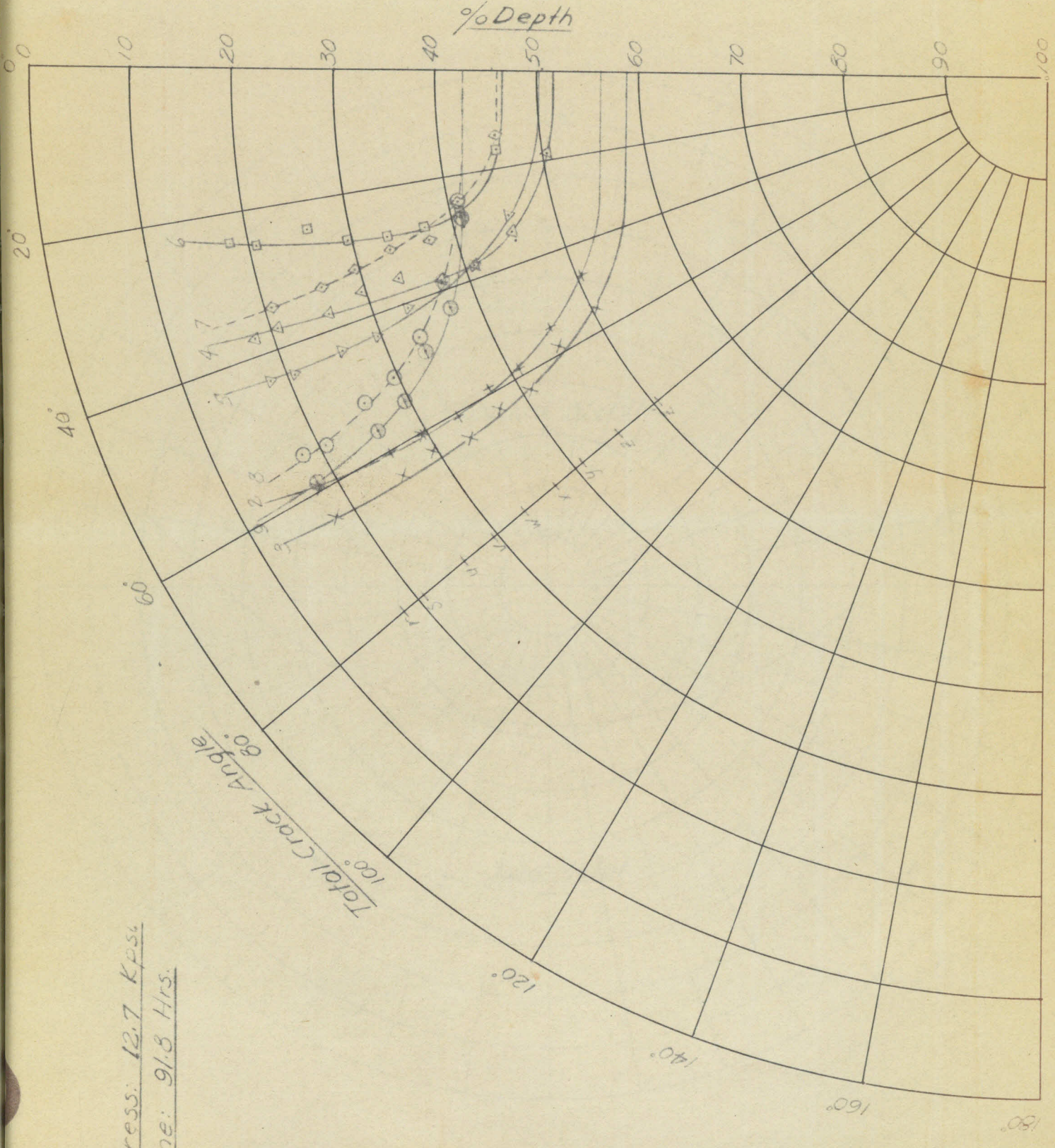

Stress: 12.7 Kpsi

Time: 91.8 Hrs.

ME 140

CALIFORNIA INSTITUTE OF TECHNOLOGY
DEPARTMENT OF MECHANICAL ENGINEERING

BY R.C.B. DATE 3-23-43

APP. W.H.L. NO. E-5-(m)-1

Crack Profile

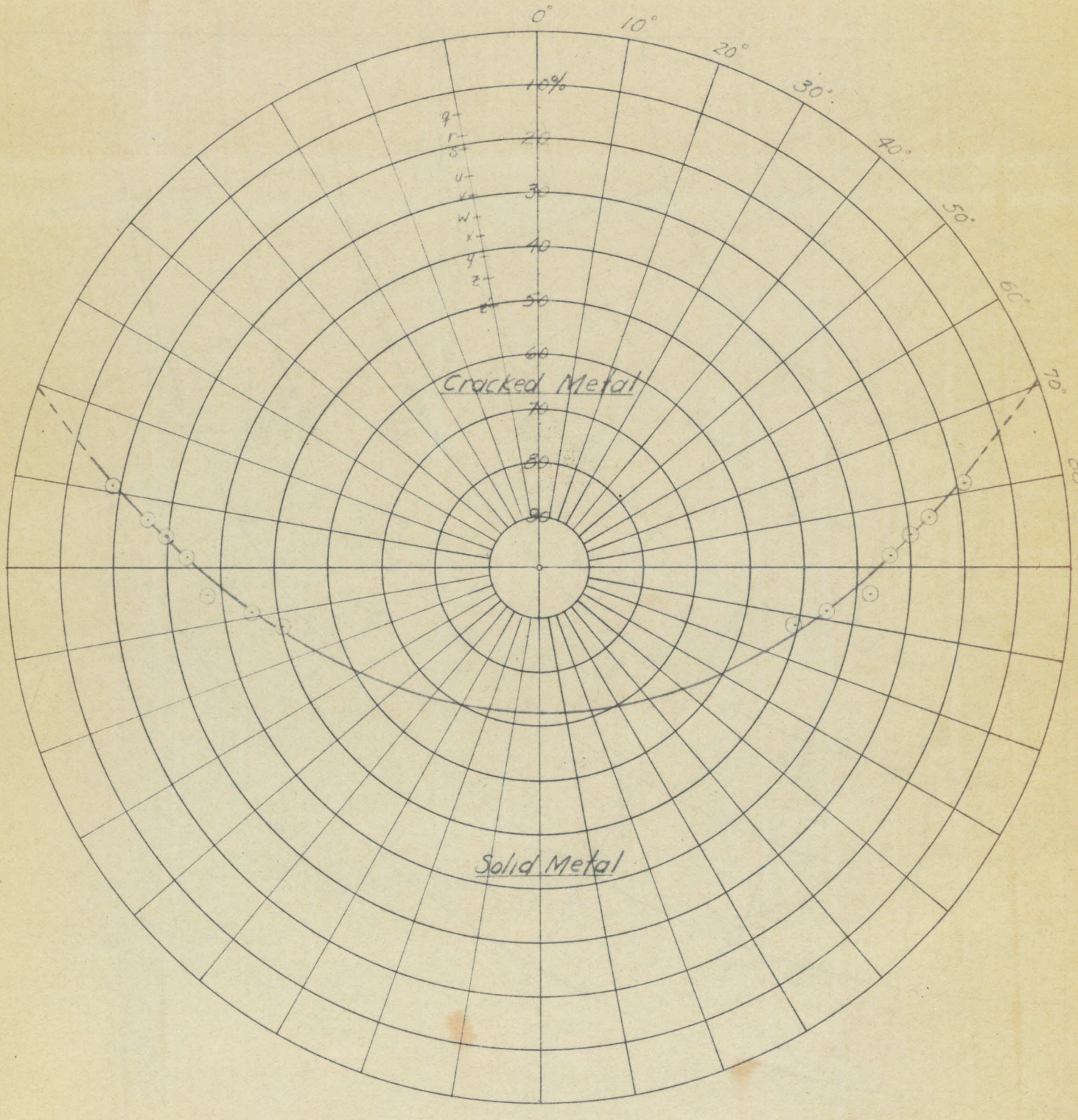

ME 140
RCB
U.N.L.

3-22-43
E-6

Crack Profiles

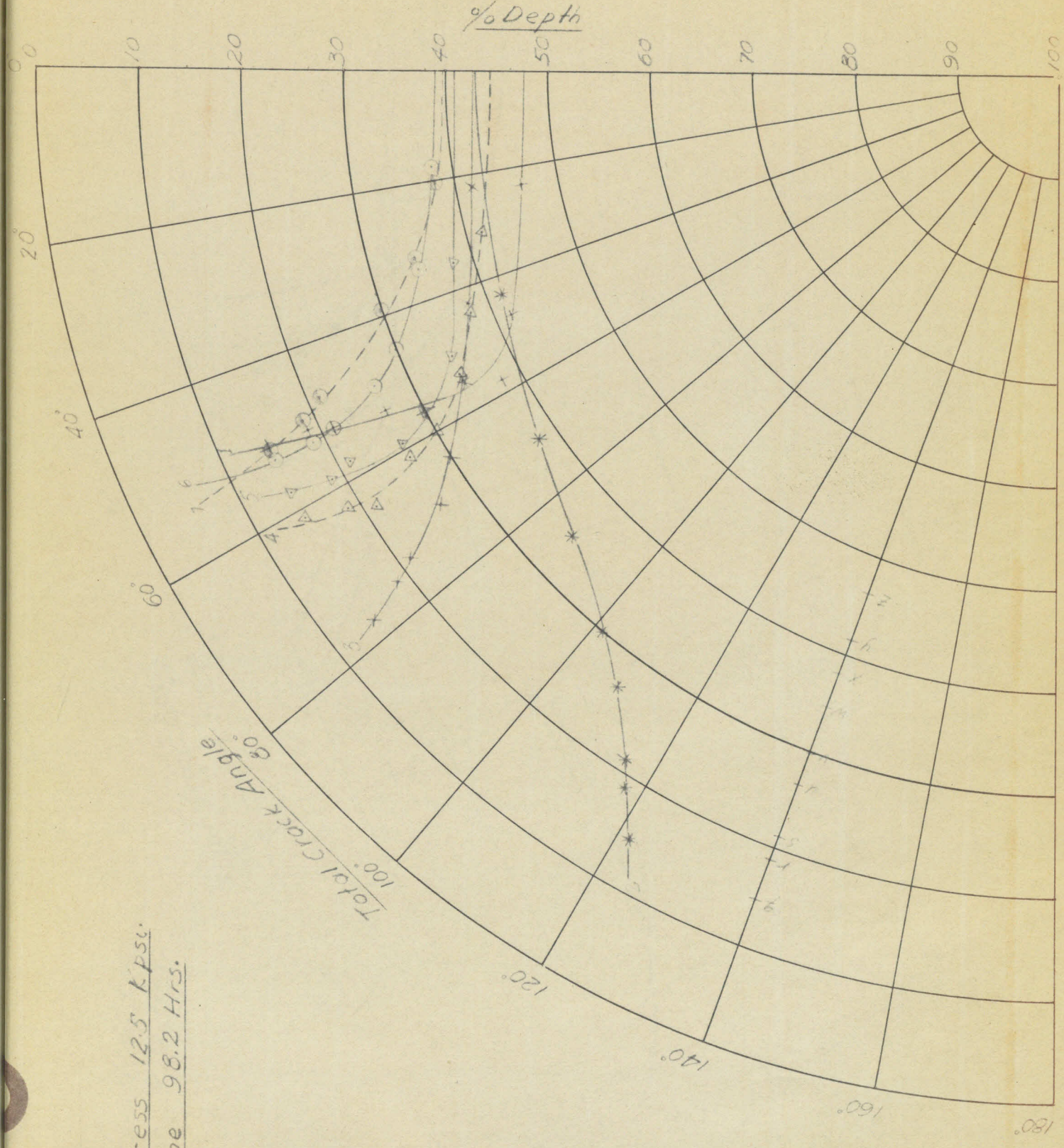

Stress 12.5 Kpsi.
Time 98.2 Hrs.

ME 140

BY R.C.B.

APP. W.H.G.

DATE 3-22-43

NO. E-7

Crack Profiles

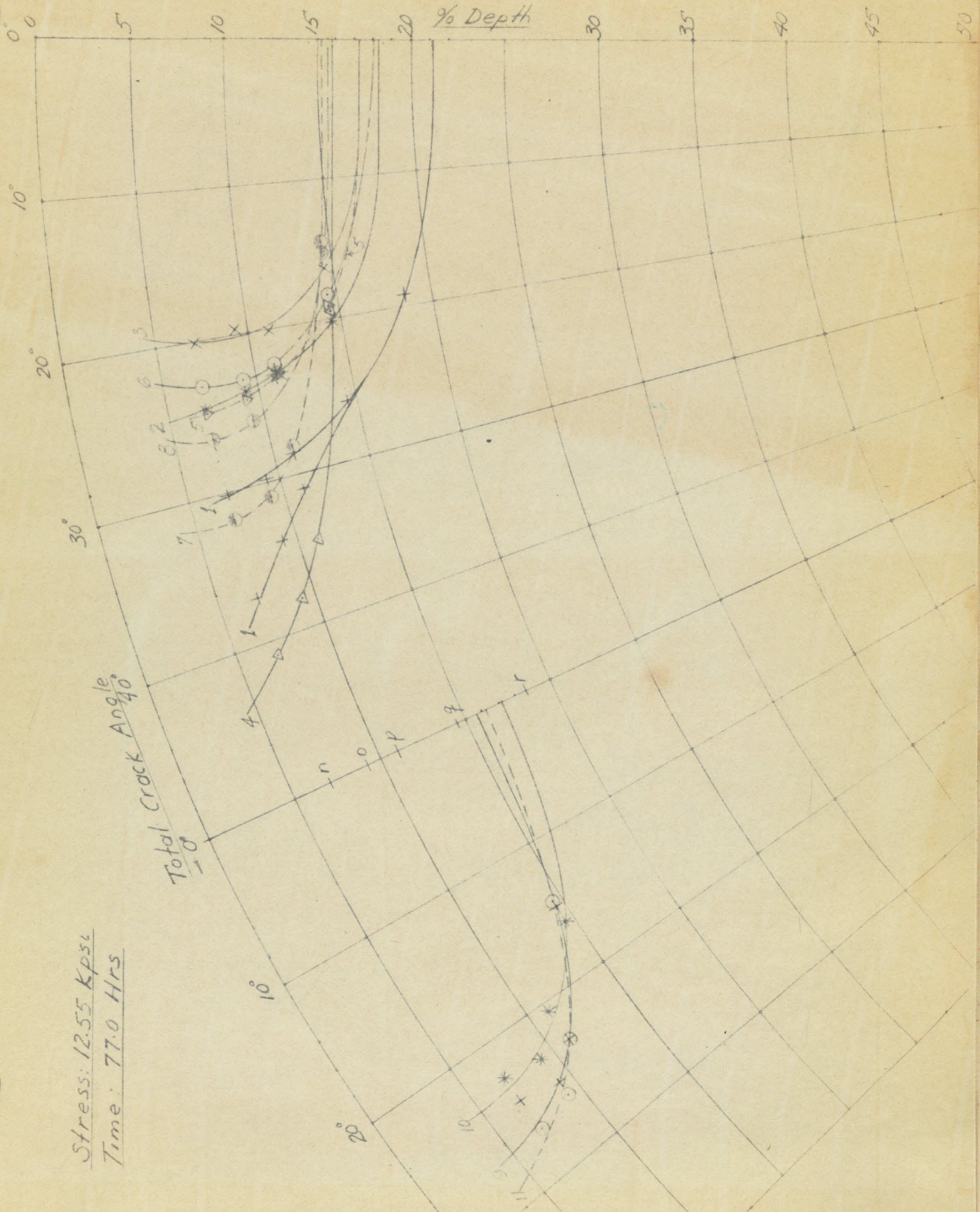

ME140

RCB

W.H.e.

3-23-73

Crack Profiles

E-8

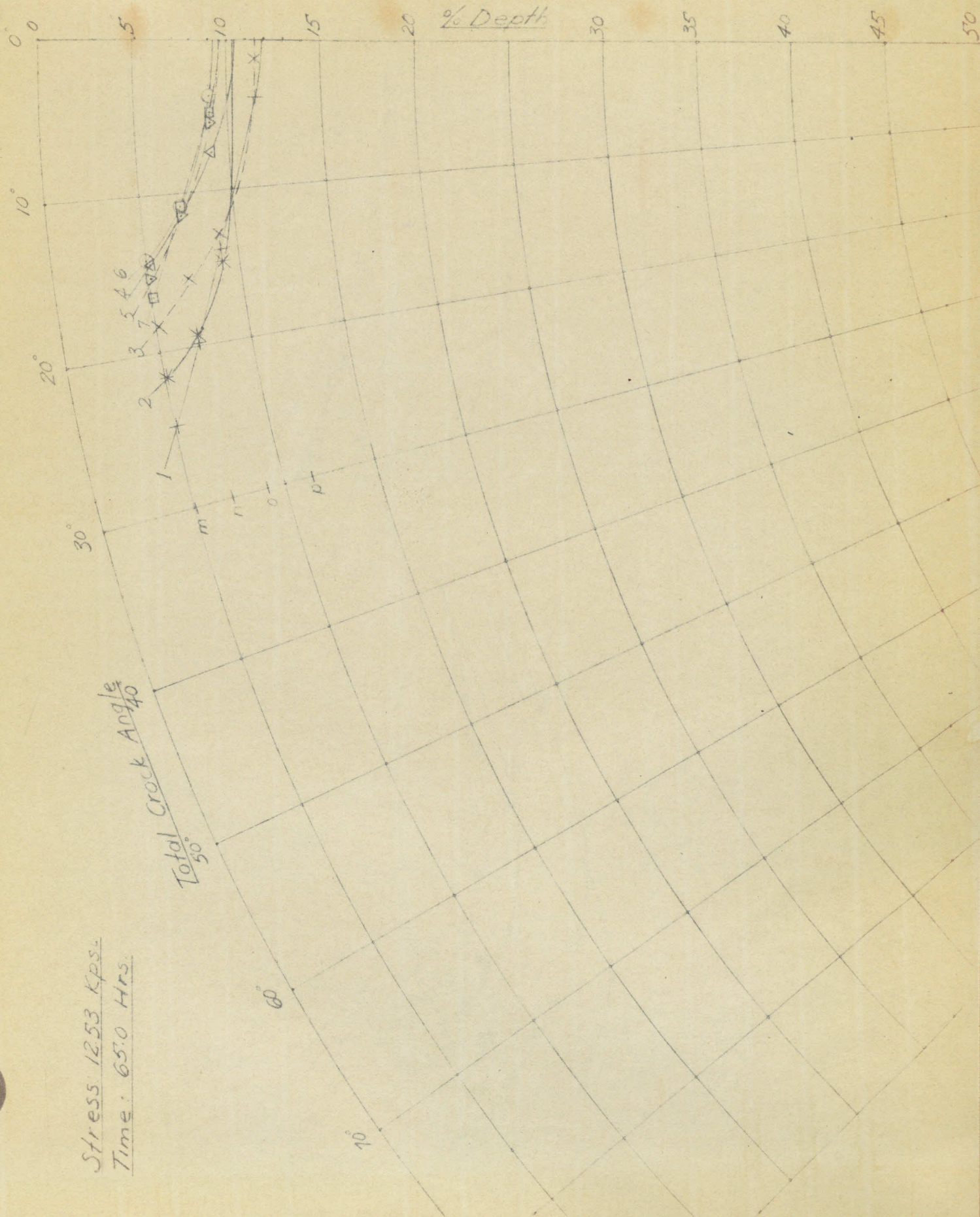

Stress 1253 Kpsi.

Time: 650 Hrs.

ME 140

K C B

Wöhler

5-23-43

E-9

Crack Profiles

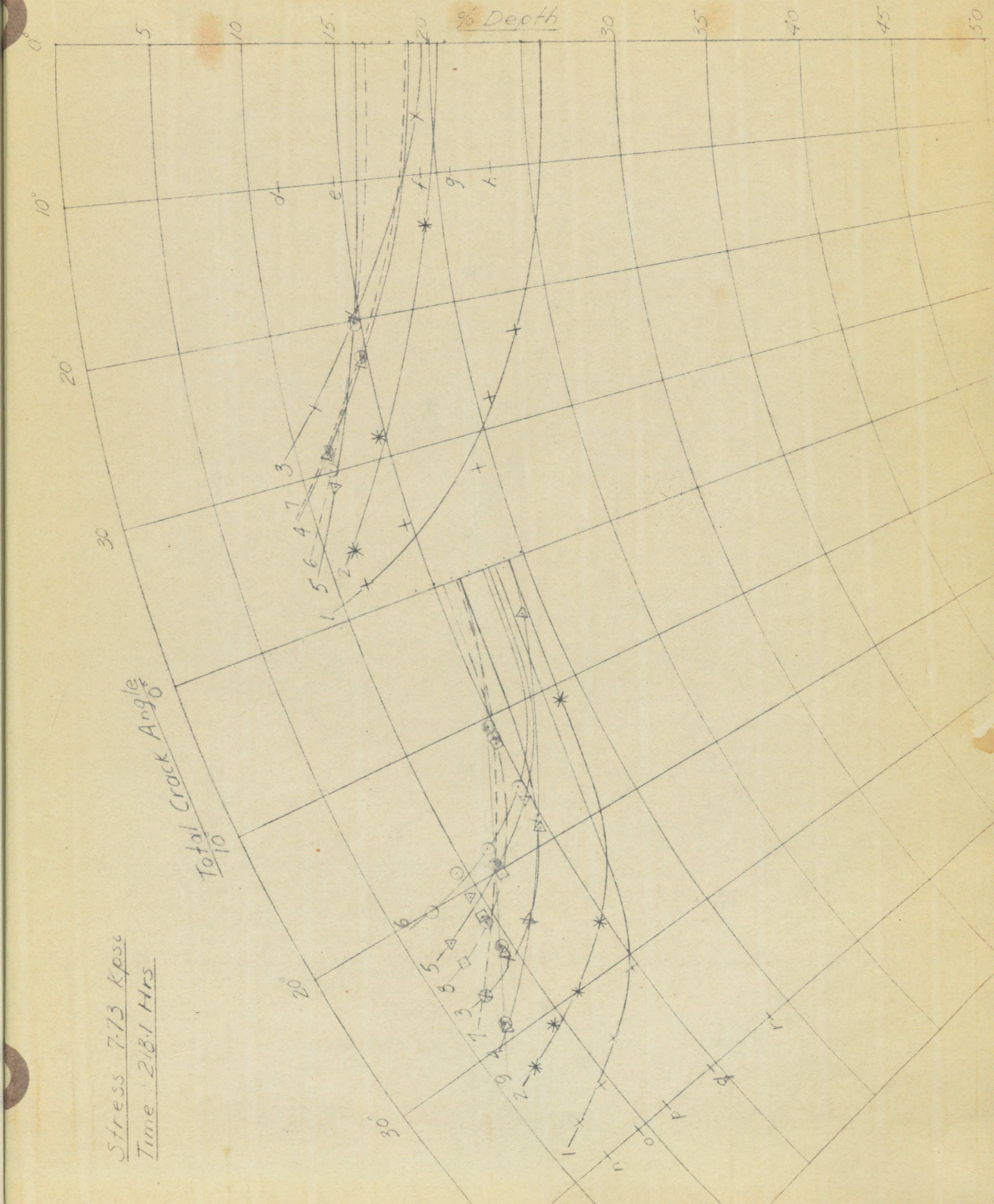

ME 140

R.C.B

Utile.

3-23-43

E-10

Crack Profiles

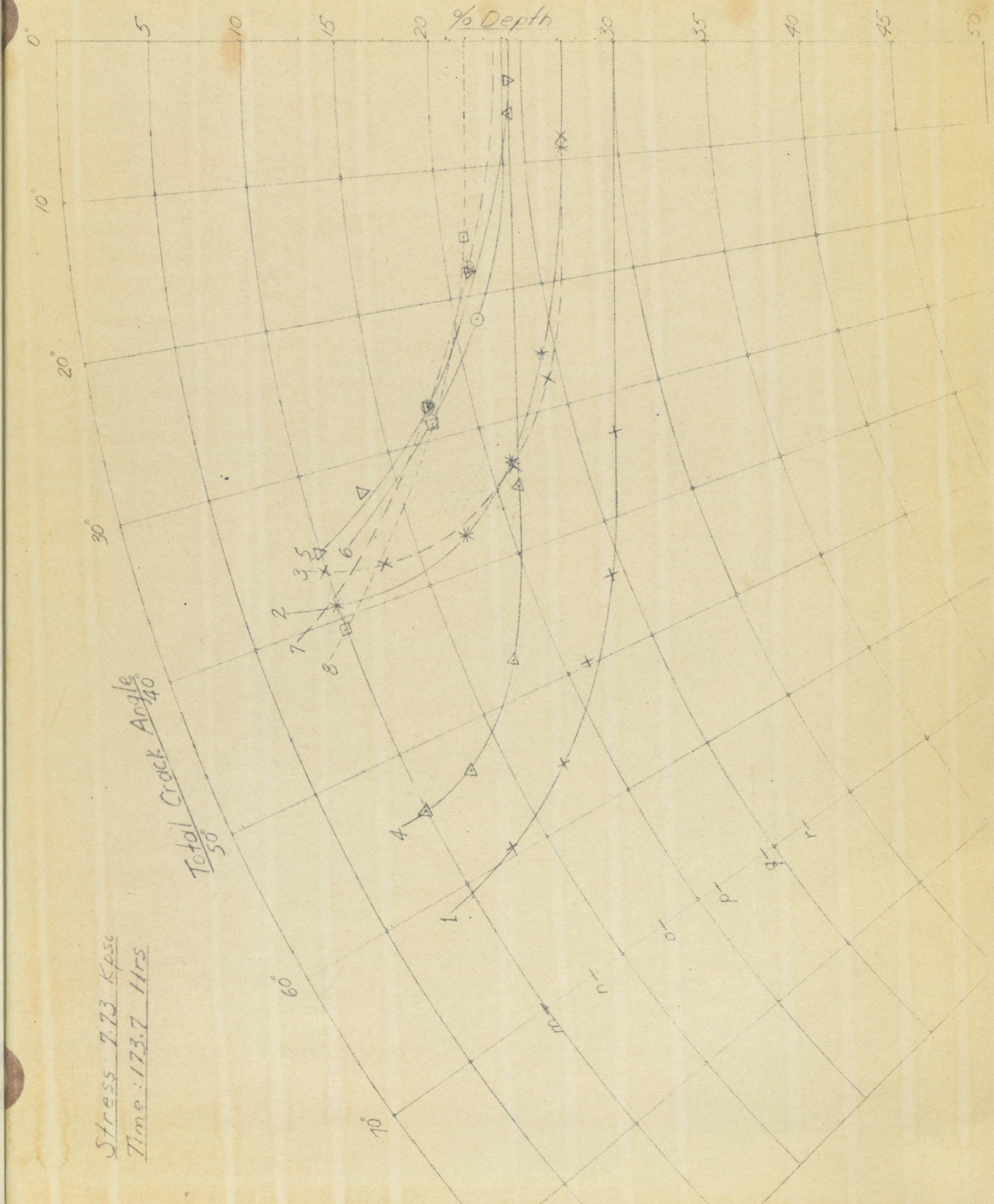

Stress: 7.73 Kpsi

Time: 173.7 Hrs